Full Scale Tests on the Performance of Hybrid Timber Connections in Real Fires

By

Samuel Bright Amankwah Boadi

A thesis submitted to
The Faculty of Graduate and Postdoctoral Affairs
In partial fulfillment of the requirements for the degree of

Master of Applied Science

In

Civil Engineering

Department of Civil and Environmental Engineering
Carleton University
Ottawa, Ontario

Abstract

Connections form an integral part of any building system. A hybrid building system is created when two or more structural construction materials are involved in its construction. There are concerns when using hybrid connections especially when they are exposed to fire. This is because different materials with varying ambient and thermal properties must perform together to ensure a safe and stable structural system.

This research seeks to present the fire behavior and resistance of unprotected hybrid connection systems involving a glulam timber beam and steel columns in typical real fires referred to as non-standard fires, and their comparison to performance under temperatures defined by CAN/ULC S-101. Three different shear tab connection systems: Concealed, Exposed and Seated were studied. These connection systems transfer beam end reactions to the columns. Each connection system was tested for two load ratios of 60% and 100% with a 12.7 mm Grade A325 bolts.

The time to failure of each assembly under the modelled non-standard fire curve reduced with increasing load ratios. Lower load ratio of 60% resulted in an increase in the times to failure by 50% - 75%. Fire resistance ratings in the modelled real fire curve were low, with a higher resistance time of 21 minutes recorded for the Seated Connection Assembly under 60% load ratio. Using the cumulative radiative energy area method to predict the severity of the standard CAN/ULC-S101 and real fire curves gave good results. The method predicted conservative equivalent times of failure for the Seated Connection Assembly under both load ratios of 60% and 100%.

Acknowledgements

My gratitude goes to the Almighty God for the opportunity, grace and wisdom that has seen me through my Master's program.

The successful completion of this program would not have come to pass without the unwavering support, motivation and guidance of my supervisor, Prof. George Hadjisophocleous. Thank you for granting me the opportunity and the trust to contribute to the existing knowledge on fire safety engineering.

This research was funded by the Natural Sciences and Engineering Research Council (NSERC), and I am grateful to them for offering me this opportunity.

I am grateful to Ba Lam-Thien for his incessant support in helping set up all the tests we ran for this research. Your effort is much appreciated. My colleagues, Marc Alam and Matt Turco were also very helpful in assisting me with working with most of the shop tools and equipment. Thank you guys for the training, encouragement and emotional support.

I am highly indebted to all who in one way or the other helped me through my Master's program. God bless you for all the moral, financial and emotional support. Finally, I want to express my utmost appreciation to my family in Ghana who raised me to where I am now. I love you!

Table of Contents

List of Tables

List of Figures

1 INTRODUCTION

1.1 Background

Wood as a construction material has been in existence for thousands of years. In recent times, the use of wood based on engineering principles has greatly evolved. The motivation behind this evolution is the need to conserve energy, to minimize environmental impact and to provide affordable and portable housing for communities. Moreover, wood and wood-based products offer the advantage of less energy consumption than other building materials, ease of production, fast erection, and versatility. Its higher propensity to be modified and dismantled when needed makes it a favourable construction material (*Tannert et al., 2012*). All these qualities that can be harnessed from wood have led to an increased demand for its usage in construction. This in turn has resulted in lot of research to comprehend the structural and thermal behavior of wood and its ability to be combined with other materials in composite construction.

Structural systems involving wood can be categorised as either heavy timber or light wood frame structures. In heavy timber structures, the main structural elements such as beams, columns and slabs are built using solid sawn lumber or glue laminated timber. In Canada, timber construction is deemed heavy when the dimensions of beams and columns, and decks exceed 150 mm and 50 mm respectively (*Buchanan, 2002*). Heavy timber structures tend to have higher passive fire resistance due to the size leading to a relatively slower charring rate as compared to light wood frame construction. The formation of char on the surface protects the unburnt wood underneath from exposure to heat.

Light wood frame construction involves beams and columns with a dimension less than 150 mm, and 50 mm for decks. It is highly employed in residential buildings of one to four storeys. Due to

their smaller size, they have less passive fire resistance compared to heavy timber construction. They must therefore be covered in protective materials such as gypsum board to improve their fire resistance (*Buchanan, 2002*). Applications of lightweight construction include wood-frame shear walls which are placed between steel columns in a structure to form the lateral load resisting elements (*He and Li, 2012*).

In Canada, buildings using wood and wood-based products fall under the category of combustible construction. These can be both residential and non-residential buildings (*Wood Design Manual, 2010*). In Canada, the University of British Columbia constructed a 5-storey building for the Earth Sciences Department using wood as the primary structural member. The north wing made of wood complemented the laboratory wing made of concrete, in terms of aesthetics and architectural value. The 5-storey building had a glulam frame with solid timber panels. To allow design and construction of the Earth Sciences Building (ESB) with wood as the only material, a Building Code Alternative Solution, which was peer-reviewed during the building permit approval process was carried out (*Canadian Wood Council, 2012*). Some examples of structures built with wood and wood-based products worldwide are listed below as reported by reThink Wood Initiative (2012);

- The Union Square Condominium in San Diego, California was constructed with wood in 2005. It houses 262 condominium units. The seven storey structure was built following the International Building Code that was introduced in the year 2000.
- The Promega GMP-Facility in Fitchburg, Wisconsin completed in October 2012 was constructed with a mixture of glue laminated timber and cross laminated timber. Design of the state-of-the-art 24,155 m^2 facility was performance based.

- The Gallery at Cameron Village in Raleigh, North Carolina is a five storey wood-framed building. The wood products in the structure are protected with fire-retardants with a 2 hour fire resistance rating.
- The Arena Stage at the Mead Center for American Theater in Washington D.C. is a hybrid structural system of wood and glass. The structure has eighteen 45 to 63 ft tall columns made of unreinforced parallel strand lumber (PSL) supporting steel roof trusses. The design team had to convince code authorities of the feasibility of the structure through computer models and extensive fire analysis (reThink Wood Initiative, 2012).

The above and many other buildings prove the ability of wood to be used alone and with other materials in construction of civil engineering structures.

Since 1992, Part 3 of the province of Ontario Building Code Act (2012) restricted the height of wood frame buildings to four storeys. Recently, the limit was increased from four to six storeys. This is due to the growing trust in wood for construction of high-rise buildings in Ontario to meet the needs of the growing population.

Despite all the great features associated with wood and wood-based products for construction purposes, there are still concerns among researchers on its fire-resisting properties, and its usage in high-rise buildings. In retrospect, researchers have tried to improve the structural and fire-resisting properties of wood related to its application in structural systems. The strength and rigidity of wood has been improved through gluing different wood products of varying properties together, and hybridization (*He and Li, 2012*). Timber based hybrid structures can be utilized in constructing high-rise timber buildings. Light-weight wood frame diaphragms can be used with steel beams to produce a floor system capable of resisting vertical loads and transferring lateral

loads. Hybrid connections also make use of the different properties of the materials involved, in transmitting loads effectively to adjoining members. However, a thorough understanding of how the materials interact in resisting loads and fire is required.

1.2 Statement of Problem

The ability of any structural system to perform its intended function depends on the strength and stiffness properties of the structural members, and the connections between those members (*Buchanan, 2002*). Connections usually constitute the weakest link in any structural system especially in fire. This problem becomes important in hybrid connections involving timber and steel. Steel, a good conductor of heat, transfers heat to connected wood members, leading to increased charring, reduction in cross-section of wood close to the connection and ultimately resulting in reduction of strength of the connection system.

Prescription-based design has been the approach used for fire safety design in buildings. In Canada, design requirements for fire safety are found in Division B, Part 3, Fire Protection, Occupant Safety and Accessibility, of the National Building Code of Canada (*NBCC, 2010*). The NBCC (2010) has no detailed engineering design provisions for the design of fire resistance of timber connections, and hybrid steel-column and timber-beam connections (*Mehaffey, 2003*). It prescribes a fire resistance rating of 45 min or 1 hour for combustible construction (*NBCC, 2010*). There is a lot of discussion among engineers that if structural design can be done based on engineering principles, then similar engineering principles can be developed to determine the fire resistance of structural members such as heavy timber connections (*Babrauskas, 2000).* Recently, the use of performance-based design approach, where systems are designed using fire safety

engineering principles and shown to satisfy the code objectives is on the rise. In order to fully understand the behavior of hybrid connections and to complement the performance based-design approach, full scale tests by Peng et al., (2010) on the behavior of connections in timber tension members, and Ali et al., (2014) on hybrid connections involving beam-column in the Standard CAN/ULC S-101 have been conducted. In their research, the influence of parameters such as load ratio, connection type, bolt diameter and properties of the materials involved were studied. To add to the research conducted by Ali et al., (2014) on the behavior of beam-column hybrid connections, this research seeks to investigate the behavior of similar assemblies in a real fire, as well as establish a relationship between the impacts of the CAN/ULC S101 fire curve and a real fire curve. Moreover, the Standard Time Temperature Curves are recognized as unrealistic (*Law, 1981; Kathleen and Almand, 2012*) in simulating severities on structural members in fires. For the past decade, several full-scale non-standard tests have been performed by researchers to study the behavior of structural elements, members, connections and assemblies in real fires (*Kathleen and Almand, 2012*). This research seeks to contribute to the gradual shift to full scale non-standard fire testing.

1.3 Objectives

The objectives of this research are to:

1. Investigate the influence of parameters of load ratio (60% and 100%) and different types of shear tab connections on the behavior of unprotected hybrid timber-steel connections in non-standard fires.
2. Compare the performance of these hybrid timber-steel connections when exposed to the standard CAN/ULC S101 and non-standard fire curves.

3. Confirm the ability of a furnace to replicate real fires.
4. Provide an understanding of the performance of hybrid timber-steel connections in real fires, and compare the resistance ratings of the different connections.

2 LITERATURE REVIEW

In this chapter, a review of the theoretical background as well as research works by others on material properties and the behavior of timber, steel and hybrid connections is presented.

2.1 Introduction to Fire Resistance

An overview of the basic methods for evaluating the fire resistance of structural components is presented in this section.

2.1.1 Fire Resistance and Fire Severity

Structural members as well as non-load bearing boundary walls of a building must be able to maintain their integrity for a given duration in a fire outbreak. The ability to withstand exposure to fire for a certain amount of time is called its Fire Resistance (*Benichou, 2000*)**.** Fire Severity refers to the potential of a fire to cause damages on the structural components. Buchanan (2002) defined it as a measure of the forces or temperatures capable of causing collapse of part or whole of the structure. To design a structure for fire safety, its fire resistance must outweigh the destructive capabilities of the fire referred to as severity. In essence, the equation below must be satisfied:

$$\text{fire resistance} \geq \text{fire severity}$$

In Canada, design requirements for fire safety are mostly based on experience (*Wood Design Manual, 2010*). The fire resistance of structural assemblies is evaluated by standard tests outlined in CAN/ULC S-101 and ASTM E119 (*Benichou et al., 2000*). These standardized tests are run to obtain the time to failure of components based on the following failure criteria;

- The stability criterion is defined as the ability of a structural component to perform its intended purpose of carrying loads throughout the test duration. Limiting deflection values are usually employed for this failure criterion (*Buchanan, 2002*)
- The integrity criterion measures the ability of structural members and barriers to restrict the movement of hot gases through them. It involves limiting the formation of cracks and fissures throughout the test duration. According to ASTM E119 (2000), failure occurs when the passage of hot gases or flames are capable of igniting a cotton waste (*Buchanan, 2002*)
- The insulation criterion involves limiting the transfer of heat through the assembly to the cold side. Insulation failure occurs when there is an average increase in temperature of 140°C or a maximum increase of 180°C at a single point and unexposed side of the assembly.

Based on standardized fire resistance tests or other approval systems, ratings are assigned to the structural elements. In the National Building Code of Canada (2010), fire resistance ratings are related to the intended occupancy, size and type of structure. It is defined as the time in minutes or hours that a material or assembly of materials will withstand the passage of flame and transmission of heat when exposed to fire under specified test conditions and performance criteria, or as determined by extension or interpretation of information derived therefrom as prescribed in the National Building Code of Canada (2010) (*Wood Design Manual, 2010*). Fire-resistance ratings may also be assigned by means of code approved calculation methods and listings. They are assigned values comparable with fire severity specified in the codes to evaluate the performance of structural assemblies. Fire resistance ratings are required for major structural systems in the National Building Code of Canada (2010).

2.1.2 Real/Parametric Fires versus Standard Fires

The first step in evaluating the fire resistance of materials is to establish a time-temperature exposure adequate enough to simulate typical fire scenarios. This time-temperature exposure can be established by fire models of Real/Parametric and Standard Fires.

2.1.2.1 Real/Parametric Fires

The term real fire or parametric fire is a modeled time-temperature curve using the parameters of compartment properties and fuel loads available *(Hertz, 2012; Purkiss, 2007)*. The influencing compartment properties comprise the type of compartment, compartment size and the amount of ventilation available. They are usually referred to as Compartment Fires. Parametric fire curves attempt to replicate heat energy and burning duration as seen in real world fire scenarios. These curves are therefore built on the principle of heat balance within a fire compartment *(Hertz, 2012)*. They tend to have three distinct phases: the growth phase known as pre-flashover; the fully developed stage known as post-flashover; and the decay phase (*Law, 1978*). The pre-flashover stage is of concern when analyzing for life safety. Peak heat release rate is reached in the post-flashover stage *(Benichou et al., 2000)*, and structural elements are exposed to the most severe heat load that may lead to collapse and loss of structural integrity (*Law, 1978*). Post-flashover fire models provide information of fire gas temperature impinging boundaries, and time of exposure, that are used as input parameters to establish the performance of compartment boundaries and members in a fire (*Harmathy et al., 1983*). According to Harmathy (1983), the post-flashover stage of a fire is influenced by five process variables: rate of air flow into compartment; mass loss rate of fuel; heat release rate within the compartment; temperature of the fire gas; and heat flux impinging and penetrating the compartment boundaries. During the decay phase, the heat intensity

gradually dies down. Apparently, this stage is also significant for structural design as heat penetrates cross-sections of exposed members due to the thermal conditions of the compartment *(Hertz, 2012)*.

In most parts of the Nordic Countries, parametric fire curves are regarded as safe fire models for the design of structures and the prediction of fire resistance of structural elements especially when safe evacuation is deemed highly important *(Hertz, 2012).* Destructive impacts of fires on structural members usually occur after flashover. Hertz (2012) defined parametric fires as the most severe flashover fires if all combustibles are ignited simultaneously. Using parametric fires is therefore regarded as a justifiable conservative fire model when safety against structural collapse is considered critical in design for evacuation *(Hertz, 2012).* They are able to model the severe destructive impact of compartment fires, and are thought to be conservative. Parametric fires are therefore suitable for the fire safety design of small compartments as well as large flat compartments, especially for areas where larger fire loads may be present such as factories. With the introduction of performance based design, the use of parametric fires in predicting the fire resistance of structural elements are highly probable.

Buchanan (2002) lists different models (Swedish Method, Lie Method, COMPF2, OZONE, Eurocode) that exist for parametric curves, with the Swedish Curves by Magnusson and Thelandersson (Fig. 2.1) being the most widely used (*Buchanan, 2002; Benichou et al., 2000*). These fire curves are functions of the available ventilation and the total fuel load, Q_t (MJ/m^2) present in a room. The available ventilation is defined by the ventilation factor which is dependent on the parameters of area of window opening A_o, height of opening H_o, and the total surface area of the room A_t. The Eurocode parametric fires were developed from the Swedish Curves as well *(Buchanan, 2002*). Unlike the standard curves, the parametric ones increase to a maximum

temperature, remain steady, and then gradually decay as fuel load and air supply diminish (*Benichou et al., 2000*).

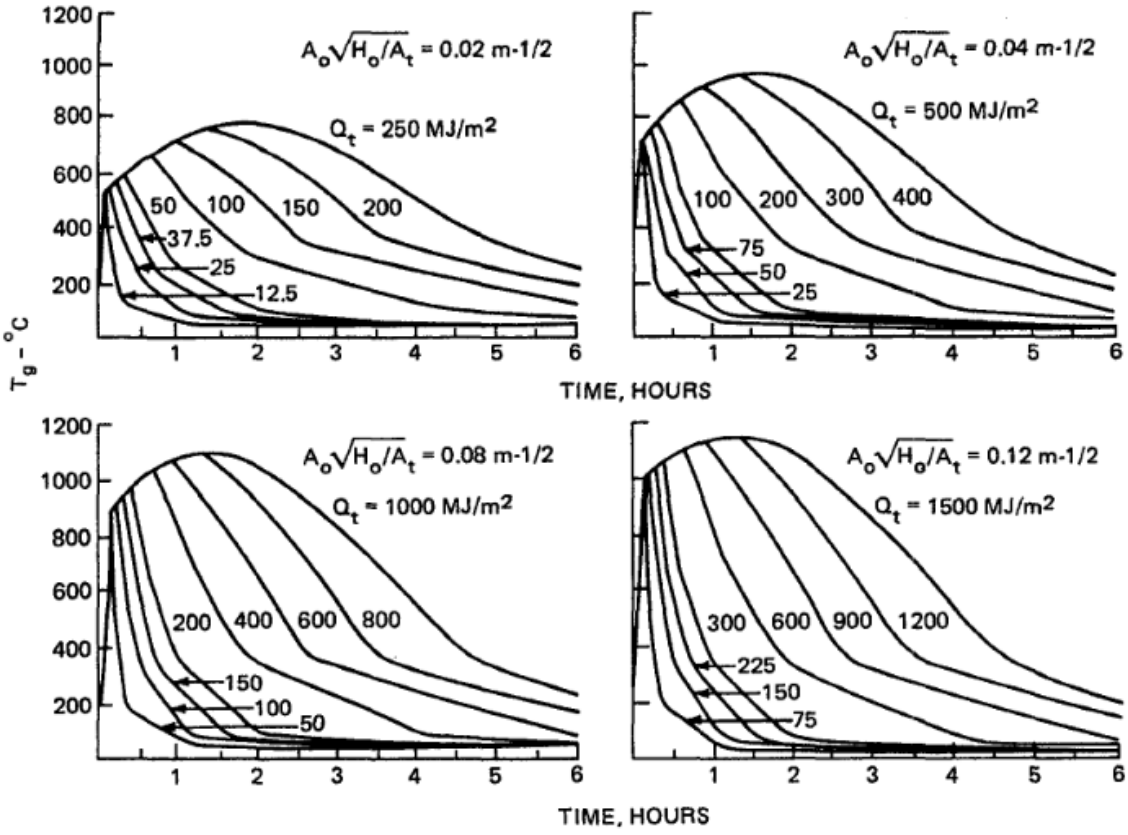

Figure 2.1 Parametric time - temperature curves for different ventilation factors and fuel loads (MJ/m^2 of total surface area) as reproduced from Walton et al., (2002)

2.1.2.2 Standard Fires

A standard fire refers to the time-temperature curve used in tests for defining the fire resistance rating of structural elements and assemblies in general. These harmonized fires are defined in standards such as the ASTM E119 and ISO 834 (*SFPE, 2002; Buchanan, 2002*), to mention a few. The standard fire curve used in Canada is in CAN/ULC S-101 which is similar to the ASTM E119

test. A differing feature between the standard time-temperature curves and the parametric one is the absence of a decay phase in the former. As such, their fire severity on specimens is greatly influenced by the dimension of the test specimen *(Hertz, 2012).* The harmonized standard time-temperature curve used in various countries is presented in Figure 2.2. The International Standards Organization's standard, ISO 834 time-temperature curve equation is given by;

$$T_g = T_o + 345\, log_{10}(8t + 1) \qquad \textbf{Equation 2.1}$$

where

T_g *is the average furnace temperature,* $°C$

T_o *is the ambient temperature,* ℃

t *is the time of exposure,* min

The CAN/ULC S101 standard time-temperature curve is represented using analytical equation shown below,

$$T_g = T_o + 750\left(1 - exp\left(-0.49\sqrt{t}\right)\right) + 22\sqrt{t} \qquad \textbf{Equation 2.2}$$

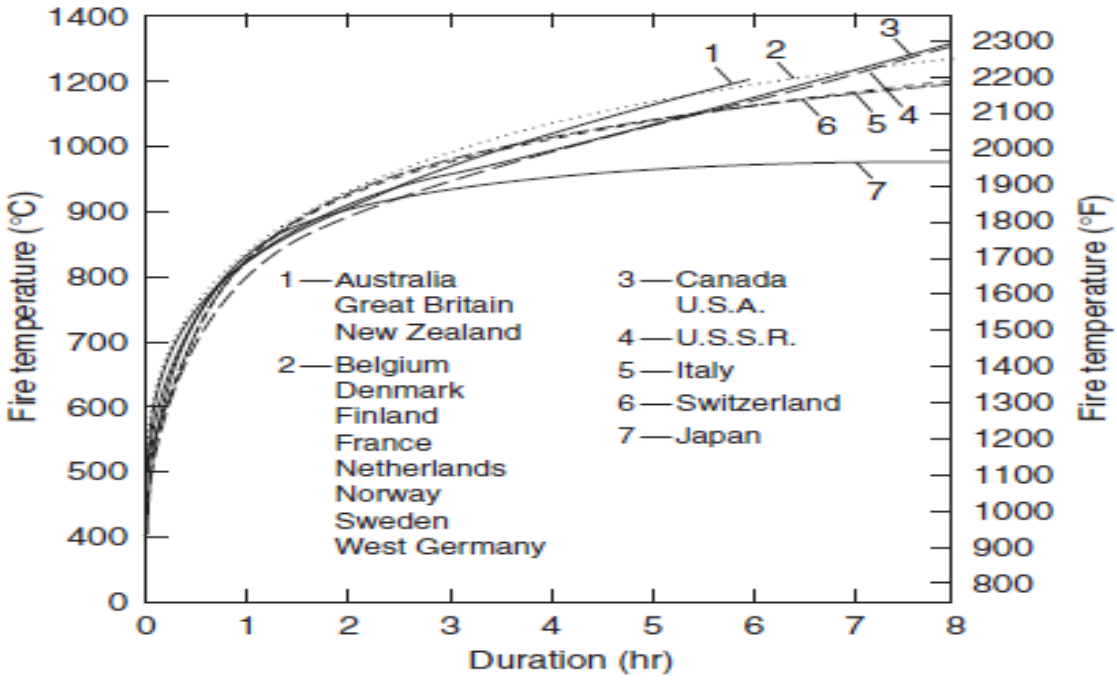

Figure 2.2 Standard time-temperature curves used in various countries for testing structural elements as reproduced from SFPE (2002)

2.2 Equivalent Fire Severity

Equivalent fire severity is a concept that compares the destructive capabilities of a fire to the severity of the standard fire. It offers an approach for comparing the fire resistance of components and structural members to real fire. Various methods to determining the equivalent severity of a fire exist. Among such methods include the equal area, maximum temperature and time equivalent approach.

2.2.1 Equal Area Concept of Fire Severity

Ingberg in 1928 (*Buchanan, 2002*) introduced the concept of equal area to compare the severity of two fires based on the integral of the time-temperature curves. By this method, two fires are

deemed to have equivalent destructive impacts on an element when the integral of their time-temperature curves above a reference point of 150°C are the same. This method though useful has shortcomings. It overlooks the contribution of fuel geometry and ventilation on fire severity. Fire severity on elements is a function of the heat energy they receive mainly by radiation. Radiation is directly proportional to the temperature build up in a compartment raised to the fourth power. Hence, this method has the potential of underestimating the fire severity of short hot fires and overestimating that of long cool fires (*Nyman, 2002*). It is rarely used now.

2.2.2 Maximum Temperature Concept

This concept compares the exposure time that would result in a maximum temperature of protected steel members in a standard fire to that which would occur in a real fire. Developed by Law (1971) and Pettersson et al. (1976), this method can be useful in estimating the equivalent severity of fires on wood products with a temperature of char of 300°C. It however gives unreliable results when the maximum temperature in the standard fire and that in the real fire at failure vary significantly.

2.2.3 Time Equivalent formula

This method relates the severity of real and standard fires by comparing their performance under both exposure models based on the governing failure criterion. For insulation criterion, it is the equivalent time of exposure of an element in a standard fire that would result in the same maximum temperature in a real fire. Based on load capacity, it is the equivalent time of exposure of an element in a standard fire that would result in the same minimum load bearing capacity as would be observed in a real compartment fire. In this case, it is referred to as the minimum load capacity concept (*Buchanan, 2002*). Time equivalence formulae developed by researchers such as

Pettersson (1973), Law (1973) and that in the Eurocode are based on maximum temperature of protected steel members in real fires.

2.3 Hybrid Timber Construction

Application of new materials and technology in the construction industry is evolving with time. Hybrid construction generally speaking involves blending different construction materials in developing one structural system. For instance, utilizing steel and timber, concrete and timber, steel and concrete, or all three materials: steel; timber; and concrete in realising a civil engineering structure. In Canada, hybrid systems comprising cast-in-place reinforced concrete at the foundation level and wood frame as the superstructure is normally found in residential buildings.

According to the Canada Mortgage and Housing Corporation (*CMHC, 2014*), millions of residential buildings in North America are constructed of wood. With time, the use of timber in construction is evolving, with advancements in technology and research methods. In Canada, the National Research Council, Canada Mortgage and Housing Corporation, and other institutions and industries have made enormous contributions toward overcoming the challenges faced with timber construction with regards to fire safety.

Notwithstanding the unavailability of clear and detailed design procedures, hybrid timber structures are being designed using conservative design approaches (*Solomon and Siegfried, 2014*). They offer the advantage of reduced self-weight, increased story height, blend of the aesthetic properties of the involved materials and optimal use of the properties of the involved materials.

Integration of the different materials in a hybrid structural system is done at either the component and/or the building system levels (*Solomon and Siegfried, 2014*). At the component level, the different materials are merged to form structural members such as hybrid beams, hybrid columns, hybrid slabs/diaphragm, hybrid shear walls, hybrid braces, hybrid bridge decks and hybrid connections. At the building system levels, the different materials are employed in the main structural framework of individual systems within the structure. Examples of such include hybrid shear wall systems, hybrid tube systems, hybrid vertical mixed systems and steel frames with wood infill walls.

2.3.1 Hybrid Timber Connections

Connections join separate structural members together in a structural system. They safely transfer loads from one member to another without undue stress, while minimizing the cost of fabrication and ensuring ease of erection (*Morris and Plum, 1996*).

Connections are designed based on realistic assumptions of the distribution of internal forces in the connecting members. They however constitute weaker links in the structural system. As such, understanding of their behavior is significant not only for fire safety considerations, but also the thermal and hydric fluxes within the connections (*Samake et al., 2014*). They must be designed to have at least a strength and a fire resistance rating equal to that of the connecting members according to the National Building Code of Canada and most building codes (*Ali et al., 2014*). Timber structures are connected either with adhesives or mechanical fasteners. Glued joints are rarely used due to their brittle mode of failure (*Johnsson, 2004*). Mechanical timber joints made of dowels, bolts, screws and nails are employed in large structural assemblies. Such joints offer warnings before failure due to their increased ductility.

Peng et al. (2010) noted that failure of timber connections may be either sudden and brittle or ductile. Ductile failure is preferred in design because it provides warnings prior to collapse. These two main failure modes are influenced by factors such as the size of timber member and fastener, the number of fasteners and their position in the wood members also known as the geometrical configuration (*Peng et al., 2010*). Under these two typical main failure modes, timber connections may fail in either block or plug shear failure, splitting failure or embedment failure (*Johnsson, 2004*) as shown in the figure below, with embedment being the only ductile failure mode. Such failure mode allows for stress redistribution (*EC5, 2004*).

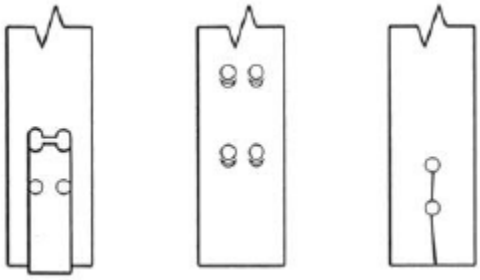

Figure 2.3 Different failure modes in timber connections: plug or block shear, embedment failure, and splitting in that order from left to right (Peng et al., 2010)

In embedment failure, the dowel or bolt compresses the area of wood underneath it during loading thereby enlarging and elongating it. Peng et al. (2010) observed that embedment failure was dominant for his connections when lower load ratios (LR<50% of ultimate ambient load) were employed (*Peng et al., 2010*). Extreme bending and yielding of bolts may also occur alone or with splitting of wood along the grain when load ratios greater than 50% of the ambient capacity are applied. All failure modes are probable for dowel joints where the diameter of the bolt or dowel is greater than 8 mm (*EC5, 2004)*.

In a fire resistant structure, both the members and the connection assembly must be able to perform their intended function under exposure to extreme temperatures (*Buchannan, 2002*). Since connections constitute weaker planes especially in hybrid structures, they must be designed to have a fire resistance rating greater than or equal to that of the members. Metal fasteners as connections have a significant impact on the charring and as such on the strength of hybrid structures involving wood due to their ability to conduct and transmit heat. The heat conducted is easily transmissible into the wood, causing charring and a subsequent reduction in its load carrying capacity (*Buchannan, 2002*). Metal fasteners with a low ratio of heated perimeter to cross-sectional area will heat up slower than those with a high ratio. The fire behavior of bolted connections depends on the amount of heat that enters the wood section through the bolts (*Buchannan, 2002*). Regardless of that, lower load ratios provide increased time of exposure before failure (*Peng et al., 2010*).

2.4 Wood and Steel

The difference in mechanical and thermal properties of wood and steel makes understanding of their behavior in a fire quite complex. Under exposure to fire, each material reacts differently depending on its thermal and mechanical properties. The rate of heat flow is being influenced by the evolution of thermal conductivity with increase in temperature (*Samake et al., 2014*)

This section briefly discusses the structural behavior of wood and steel under normal and elevated temperatures.

2.4.1 Wood at Ambient Temperature

Wood is a multipurpose raw material which is widely used in all fields of construction. It is an organic material composed of cellulose fibres, and is heterogeneous, hygroscopic and anisotropic.

One feature that truly distinguishes wood from all other construction materials is that it occurs naturally and in abundance. As such, it was widely used as a construction material in the ancient times, and still remains a common material for construction in these modern times. It is widely used in countries such as Canada, Sweden, Finland, Norway and Poland, where there is abundance of quality wood. Its application ranges from residential construction to highly sophisticated and heavy civil engineering constructions such as bridges and cofferdams.

Wood has three mutually perpendicular planes of symmetry defined in the longitudinal, tangential and radial directions as shown in Figure 2.4 below.

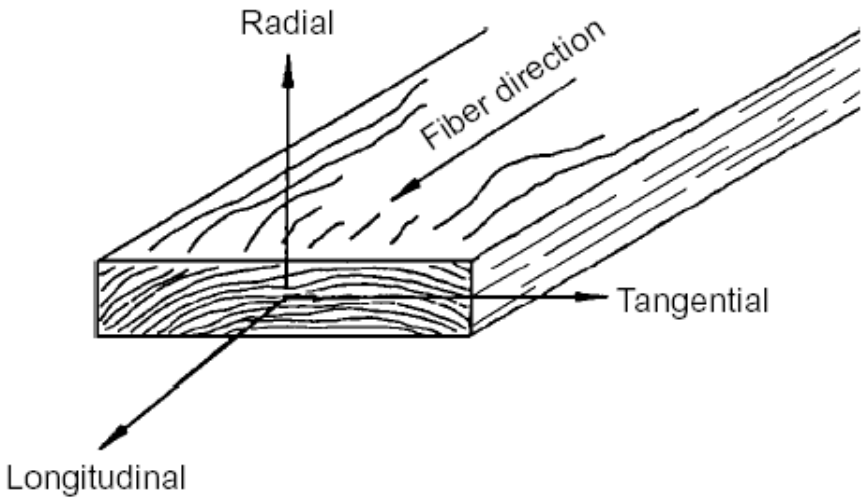

Figure 2.4 The planes of symmetry in wood (Wood Handbook, 1999)

The longitudinal direction is parallel to the grain, the radial direction runs along the annual growth rings, and the tangential direction runs tangential to the annual growth rings. The structural behavior of wood in each of these directions varies, and as such it is recognised as an orthotropic material.

The figure below (Fig. 2.5) shows the stress-strain relationship for small specimen of wood void of any defects.

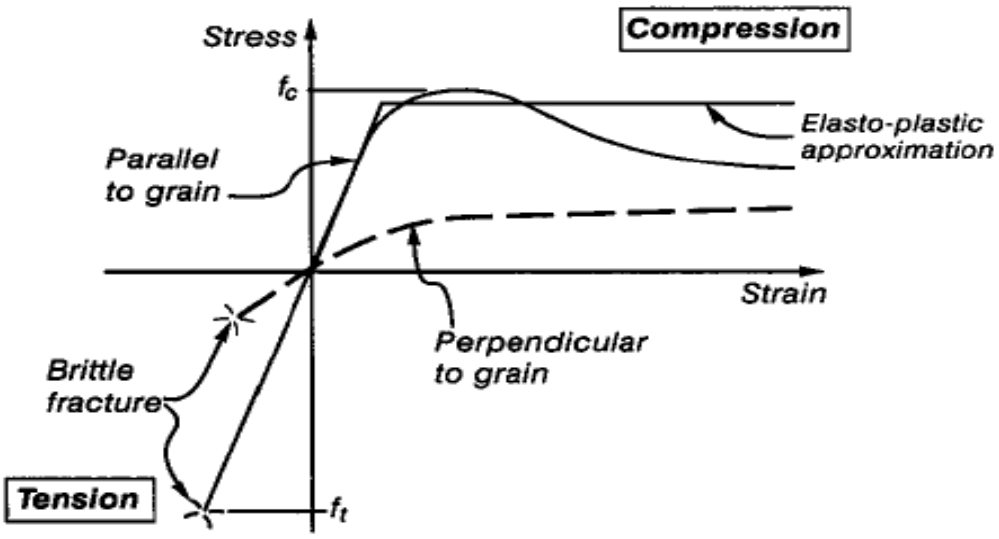

Figure 2.5 Stress-Strain relationships for clear wood (Buchanan, 2002)

When wood is loaded parallel to the grain, it exhibits a fairly high elasticity in tension, but with a failure mechanism which is abrupt and brittle at a tensile stress f_t. Compressive loading also produces such high elasticity with a modulus of elasticity equal to that in tension. However, unlike tension, the non–linearity in compression is characterised by yielding at the maximum compressive stress f_c with subsequent reduction in strength and increase in deformation as the wood crushes further. Short columns crush under this load, whereas long slender columns buckle.

Loading perpendicular to the grain produces a similar stress-strain relationship but with a lower modulus of elasticity and as such modulus of resilience and toughness. Splitting in tension occurs at very low stress as the material is pulled apart along the fibres which happen to be weaker planes. Also, it has higher ductility under compressive loading as the strains increase with fairly gradual increase in the load.

2.4.2 Steel at Ambient Temperature

Steel is one of the most widely used materials in construction. It is a man-made with iron being the main raw material used. It can be hot-rolled, cold-rolled or welded. It is employed in the construction of hybrid connections and manufacturing of connectors such as bolts and nails.

Tensile tests done on a coupon to analyze the material behavior of steel (Fig. 2.6) show that it exhibits an initial linear elastic behavior, followed by a yield plateau during which the strains increase at a constant stress value. Beyond this plateau, increase in stress results in an increase in deformation, a phenomenon known as strain hardening, until the ultimate stress value is reached. The material eventually fails in fracture. Usually the yield stress is used for design since the material would have undergone severe plastic deformation before the ultimate strength capacity is reached. As such, an assumption of elasto-plastic material behavior can be assumed especially when steel is used in the design of connections where we don't expect severe plastic deformations.

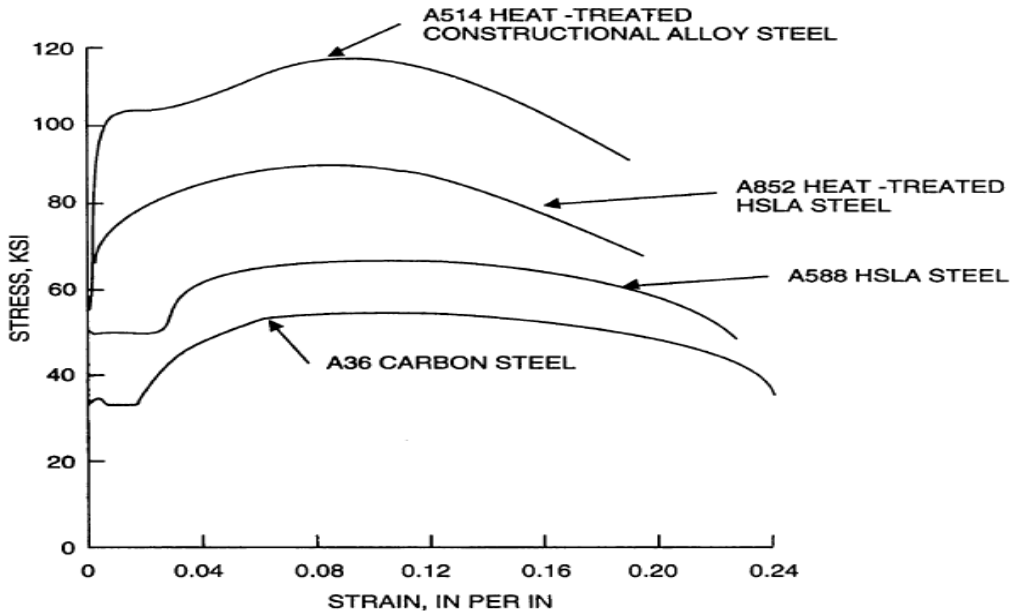

Figure 2.6 Typical Stress - Strain Curves for Structural Steel

2.4.3 Wood at elevated temperatures

Under exposure to a severe fire, materials go through physiochemical changes. Wood is not an exception, and the process involved is known as pyrolysis. Under severe heat, bound water stored in wood starts to evaporate at temperatures above 100°C. Part of the water vapor escapes through the cells to the outside while the remaining fraction travels to the less heated section of the wood, where it condenses. The heated section of the wood then starts to degrade thermally at temperatures ranging from 250°C to 300°C. In Canada, 288°C is the accepted temperature at which thermal degradation commences *(Buchanan, 2002).* The cross-section, and as such the density of wood starts to decrease at this temperature as the outer layer converts to char. The ratio of density of wood at room temperature to that at elevated temperature reduces to 0.9 at 200°C and then decreases significantly to about 0.2 at about 350°C *(Benichou et al., 2000)*. The layer of char formed, though structurally inactive, acts as a barrier protecting the unheated section of wood underneath. Beneath the char layer is the pyrolysis zone which contains wood just at the verge of undergoing thermal decomposition. In this zone, wood starts to decompose and release volatiles or combustion products to sustain the fire. The boundary between the char layer and the pyrolysis zone is known as the char base. Beneath the zone of pyrolysis lies unheated normal wood. This section of wood is at initial room temperature, and is protected by the layers of char above it.

2.4.3.1 Charring Rate of Wood

The charring rate of wood is an important parameter in defining the load capacity of a wood member exposed to elevated temperatures. The residual cross-section after charring is used to determine the reserve of capacity during and after exposure to extreme temperatures. It therefore serves as a guidance to structural engineers in estimating the capacity of wood members during

fire exposure. Moreover, it is used by fire investigators in establishing the duration and the effects of fires, and to some extent the causes of the fire. However there is limited scientific discussion on how it influences such investigations (*Maciulaitis et al., 2005*). NFPA 921 even goes ahead to state that "The investigator is cautioned that no specific time of burning can be determined based solely on the depth of char." Nonetheless, there is a lot of discussion on how to measure charring depth and draw significant conclusions such as the onset of a fire, which could be of help to fire investigators.

Theoretically, a linear relationship is assumed to exist between the charring depth and the time of exposure to elevated temperatures of a standard fire. The charring rate of wood is defined as the ratio of the charring depth to the exposure time. The charring depth which refers to the depth from the exposed surface of wood to the char front is assumed uniform over the entire section of the wood. The charring rate of wood in a standard fire is predictable, depending on the density and the moisture content of the wood *(Buchanan, 2002).* As shown in Figure 2.7, the charring rate of wood decreases with increase in density for all moisture contents measured. The dryer the sample, the higher the rate of charring as less heat energy is spent in evaporating bound water at 100°C before thermal degradation and pyrolysis commence. As it can be seen, this difference is not that profound.

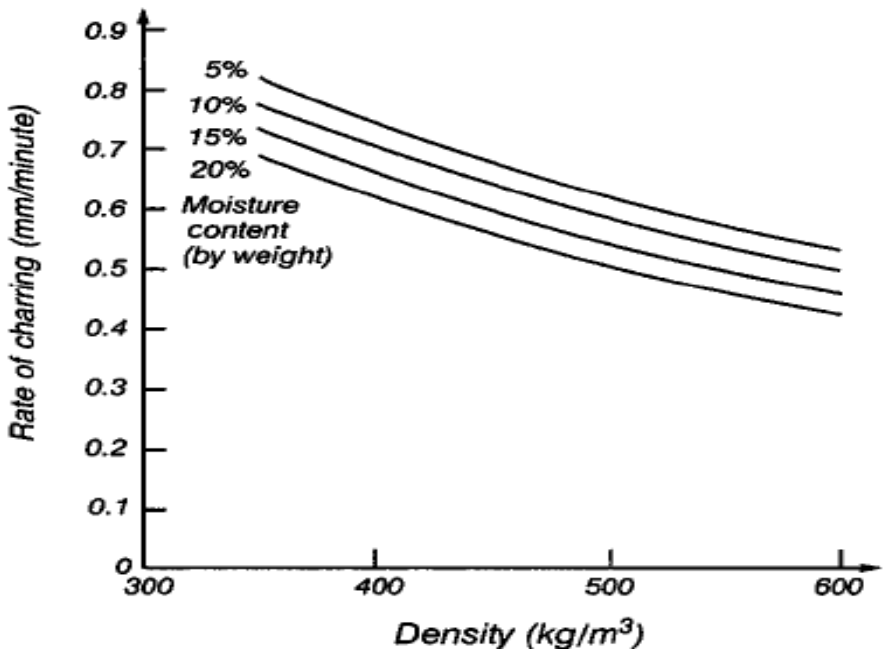

Figure 2.7 Effect of density and moisture content on charring rate of wood as reported by Lie, 1972

For solid beams and columns, a constant charring rate (Fig. 2.8) ranging from 0.5 to 0.8 mm/min is specified based on tests run in a fire resistance test furnace (*Babrauskas, 2004*). The New Zealand code (*SNZ, 1993*) gives a notional charring rate of β = 0.65 mm/min. In the Eurocode 5 (EC5, 2004), a notional charring rate of β = 0.65 mm/min is given for softwoods, and β = 0.50 mm/min and 0.65 mm/min is given for hardwood with densities greater than 450 kg/m^3 and 290 kg/m^3 respectively. The charring rates increase by approximately 10% if the effect of corner rounding is considered. In Australia, a charring rate as a function of the density and moisture content of wood is presented by the code (SAA, 1990 (b)), and is given by the equation;

$$\beta = 0.4 + (280/\rho)^2 \qquad \textbf{Equation 2.3}$$

Where ρ is the wood density in kg/m^3.

In North America, the proposed charring rate is given by recommendations by AFPA (1999) (Fig. 2.8) as

$\beta = 2.58\beta_n/t^{0.187}$ **Equation 2.4**

where β_n is the nominal charring rate after 1 hour fire exposure. The recommended value for β_n is 0.635 mm/min for glulam and solid wood.

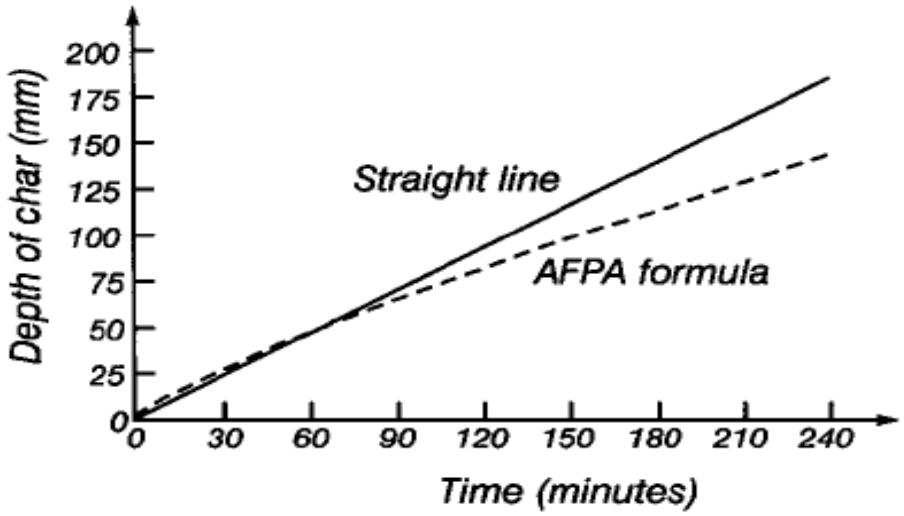

Figure 2.8 Charring rate from North American Recommendations (Buchanan, 2002)

Annex A of Eurocode 5 (1995-1-2) addresses the charring rates of wood under exposure to real or parametric fires. The relationship between the charring rate and the exposure time is represented in Figure 2.9 below;

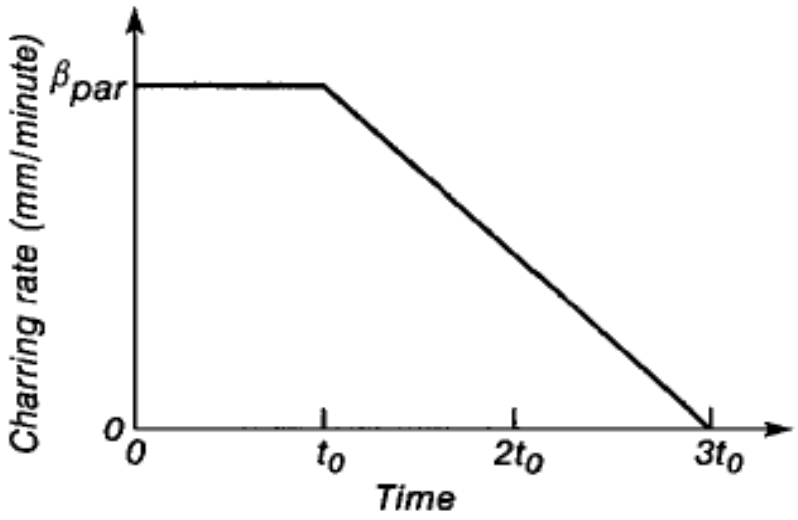

Figure 2.9 Charring rate with time for parametric fire exposure (Buchanan, 2002)

The initial charring rate is assumed constant over a period of time t_o during the incipient heating phase. It then decreases linearly to zero after a time $2t_o$ has elapsed.

The initial charring rate β_{par} is given as a function of a certain parametric char factor k_p and the notional char rate β_n.

$$\beta_{par} = k_p \beta_n \qquad \textbf{Equation 2.5}$$

$$k_p = 1.5(5F_v - 0.04)/(4F_v + 0.08)$$

$$F_v = (A_v/A_t)\sqrt{H_v} \ \textit{is the opening factor}$$

The initial char time t_o is given as

$$t_o = 0.006 e_t / F_v \qquad \textbf{Equation 2.6}$$

Where e_t is the design fire load density in MJ/m^2 of the bounded internal surface area of the fire room. Also the total char depth, c at the end of the exposure is given as

$$c = 2\beta_{par} t_o \qquad \textbf{Equation 2.7}$$

It is however important to note that though provisions are made for the calculation of the charring rate under parametric fires, the thermal and mechanical properties employed still remain functions of the standard fire exposure (*Lange et al., 2014*) without considering the effects of the cooling phase. Tests however have shown that burning of wood specimens progresses to a significant extent even in the cooling phase till subsequent failure (*Konig, 2006*).

2.4.3.2 Thermal Properties of Wood

Strength calculations for wood are based on the properties of the unheated core. As such thermal properties are not really significant in predicting its strength ***(****Purkiss, 2007****)***. However a knowledge of its thermal properties, mainly thermal conductivity, specific heat and density is

needed to understand and model their interaction with fire. They are also required as input parameters when finite element numerical methods are employed in validating experimental projects.

Thermal conductivity is a quantitative measure of the ability of a material to conduct heat. Materials with high thermal conductivity allow heat transfer through them at a faster rate as compared to those with low thermal conductivity. Its unit of measurement is given as Watts per meter Kelvin (W/m.k). Wood in general has a lower thermal conductivity value than most construction materials. A lot of research on the thermal conductivity of wood has been undertaken by various scholars and researchers. It has been shown that the thermal conductivity of wood varies significantly (*Zi-Tao et al., 2011)*, and is mainly dependent on the wood type, its density and moisture content, as well as temperature and the test method employed (Fig. 2.10). Thermal conductivity of wood is shown to increase with increase in density. Tao et al. (2011) in his experiment to measure the conductivity of wood species in China, presented the result below which shows the variation of the thermal conductivity of ovendry wood with density at a constant temperature of 30°C. In his experiment, ovendry samples were obtained by dry heating the samples at 105°C to drive out most of the bound water till a constant mass was achieved. At this temperature, the density of the wood is reduced to about 90% of its original value *(Buchanan, 2002)*.

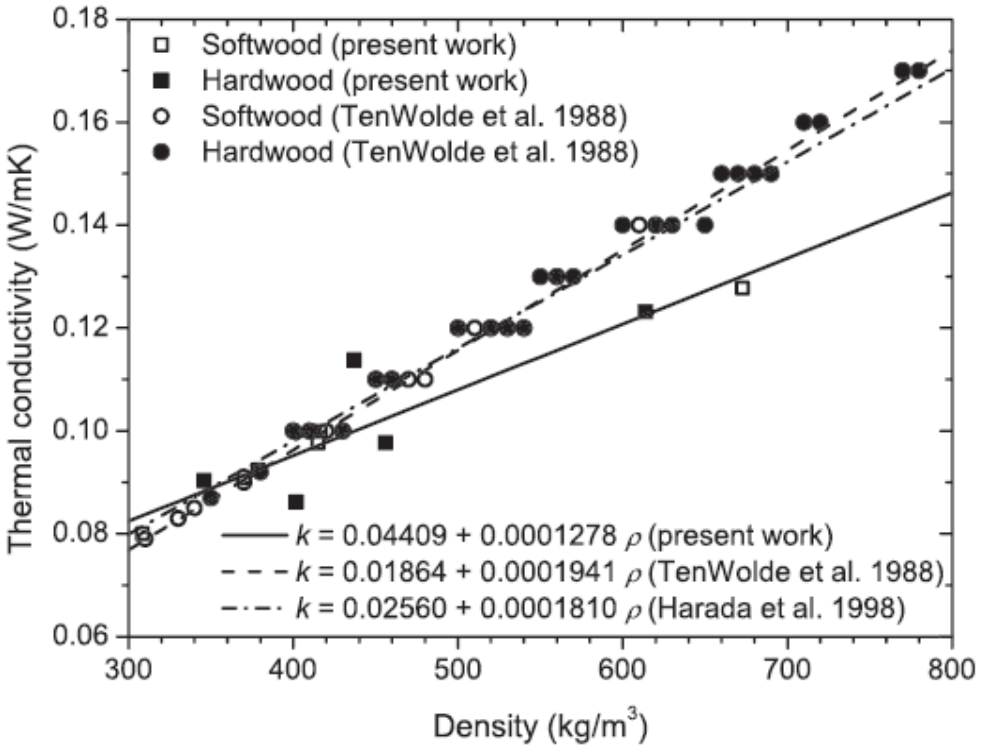

Figure 2.10 Transverse thermal conductivity of wood at 30°C as a function of oven-dry density (Zi Tao et al., 2011)

As wood decomposes to char at temperatures above 300°C, its density reduces to about 20% of its original value. The layer of char formed has even lower thermal conductivity and acts as insulation thereby reducing heat transfer to the unburnt layer underneath. This reduced thermal conductivity persists till fissures and shrinkage cracks appear in the char layer at temperatures above 500°C, initiating an increase in the rate at which heat transfers to the unburnt section of wood ***(EC5, 2004)***. For standard fire exposure, Eurocode gives the variation of thermal conductivity with temperature as shown below (Fig. 2.11).

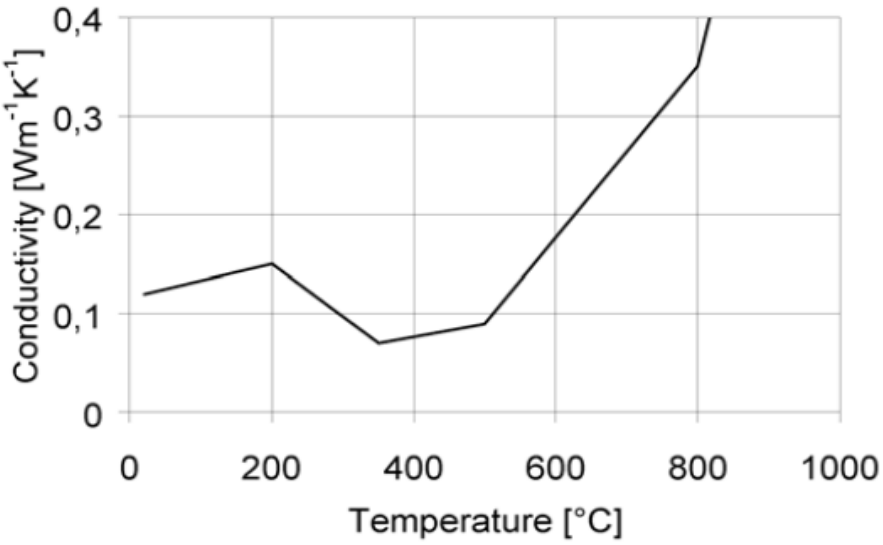

Figure 2.11 Temperature - thermal conductivity relationship for wood and the char layer (EC5, 2004)

Specific Heat (KJ/kg. K) is a measure of the amount of heat energy required to increase the temperature of 1 kg of an object by 1 K. The variation of specific heat of wood with temperature is presented in the figure below obtained from Eurocode 5.

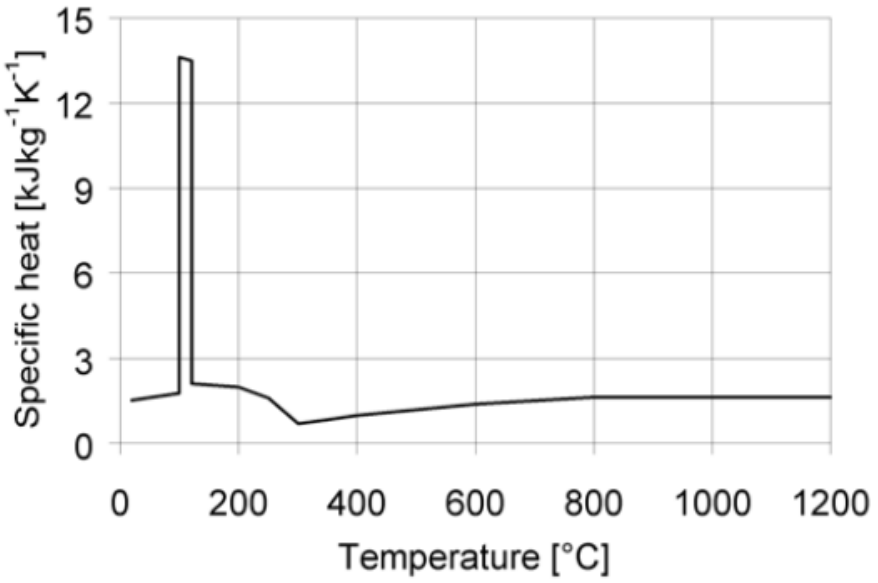

Figure 2.12 Variation of specific heat of wood with temperature (EC5 (2004))

As seen in Figure 2.12, the spike represents the higher amount of energy utilised to drive out bound and free water in the wood at temperatures slightly above 100°C, before further increment in temperature of wood ***(Buchanan, 2002)***. As wood becomes dry, relatively lower energy is required to raise its temperature.

The density of wood decreases as temperature increases resulting in evaporation of bound moisture, and thermal decomposition of the wood material. The density ratio of wood as a function of temperature is presented in Figure 2.13 below.

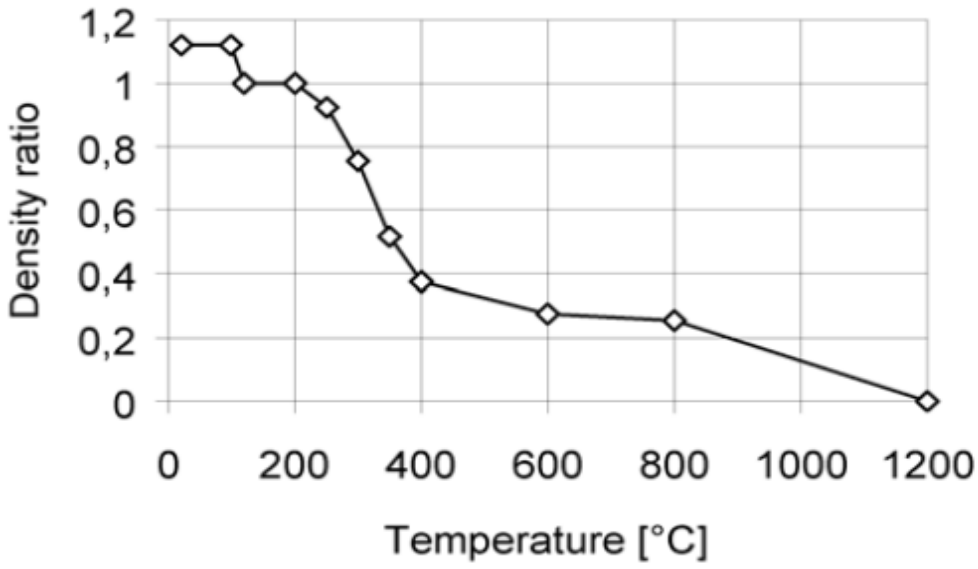

Figure 2.13 Temperature - density ratio relationship for softwood with an initial moisture content of 12% (EC5, 2004)

The ratio of the density of wood at elevated temperatures to that at ambient is referred to as the density ratio. The density ratio reduces to approximately 1 as moisture is evaporated at temperatures beyond 100°C. It then undergoes significant drop to 0.38 as thermal decomposition begins at temperatures beyond 350°C.

2.4.3.3 Mechanical Properties of Wood

The mechanical properties of wood are temperature dependent. Owing to the reduction of cross-section of wood in fires, its capacity can significantly reduce and ultimately affect its fire performance.

Gerhards (1982) in his research on the modulus of elasticity of wood perpendicular to grain reported a scatter for temperatures below 100°C. This variability becomes prominent as the temperature increases from ambient to about 100°C. As temperature approaches 100°C, bound water is lost, and moist wood starts to lose most of its stiffness. In general, it was reported by Gerhards (1982) that the strength of wood increases with decrease in temperature as is evident in the below figure (Fig. 2.14). Timber with higher moisture content exhibits higher variability and relatively lower stiffness with increase in temperature (*Drake et al., 2015*).

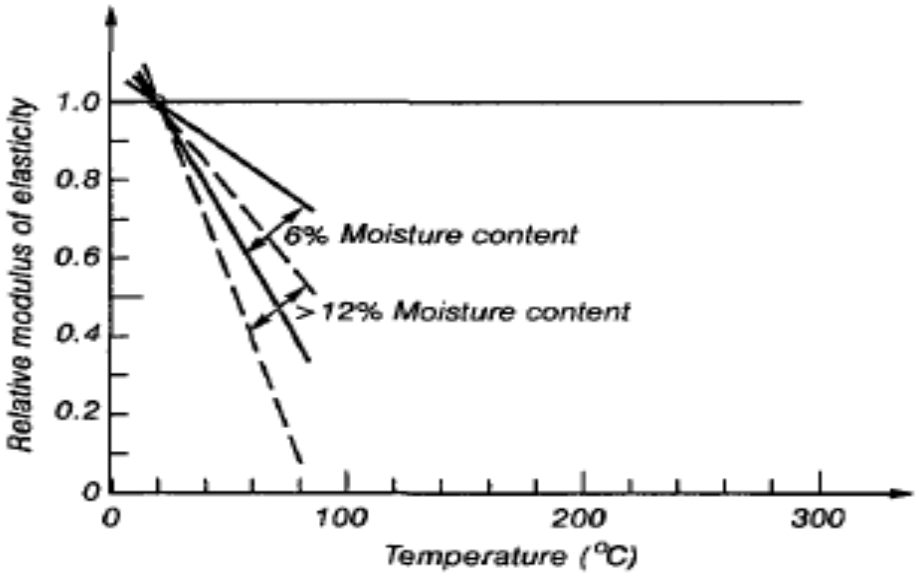

Figure 2.14 Effect of temperature on modulus of elasticity perpendicular to grain (Buchanan, 2002)

The effect of elevated temperatures on the tensile and compressive strength of wood perpendicular to grain follows a similar trend to the effects on stiffness. They show a scatter from ambient

conditions to temperatures in the 100°C vicinity. Generally the tensile and compressive strength reduces with the increase in temperature with a higher reduction for higher moisture content specimens (Fig. 2.15).

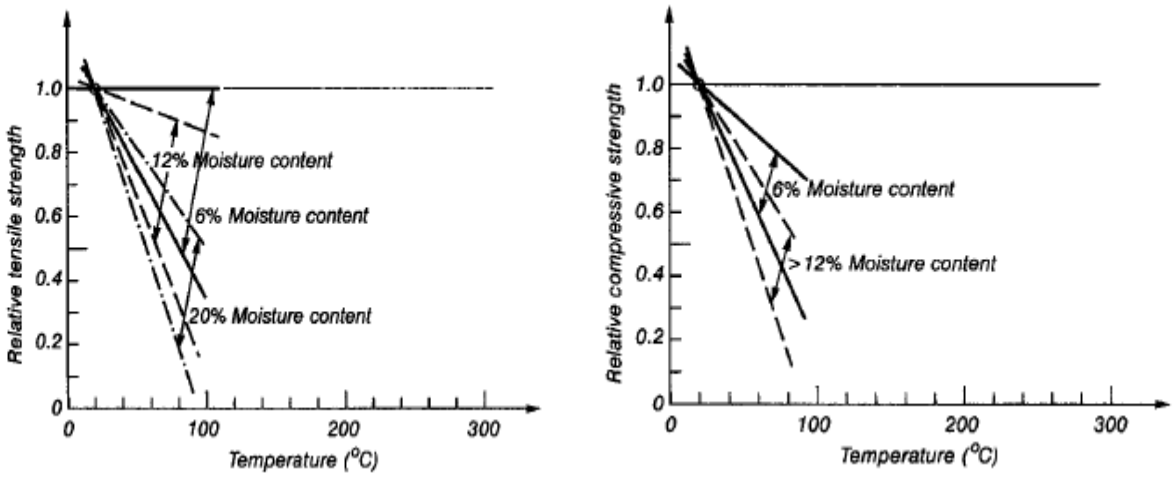

Figure 2.15 Effect of temperature on the tensile and compressive strengths of wood (Buchanan, 2002)

Temperatures of interest in wood ranges from ambient (20°C) to 300°C as wood goes through the process of losing bound water (100°C), pyrolysing (200°C) and finally losing strength in the char layer (280 - 300°C). In Figure 2.16 below, Buchanan (2002) discusses the assumed effect of temperature on the mechanical properties of glue laminated beams. The modulus of elasticity drops linearly to 50% of its ambient value at 300°C. The tensile strength follows a similar trend to 200°C after which the gradient changes reaching zero strength at 300°C. The reduction factors for the modulus of elasticity and tensile strength apply to both wet and dry specimens. Under compression, dry specimens' strength reduce linearly to zero at 300°C. The compressive strength of wet specimens however drops to 50% of the ambient value at 100°C and exhibits the same strength value up to 160°C before it finally reduces linearly to zero strength at 300°C.

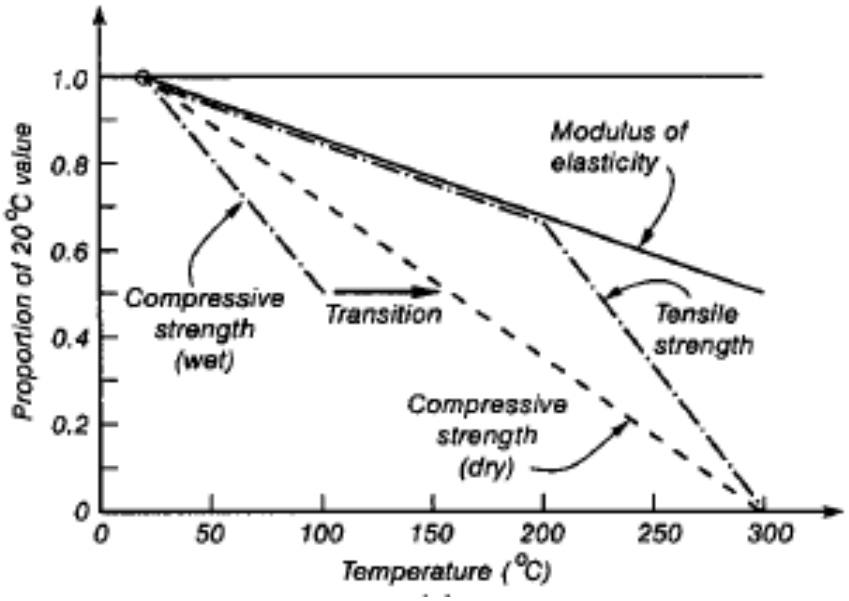

Figure 2.16 Effect of temperature on mechanical properties of wood (Buchanan, 2002)

Gerhards (1982) also reported summaries on the shear modulus and strength of wood. Shear failure in wood is characterised by longitudinal split along the grain structure. Increase in temperature results in reduction of the shear strength of wood (Fig. 2.17) with a rapid drop in wet woods at 150°C.

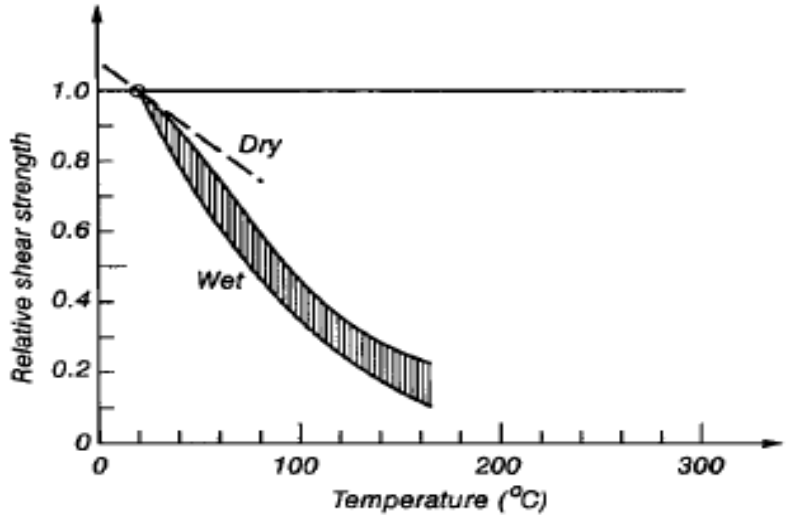

Figure 2.17 Effect of temperature on shear strength of wood (Buchanan 2002)

Gerhards reported a reduction in the shear modulus by 0.2 to 0.5 of the ambient values at temperatures above 80°C.

2.4.4 Steel at Elevated Temperatures

Steel structures are very sensitive to extreme temperatures due to their higher conductivity and ability to store heat. They undergo various changes in the crystalline structure under exposure to high temperatures leading to significant reduction in stiffness and strength, and increased deformations. Owing to the reduced size of steel structures, they usually underperform in fire compared to their neighbouring concrete and wood structures.

The effect of temperature on the thermal and mechanical properties of steel as a structural material with regards to information from Eurocode 3 (1995) is considered under this section.

2.4.4.1 Thermal Properties

Understanding of the thermal properties of steel are required prior to its usage in construction of fire-exposed structures. Changes in its thermal properties significantly affect the heat transfer and temperature profile within the member. The density of steel may be assumed constant (7850 kg/m^3) with temperature (*Eurocode 3, 1995*).

As shown in Figure 2.18, the specific heat of steel varies with temperature. The sudden rise is as a result of the metallurgical changes at 730°C.

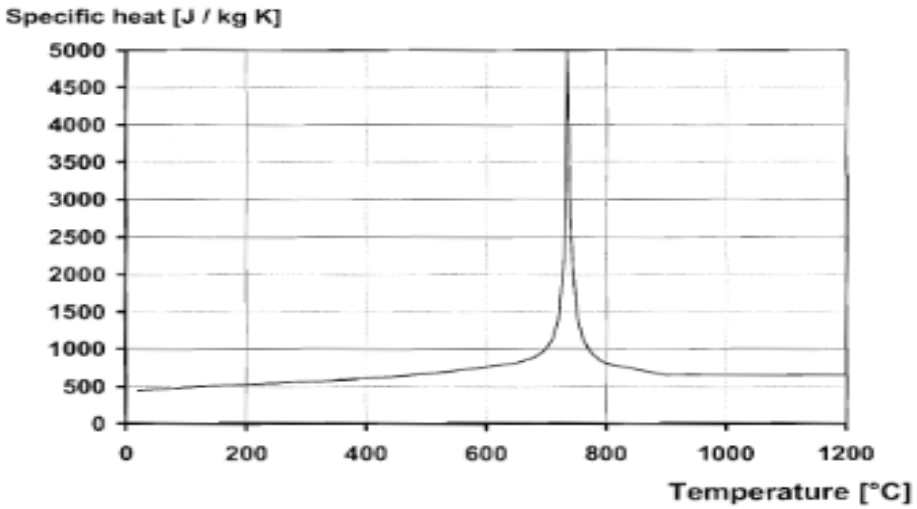

Figure 2.18 Specific heat of steel as a function of temperature (EC3, 1995)

For simple calculations, a constant value of 600 J/kg K can be assumed for all temperatures. However for more accurate predictions, the equations below from Eurocode 3, as functions of temperature (T °C) can be utilised in estimating the specific heat.

$$c_p = 425 + 0.773T - 1.69 \times 10^{-3}T^2 + 2.22 \times 10^{-6}T^3 \qquad 20℃ \leq T < 600℃ \qquad \textbf{Equation 2.8}$$

$$= 666 + \frac{13002}{738 - T} \qquad 600℃ \leq T < 735℃$$

$$= 545 + \frac{17820}{T - 731} \qquad 735℃ \leq T < 900℃$$

$$= 650 \qquad 900℃ \leq T \leq 1200℃$$

A bilinear relationship exists between the thermal conductivity of steel and temperature as shown in Figure 2.19. Thermal conductivity of steel decreases linearly from 54 W/m K at ambient temperature to 27.3 W/m K at 800°C, beyond which it remains steady (*Eurocode 3, 1995*).

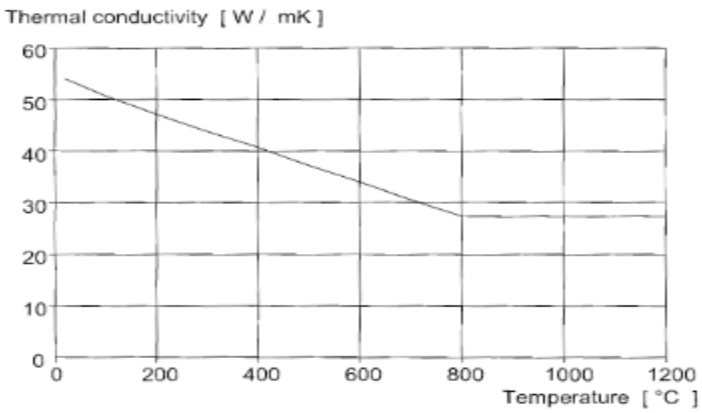

Figure 2.19 Thermal conductivity of steel as a function of temperature (EC3, 1995)

The governing equations are given as;

$$\lambda = 54 - 0.0333T \qquad 20℃ \leq T < 800℃ \qquad \textbf{Equation 2.9}$$

$$= 27.3 \qquad 800℃ \leq T \leq 1200℃$$

For simple calculations, a constant value of 45 W/m K may be assumed.

2.4.4.2 Mechanical Properties of Steel

The mechanical properties of steel degrade with the increase in temperature as shown below (Fig. 2.20) for a typical hot-rolled steel.

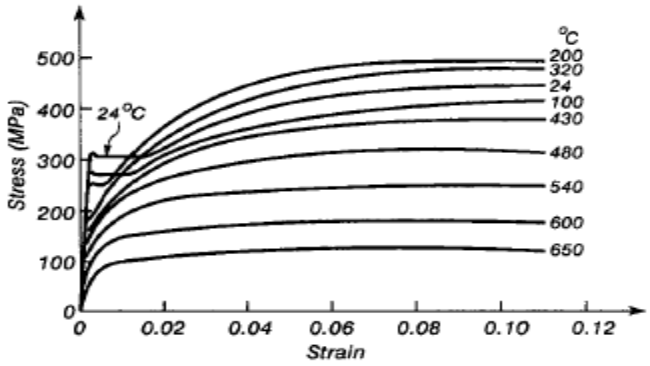

Figure 2.20 Stress-strain curve for typical hot-rolled steel at elevated temperatures (Buchanan, 2002)

Increase in temperature reduces the yield strength of steel. However, the ultimate strength increases slightly at moderate temperatures before starting to decrease at higher temperatures (*Buchanan, 2002*).

To account for the reduction in stiffness of steel with increasing temperature, Eurocode 3 provides the reduction factors shown in Figure 2.21 below.

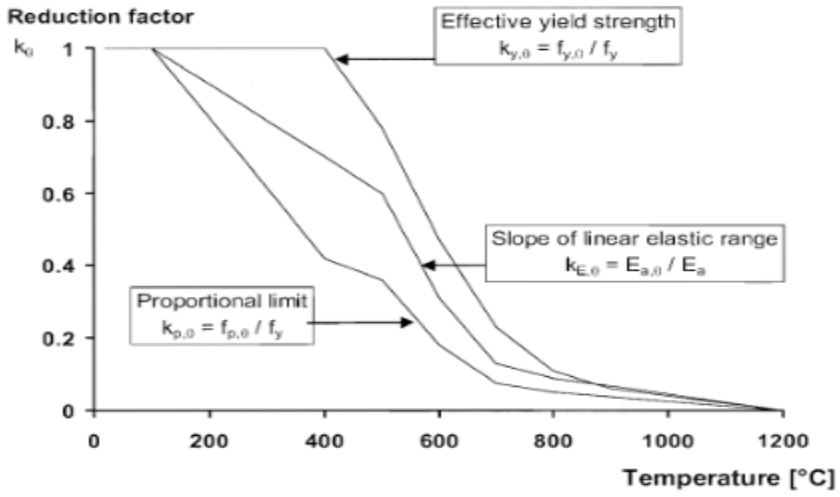

Figure 2.21 Reduction in yield strength and modulus of elasticity with temperature (Eurocode 3, 1995)

The stress-strain relationship of steel at elevated temperatures (Fig 2.22) is estimated by the set of equations below according to Eurocode 3 (1995).

$$\sigma = \varepsilon E_{a,T} \quad for\ \varepsilon \le \varepsilon_{p,T} \qquad \textbf{Equation 2.10}$$

$$= f_{p,T} - c + \left(\frac{b}{a}\right)\left[a^2 - \left(\varepsilon_{y,T} - \varepsilon\right)^2\right]^{0.5} \qquad for\ \varepsilon_{p,T} < \varepsilon < \varepsilon_{y,T}$$

$$= f_{y,T} \qquad for\ \varepsilon_{y,T} \le \varepsilon \le \varepsilon_{t,T}$$

$$= f_{y,T}\left[1 - \frac{\left(\varepsilon - \varepsilon_{t,T}\right)}{\left(\varepsilon_{u,T} - \varepsilon_{t,T}\right)}\right] \qquad for\ \varepsilon_{t,T} < \varepsilon < \varepsilon_{u,T}$$

$$= 0.00 \qquad for\ \varepsilon = \varepsilon_{u,T}$$

where $f_{y,T}$ is the effective yield strength, $f_{p,T}$ is the proportional limit, $E_{a,T}$ is the slope of the linear elastic range, $\varepsilon_{p,T}$ is the strain at the proportional limit, $\varepsilon_{y,T}$ is the yield strain, $\varepsilon_{t,T}$ is the limiting strain for yield strength, $\varepsilon_{u,T}$ is the ultimate strain, and the parameters are expressed as;

$$\varepsilon_{p,T} = \frac{f_{p,T}}{E_{a,T}}$$

$$\varepsilon_{y,T} = 0.02$$

$$\varepsilon_{t,T} = 0.15$$

$$\varepsilon_{u,T} = 0.20$$

$$a^2 = (\varepsilon_{y,T} - \varepsilon_{p,T})\left(\varepsilon_{y,T} - \varepsilon_{p,T} + \frac{c}{E_{a,T}}\right)$$

$$b^2 = c(\varepsilon_{y,T} - \varepsilon_{p,T})E_{a,T} + c^2$$

$$c = \frac{(f_{y,T} - f_{p,T})^2}{(\varepsilon_{y,T} - \varepsilon_{p,T})E_{a,T} - 2(f_{y,T} - f_{p,T})}$$

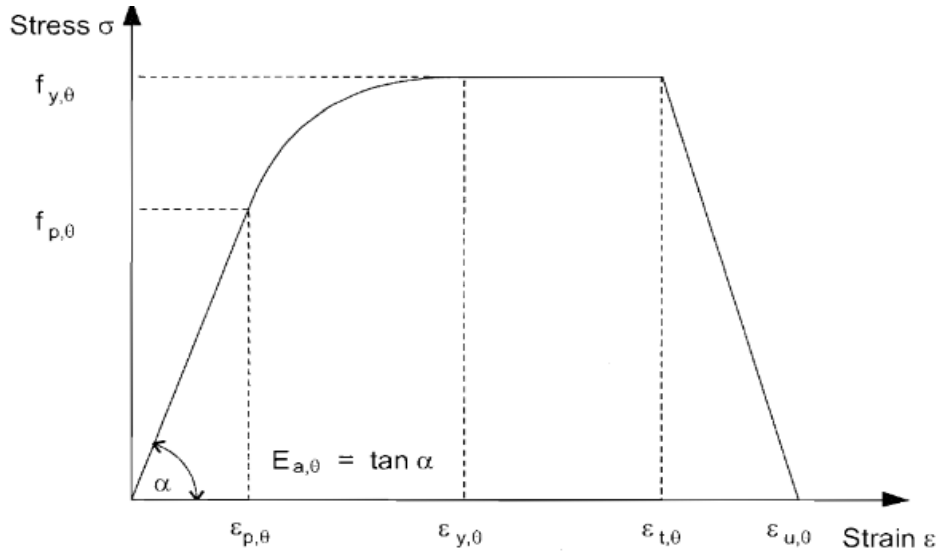

Figure 2.22 Stress-strain relationship for carbon steel at elevated temperatures (Eurocode 3, 1995)

2.5 Review of Pertinent Literature to Connections

Fire Design of steel-to-timber dowelled connections (2010)

Authors: Erchinger C, Frangi A, and Fontana M.

In this research, the authors sought to design a model for the calculation of the fire resistance of multiple shear steel-to-timber dowelled connections with slotted in steel plates under a tensile load through experimental and numerical analysis. To achieve this, 25 ambient tests to determine the load carrying capacity, and 18 fire tests under constant tension load with exposure to the ISO fire curve (*ISO 834, 1999)* were conducted in a horizontal furnace at the Swiss Laboratories for Materials Testing and Research (Empa) in Duebendorf.

The cross-sectional dimension of the timber beam tested was 200 mm x 200 mm (strength class GL24h) with two or three slotted in steel plates of thickness 5 mm and steel dowels. The main variables were as listed below;

- Load ratio (30%, 15% and 7.5% of the average measured load carrying capacity of five tensile tests at ambient)
- Dowel diameter (6.3 mm and 12 mm)
- Number and configuration of the steel dowels
- Thickness of the timber side members

Details of the tested specimens and setup is provided in Table 2.1 and Figure 2.23.

Table 2.1 Overview of the test programme (Erchinger et al., 2010)

Test name	Number of tests	Type of test	Tensile load (kN)	Fire resistance (mean value) (min)	Remarks
D1.1	5	Ambient temp.	Until failure F_u	–	200 × 200 mm (GL24h), 3 steel plates, 2 × 9 steel dowels (6.3 mm); (see Fig. 1 (right))
	2	ISO-fire	$0.3 \cdot F_u = 145$	33.0	
	2	ISO-fire	$0.15 \cdot F_u = 72$	36.0	
	2	ISO-fire	$0.075 \cdot F_u = 36$	41.0	
D1.2	5	Ambient temp.	Until failure F_u	–	280 × 280 mm (GL24h), 3 steel plates, 2 × 9 steel dowels (6.3 mm)
	2	ISO-fire	$0.3 \cdot F_u = 173$	73.0	
D1.3	2	ISO-fire	$0.3 \cdot F_u = 145$	64.5	Same as D1.1; protection by three-layered timber boards (27 mm)
D1.4	2	ISO-fire	$0.3 \cdot F_u = 145$	60.5	Same as D1.1; protection by gypsum plasterboards (15/18 mm)
D2.1	5	Ambient temp.	Until failure F_u	–	200 × 200 mm (GL36h), 3 steel plates, 3 × 9 steel dowels (6.3 mm)
	2	ISO-fire	$0.3 \cdot F_u = 188$	31.0	
D3.1	5	Ambient temp.	Until failure F_u	–	200 × 200 mm (GL24h), 3 steel plates, 3 × 3 steel dowels (6.3 mm)
	2	ISO-fire	$0.3 \cdot F_u = 69$	32.5	
D4.1	5	Ambient l temp.	Until failure F_u	–	200 × 200 mm (GL24h), 2 steel plates, 2 × 4 steel dowels (12 mm)
	2	ISO-fire	$0.3 \cdot F_u = 124$	34.5	

Figure 2.23 Fire Test Arrangement (Erchinger et al, 2010)

After the series of fire tests, it was observed that all connections achieved a fire resistance rating of thirty minutes or more. A change in the number and diameter of dowels resulted in no significant increase in the fire resistance as seen in results from Connections D2.1, D3.1 and D4.1 (Table 2.1). Moreover, reduction of the load level unusually led to no significant increase in the fire resistance. Increase in fire resistance was observed when the thickness of the side members and end distance of the dowels were increased. This delayed transfer of heat flux from dowels to the outer surface thereby reducing the char rate of the outer layer and rate of travel of the char front to the sections within. By ao doing, connection D 1.2 had an increased fire resistance rating of 70 min. It was also

observed that connections protected by three-layered 27 mm thick cross-laminated timber boards could withstand exposure for 60 min before failure. Failure of all specimens was characterised by enlargement of the dowel holes due to transfer of heat from the heated dowels into the layer of wood in the holes leading to loss of mass; a phenomenon referred to as embedment failure (Fig. 2.24).

Figure 2.24 Typical specimen after the fire characterised by embedment failure (Erchinger et al., 2010)

From the Finite Element (FE) Analysis, the mean value of the temperature of elements less than 300°C was calculated in order to come up with an equation for the load-carrying capacity of the connections in fire. Temperature of elements exceeding 300°C were ignored since such elements were assumed to have already charred and of zero embedment strength.

The authors came up with the equation below for estimating the load carrying capacity of multiple shear steel to timber dowelled connections.

$$R_{fi} = n_{tot} \cdot \sum_{i=1}^{n} \left(f_{h,i(\theta_{mean,i})} \cdot b_i \right) \cdot d \qquad \textbf{Equation 2.11}$$

Where

R_{fi} is the load carrying capacity of the connection in fire (N)

n_{tot} is the number of dowels in a connection

$\theta_{mean,i}$ is the mean temperature of element i (°C)

b_i is the width of element i (mm)

d is the diameter of the steel dowel (mm)

From the FE thermal analysis, it was also inferred that the charring of the side members is greatly influenced by the thickness of the side member. They concluded that a required minimum thickness of the side members of 35 mm is needed for a fire resistance rating between 30 and 60 min. Based on this, a simplified charring model based on the one dimensional charring rate ($\beta_0 = 0.65\ mm/min$) was established as follows:

$$d_{char,s} = \beta_0 \cdot t \ \ for\ 0 \leq t \leq 30\ min \qquad \textbf{Equation 2.12}$$

$$d_{char,s} = \beta_0 \cdot 30 + 1.5 \cdot \beta_0 \cdot (t - 30) for\ 30 \leq t \leq 60\ min \qquad \textbf{Equation 2.13}$$

The increased charring rate of $1.5\beta_0$ in the second phase is as a result of the heat flux from the steel influencing charring after almost 30 min exposure.

The top/bottom charring was also calculated assuming an increased charring rate of $1.1\beta_0$ throughout the time of exposure to a fire duration of 60 min.

$$d_{char,o} = 1.1 \cdot \beta_0 \cdot t \ \ for\ 0 \leq t \leq 60\ min \qquad \textbf{Equation 2.14}$$

It was concluded that the load carrying capacity of multiple shear steel to timber dowelled connections is a factor of the charring of the timber side members and temperature distribution within the residual cross-section.

Structural Fire Design of Timber Structures According to Eurocode 5 (2005)

Author: Jurgen Konig

The author in this paper presented an overview of Eurocode 5 (2004) dealing with structural fire design of timber structures. In this review, rubrics and guidance on the design of timber beams from the Eurocode 5 was looked at. In general, two main strategies can be employed in satisfying the requirement for safety in fire as required by the Construction Products Directive. These are;

- Application of nominal fire scenarios such as the Standard Fire Scenarios (ASTM E119 or CAN/ULC S-101)
- Application of natural fire scenarios such as parametric fire curves.

Provisions made in Eurocode 5 (2004) apply to design of timber members exposed to standard fires.

The requirements of design are spread over the three main failure criteria of Stability, Integrity and Insulation. To satisfy the stability criterion, the structure must serve its load bearing purpose without collapse throughout the complete duration of the fire. The insulation criteria allow a maximum increase in temperature of 180K and a total average temperature of 140K on the unexposed side of a member under standard fire exposure. It however allows a maximum increase of 200K and an average of 240K in the decay phase of natural fires.

The design strength of timber in fire, $f_{d,fi}$ is given as a factor of the 20% fractile of the cold strength properties, f_{20} which is in turn a factor of the characteristic strength property, f_k (5% fractile). Based on these two factors, the design strength in fire is given as;

$$f_{d,fi} = k_{mod,fi}\frac{f_{20}}{\gamma_{M,fi}} \ , \ where\ f_{20} = \ k_{fi}f_k \qquad \textbf{Equation 2.15}$$

k_{fi} is a factor dependent on the coefficient of variation of the material. It is given as 1.15 for glulam members. $k_{mod,fi}$ is a modification factor which accounts for the reduction in strength properties of sections below the char layer. $\gamma_{M,fi}$ is a partial factor of safety chosen as unity in fire designs.

Verification methods of strength and performance involve either a global analysis of the entire structure and assembly, or one – member analysis which involves performing full scale fire tests to ascertain performance of individual members. For timber members' performance in fire, member analysis alone is enough for verification purposes. Timber chars from the outer surface and loses mass upon heating without elongating. As such, even when involved in other structural members, it offers negligible impact to their structural stability in fire. A global analysis of the entire structural system will be required only when very detailed and accurate results are a necessity.

In order to determine the reduced cross-section of a timber member after exposure to extreme temperatures, the char rate and depth must be estimated. This can be done experimentally by a more accurate method of laser scanning, or by a commonly used measurement method. Laser scanning offers the advantage of producing 3D models of the residual timber members (*Erchinger et al., 2010*). Theoretically, these two parameters can be found from provisions in the Eurocode. The author defined charring as the dominating effect of a fire exposure on the mechanical resistance of timber members. In Eurocode 5 (2004), the one-dimensional charring rate β_0 defined as the charring rate as seen under exposure of a semi-infinite slab to one dimensional heat transfer is chosen as the basic value. When the one dimensional charring rate is used in evaluating the residual strength, then effect of corner rounding must be accounted for in estimating the residual properties. A simpler approach however is to use the notional charring rate β_n which implicitly accounts for the effect of corner rounding.

Eurocode 5 (2004) provides two alternative methods for finding the residual cross-section properties of timber beams and columns. These are the *reduced cross-section method* and the *reduced properties method*. The *reduced cross-section method* takes into account loss of strength in the heat affected layers just beneath the pyrolysis zone. It does so by reducing the residual cross-section by an extra 7 mm. It is the most recommended method.

The *reduced properties method* however introduces a factor $k_{mod,fi}$ for compressive, tensile and bending strength to account for the loss of strength in the heat affected zones. It comes with some disadvantages as listed below;

- There are no modification factors for shear strength
- Method cannot be verified using advanced methods
- Method applies to only three and four – sided exposure, and cannot be employed for slabs.

Provisions for the design of connections are also made for laterally loaded symmetrical three-member connections in shear, connections with screws and axially loaded fasteners. Unprotected connections designed to comply with code requirements at ambient conditions are sure to meet fire resistance durations of 15 minutes for nails, screws and bolts or 20 minutes for dowels. With the exception of bolted connections, fire resistance rating of 30 minutes is achieved only by increasing the thickness of the side members and of course the length of the fasteners. To achieve a fire rating of 60 minutes, all connections must be protected with gypsum board, wood-based panels or any heat resisting layer. Reducing the load ratio will also increase the fire rating of the connections.

The author also recognized provisions made in the Eurocode for advanced calculation methods involving the use of finite element methods for the structural and thermal analysis, evaluation and verification of timber structures. Provisions are given for the effective thermal properties of timber

as functions of char. These properties are however not recommended for exposures other than the standard fires.

To conclude, he established the importance of the Eurocode 5 in the design of safe timber structures for fire without tests, despite the gaps in knowledge.

Charring rates and temperature profiles of wood sections (2003)

Authors: Frangi A. and Fontana M.

In this experimental research, a series of glued-laminated timber beams and slabs made of nailed timber planks or hollow core timber elements were tested under standard fire exposure. The beams and slabs were subjected to three sided and one sided exposure respectively. The authors sought to evaluate the global structural behavior of timber in terms of measuring and analysing the charring depth and temperature distributions at different locations in the sections.

Statistical data of the specimens tested are produced in Tables 2.2 and 2.3 below;

Table 2.2 Statistical values of the measured density r_w and moisture content w for the timber specimens tested under the Standard Fire (Frangi and Fontana, 2003)

Specimen	Parameter	n	$\bar{x}$	s	v
Solid timber beams	r_w (kg/m^3)	28	378	13	0.03
	w (%)	28	13	1	0.10
Glued laminated timber beams	r_w (kg/m^3)	12	453	22	0.05
	w (%)	12	13	2	0.12
Timber planks	r_w (kg/m^3)	122	425	37	0.09
	w (%)	122	13	1	0.07
Hollow core timber members	r_w (kg/m^3)	—	450	—	—
	w (%)	28	10	2	0.18
All	r_w (kg/m^3)	162	419	39	0.09
	w (%)	190	13	2	0.14

n – *the number of elements* $\bar{x}$ – *mean value* s – *standard deviation* v – *coefficient of variation*

Table 2.3 Statistical values of the measured charring rates for the timber specimens tested under the standard fire exposure (Frangi and Fontana, 2003)

Specimen	Charring rate	n_1	n_2	$\bar{x}$	s	v
Solid timber beams	β_s (mm/min)	14	83	0.67	0.07	0.11
Glued-laminated timber beams	β_s (mm/min)	10	72	0.70	0.05	0.07
Nail-laminated timber planks	β_u (mm/min)	90	180	0.70	0.07	0.10
Hollow core timber members	β_u (mm/min)	25	25	0.67	0.06	0.08
All	β (mm/min)	139	360	0.69	0.07	0.10

$n_1 - the\ number\ of\ timber\ members\ \ n_2 - number\ of\ measurements$

For the members exposed on three sides, charring was measured from either the side β_s or from the underside of the cross-section β_u as shown in the figure below (Fig. 2.25);

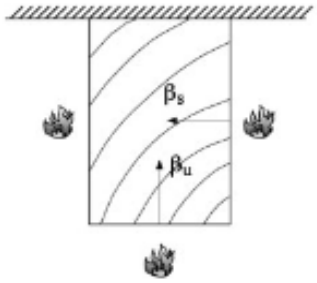

Figure 2.25 Timber member exposed to the ISO fire on three sides (Frangi and Fontana, 2003)

It was observed from the normal probability curves (Fig. 2.26) plotted by the authors that an assumption of a normal probability distribution of the charring rate is valid for the members tested. The measured charring rates in the range of 0.67 to 0.70 mm/min compared well with other fire tests.

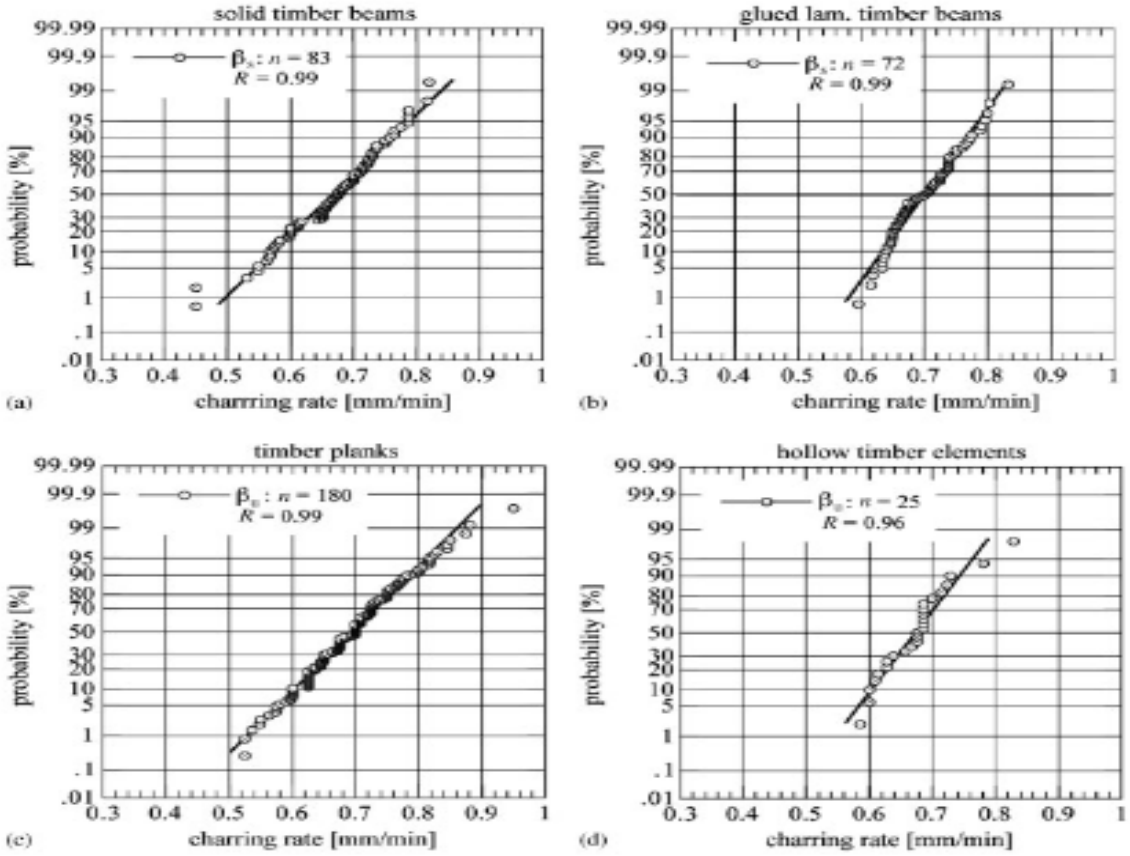

Figure 2.26 Measured charring rates for different types of timber specimens (Frangi and Fontana, 2003)

Measured mean values of the charring depth as functions of the failure time also revealed that a constant charring rate may be assumed for fire durations between 30 and 120 min under the ISO fire curve (Fig. 2.27).

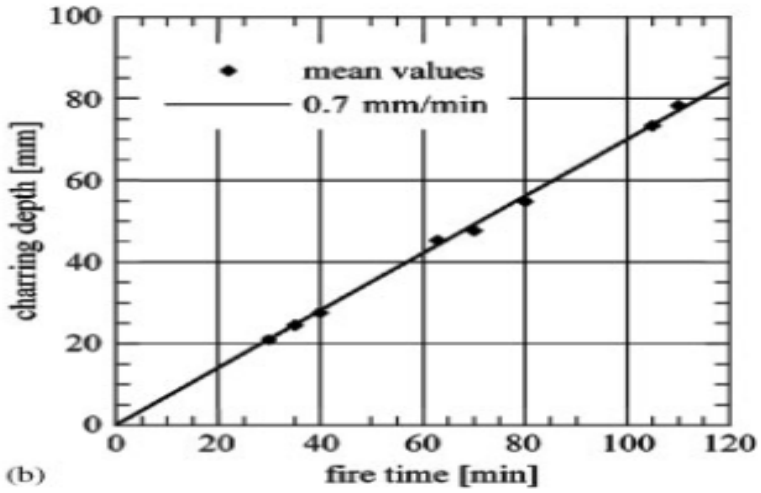

Figure 2.27 Measured charring depth as a function of time (Frangi and Fontana, 2003)

It was also observed that charring rates measured from the underside of the beam remained similar to that measured from the sides as long as the width of the residual cross-section is larger than 60 mm. Smaller residual sections between 40 and 60 mm had relatively higher charring rates measured from the underside of the beams (Fig. 2.26 (b)).

It was then concluded that a constant charring rate can be assumed for all sides exposed to the fire if the width of the unburnt cross-section exceeds a certain minimum value, $b_{o,min.}$ This value may be found for different values of the critical width of the residual cross-section $b_{fi,min}$ using a charring rate of 0.7 mm/min (Fig. 2.28 (b)).

The authors could not find any relationship between the charring rate of timber and density, as well as that between charring rate and moisture content of specimens (Fig. 2.29 (a) and (b)).

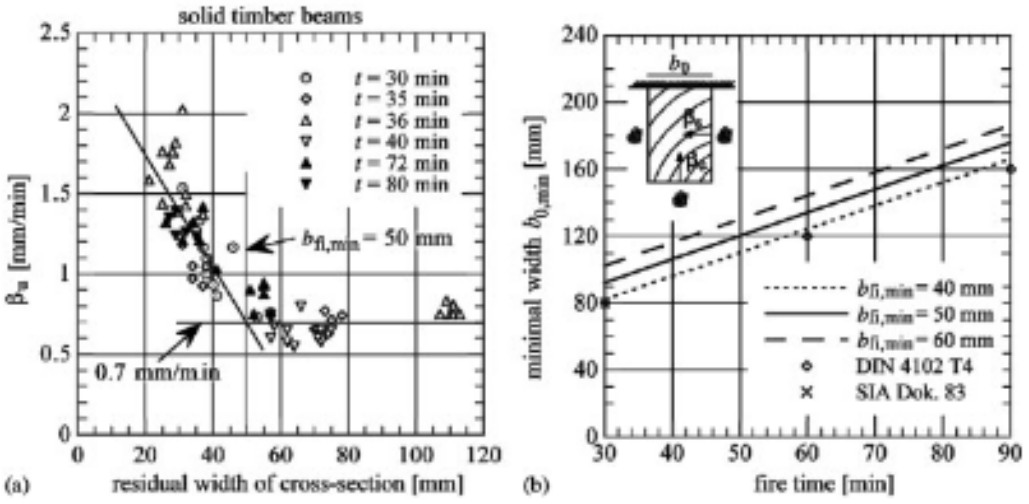

Figure 2.28 (a) Measured charring rates as a function of the residual width of the cross-section; (b) calculated and recommended minimum width of the cross-section as a function of the fire time (Frangi and Fontana, 2003)

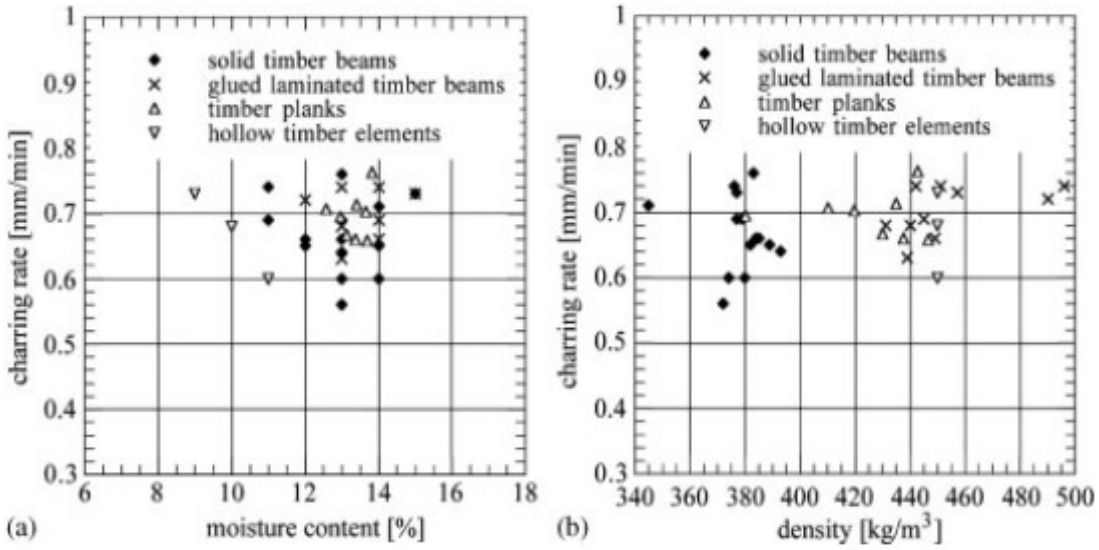

Figure 2.29 Measured charring rates as a function of (a) moisture content (b) density for the timber elements under the standard fire exposure. (Frangi and Fontana, 2003)

Temperature profiles within a timber member exposed to severe temperatures usually have a steep thermal gradient due to the insulation from layer of char and unburnt wood. Based on the influence of the charring rate, the heat flux from the sides, time of exposure and the cross-section properties,

the authors came up with the below equation for predicting the temperature profile in timber beams exposed to fire on three sides.

$$\theta(x,y) = 20 + 180(\beta t)^{\propto}\left\{\left(\frac{1}{x}\right)^{\propto} + \left(\frac{1}{b-x}\right)^{\propto} + \left(\frac{1}{y}\right)^{\propto}\right\} \quad \textbf{Equation 2.16}$$

Where

θ *is the temperature in* ℃ *as functions of the depth* x *and* y

β *is the charring rate in* mm/min

t *is the time in* min

x *is the depth measured from the side surface of beam*

y *is the depth measured from the underside of cross* $-$ *section*

$\propto (t) = 0.025t + 1.75$

In conclusion the authors confirmed the significance of thermal degradation and temperature distribution in predicting the resistance of timber structures.

Thermo-hydric transfer within timber connections under fire exposure: Experimental and numerical investigations (2014)

Authors: Abdoulaye Samake, Mustapha Taazount, Philippe Audebert, Patricio Palmili

The authors presented their observations and findings on the experimental and numerical thermo-hydric transfer of timber connections under exposure to the ISO-834 standard fire curve. Thermo-hydric flow involves transfer of heat between the hybrid materials, and the outward flow of bound water to the timber/steel interfaces. Hydric flux involving the transfer of bound water from a region of high partial pressure to a lower one in wood after 100°C, has the capacity to retard material combustion depending on the moisture content of the timber. A series of six experimental tests was conducted on single rod connections for this study using a gas oven. Three specimens had 16

mm diameter rods (T-T with dowel fastener, T-S-T with dowel fastener and T-S-T with bolt fastener), and the remaining three had 20 mm diameter rods. Temperature profiles within the steel plates and timber members were measured with thermocouples (TC) embedded in them. Details of the specimen are shown in Figure 2.30 and Table 2.4.

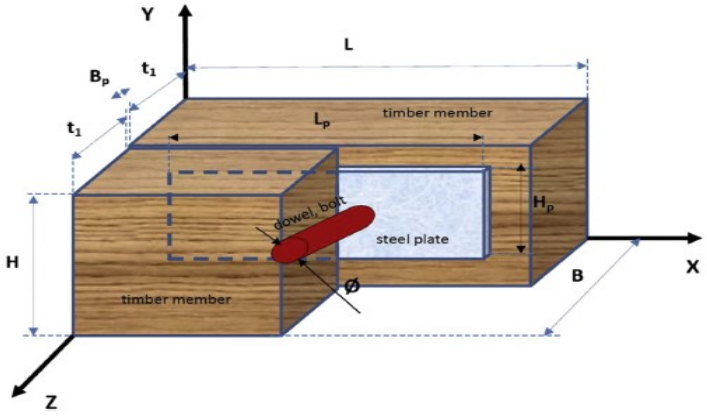

Figure 2.30 Geometrical configuration of specimens (Samake et al., 2014)

Table 2.4 Specimen details (Samake et al., 2014)

N°	Type	Fastener type	L (mm)	B (mm)	H (mm)	L_p (mm)	B_p (mm)	H_p (mm)	t_1 (mm)	Ø (mm)
S_1	T–T	Dowel	300	155	130	–	–	–	77.5	16
S_2	T–S–T	Dowel	300	155	130	260	8	64	77.5	16
S_3	T–S–T	Bolt	300	155	130	260	8	64	77.5	16
S_4	T–T	Dowel	300	210	130	–	–	–	105	20
S_5	T–S–T	Dowel	300	210	130	260	10	64	105	20
S_6	T–S–T	Bolt	300	210	130	260	10	64	105	20

16 thermocouples were employed to measure temperature distributions. Thermocouples TC1, TC2, TC3 and TC4 measured the temperature change in the fasteners. TC5, TC6, TC7 and TC8 were installed in the wood, TC9, TC10, TC11 and TC12 in the wood-metal interface and the remaining four in the oven to control the gas flow.

The authors reported an average charring rate of 0.71 mm/min which was close to the recommended 0.70 mm/min in EN 1995-1-2. At the fastener location, temperatures recorded in the bolted Timber-Steel-Timber joints were twice as high as those recorded in the doweled Timber-Steel-Timber joints. In addition to that, the ability of the fasteners to conduct heat is related to the perimeter in contact with fire. The temperature profile around the fastener region is shown in Figure 2.31 (a) where there is a change in phase at 100°C as heat is utilised in evaporating water within the joint. They concluded that extreme temperatures in timber areas close to the fasteners can significantly induce failure if the joints are mechanically stressed under fire exposure.

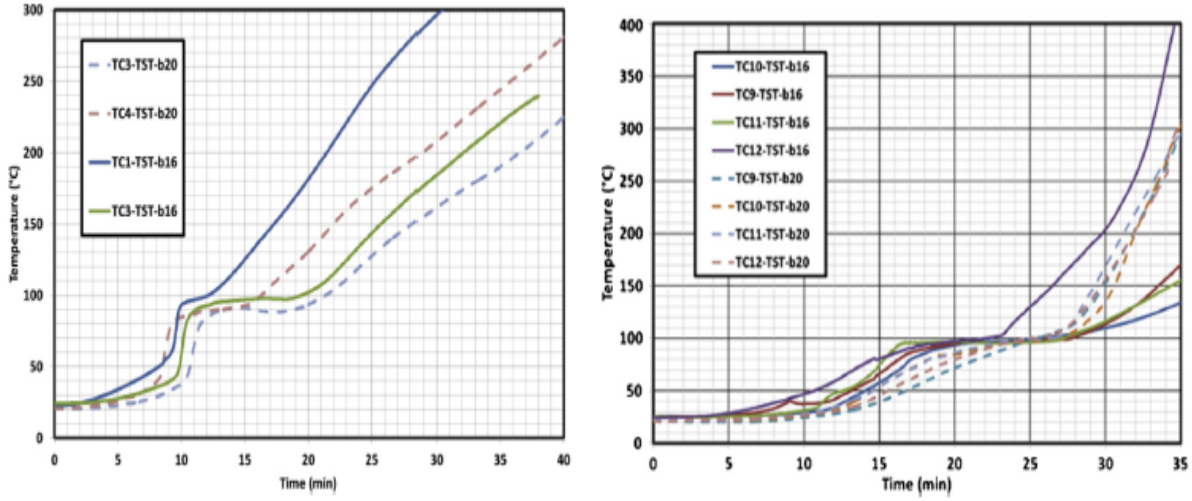

(a) (b)

Figure 2.31 Dowelled Timber-Steel-Timber (a) joint; temperature-time evolutions (near bolt) (b) Bolted Timber-Steel-Timber joint; temperature-time evolutions (Samake et al., 2014)

The timber-metal plate interface was exposed to significant temperatures for the bolted members. Temperatures were as high as 400°C, and water stagnation and phase change at 100°C were clearly obvious from the plot (Fig. 2.31 (b)). The presence of the metal plate in the joint contributed to preventing escape of evaporated water in wood. This trapped water slowed the burning process as is seen in Figure 2.31 (b). Thermocouples on the periphery of the timber member (TC5 and TC8)

recorded temperatures as high as 400°C regardless of the configuration confirming the uniformity of thermal diffusivity velocity from the exterior surface toward the inside of the specimen.

Charring Rate of Timber in Natural Fires (2014)

Authors: Lange D., Bostrom L., Schmid J., and Albretsson J

To investigate the load carrying capacity and charring rates of timber beams under natural fires, 32 glulam beams (140 x 270 x 5400 mm) were subjected to three different time-temperature curves and varying load levels in Sweden. The simply supported beams were tested on a horizontal furnace and loaded to failure under a four-point loading. The sides and underside of the beams were exposed while the top surface was covered with aerated concrete blocks and mineral wool. Thermocouples were installed within the specimens at various depths to record the temperature profile. The temperature in the furnace was measured by 20 equally distributed plate thermometers. For their exposure, the authors looked at a standard fire curve, a slow heating rate real fire and a fast heating rate real fire curves. The fast or rapid rise real fire was modelled to peak at 1100°C after about 20 min from the start of the test. It decayed rapidly to room temperature after about 50 min from start of test. The slow heating real fire however was modelled to grow steadily and slowly, peaking at almost 800°C after 1 hour. The decay phase had a very gentle slope reaching 600°C after 2 hours of testing.

The average charring rate was calculated based on the time taken for the isotherm of the charring temperature to reach a thermocouple from the start of the test. An average charring rate of 1.1 mm/min over the first 20 mm depth of installation from bottom of beam was recorded under exposure to the rapid heating real fire. This however decreased to 0.7 mm/min over 50 mm depth

of installation. Under the slow heating real fire curve, a charring rate of 0.22 mm/min was recorded for the first 10 mm depth, and remained constant at an approximate value of 0.3 mm/min from 20 mm to 50 mm depth. They reported a relatively higher average charring rate for rapid rise fire curves as opposed to the slow rise and standard EN 1363-1 fire curves. The authors reported that the charring rate is dependent on the heating rate as well as the rate of cooling for exposure under real fires.

Fire Performance of Hybrid Timber Connections with Full Scale Tests and Finite Element Modelling (2014)

Ali S. G., Akotuah A. O., Erochko J., and Hadjisophocleous G. V.

In order to investigate the influence of various design parameters on the behavior and performance of hybrid connections in fire, the authors conducted a series of 11 full-scale tests on connections involving a glulam beam and steel columns. The tests were conducted in the connection furnace located at the Full-Scale Fire Research Facility of Carleton University in Almonte, Ontario. The beam (140 x 191 x 1900 mm) with its top surface protected was connected to two pin-pin heavily insulated steel columns (W150 x 37) using three different shear tab connections. It was then subjected to a two point loading at 1/3 points along the length of the beam. The specimens were subjected to the standard time-temperature curve as defined by CAN/ULC S-101.

The main parameters considered by the authors were the type of connection, the load ratio and the bolt diameter. 30%, 60% and 100% load ratios were investigated. The influence of bolts of diameters ½" and ¾" were studied as well. The three different connection types investigated were the Concealed (CN), Exposed (EX) and Seated (SE) shear tab connections (Fig 2.32)

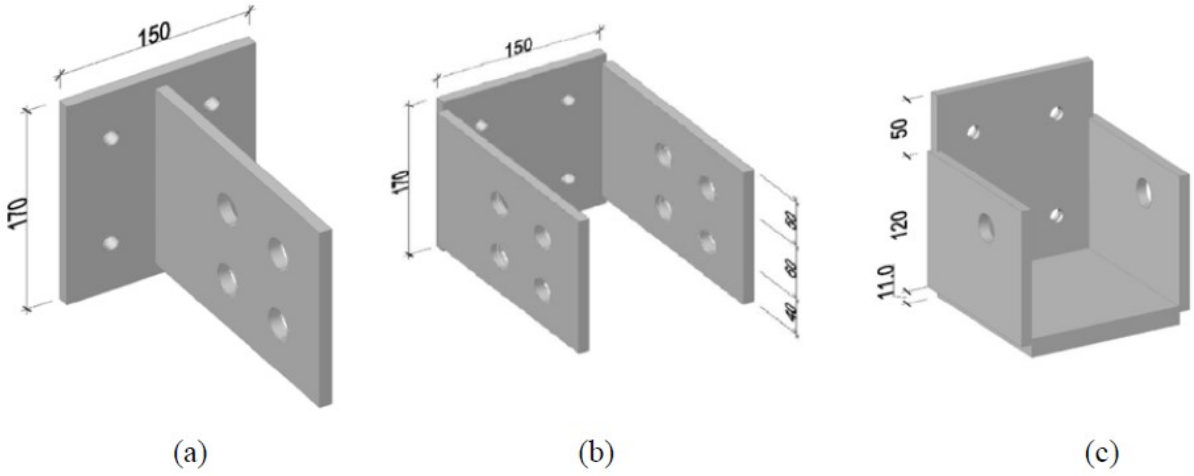

Figure 2.32 Different connections considered: (a) CN (b) EX (c) SE (Ali et al., 2014)

The authors reported brittle failure involving splitting of the wood along the grain at the connection ends as the main mode leading to loss of structural capacity of the system. Initial cracks at the bolt-hole edges grew as the bolt shank exerted compressive stresses on the wood below ultimately leading to splitting failure. It was reported that applying a 100% load ratio on the beam increased internal stresses significantly. It however did not lead to premature failure since the full vertical load ratio was only a fraction of the ultimate load.

The authors discussed the fire resistance as observed for the Concealed and Exposed Connections using ¾" diameter bolts under 30% and 60% load ratios. The Concealed Connection recorded a time to failure of 35 min as compared to 25 min for the Exposed Connection. It was reported that heat transfer to sections located in the bottom corner of beam had higher temperature profile over time than sections in the middle of the cross-section. This was attributed to the transfer of heat from two boundary surfaces for sections in the bottom corner as opposed to transfer from one boundary surface for sections in the middle of the cross-section. At a 20 mm depth from the sides the temperatures range from 650 - 750°C after 35 min of exposure. The temperature distribution

within the 40-100 mm range of the cross-section depth varied from ambient temperature at the center to 100°C at the edges. At the connection ends, a charring rate of 0.56 mm/min was recorded for the EX connection compared to 0.94 mm/min for the CN connection. This significant protection of wood at the connection end of the EX system was attributed to the presence of the steel plates on the sides of the beam which offered partial protection and delayed charring of wood underneath. As explained by Samake et al. (2014), this partial protection could also be attributed to stagnation of evaporated water between the steel plates and wood underneath it. This causes delay of rise in temperature at the interface between the wood and the steel plate thereby delaying charring. An increased in the charring rate at the connection ends of the CN system was also attributed to transfer of heat flux to middle of beam cross-section due to the ability of the exposed bottom of inserted plate and bolt to directly conduct and transfer heat.

3 METHODOLOGY

In order to investigate the fire resistance and behavior of hybrid steel column and glulam beam connections in real fires, eight (8) glulam beams were tested at the Full Scale Fire Research Facility of Carleton University in Almonte, Ontario. This chapter gives a brief description of the test facility, specimens and the testing procedure.

3.1 Facilities

3.1.1 Furnace

The furnace was especially designed to test the fire performance of various connection assemblies. The interior of the furnace is 2700 mm x 2700 mm x 2200 mm high. It is heavily insulated with 25-mm thick Fibrefrax® mineral blanket. Inside the furnace are two propane line burners, one on each side of the wall. Figure 3.1 shows an exterior view of the furnace and the testing load frame on the left, and a typical propane burner on the right. Burners are located on both sides of the furnace wall for a better distribution of heat in the room. On the exterior burner sides of the walls are two blowers installed to supply air to the furnace and maintain a positive pressure. The furnace temperature can be monitored and controlled to simulate any time – temperature curve.

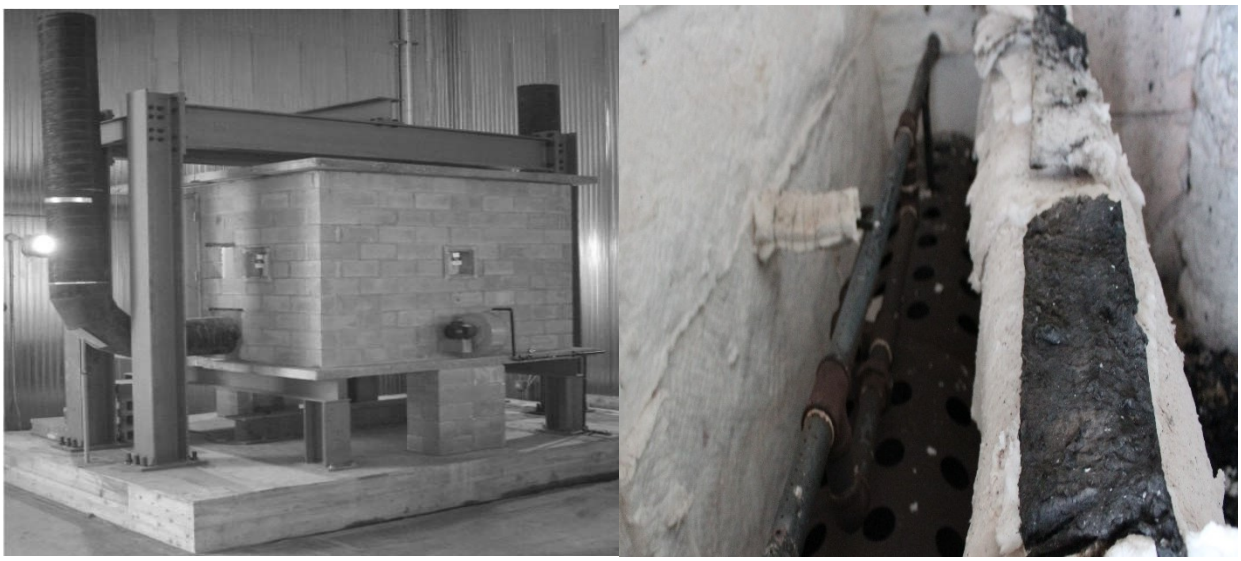

Figure 3.1 Exterior view of furnace and propane burner

3.1.2 Thermocouples and Plate Thermometers.

Six (6) shielded rod thermocouples and four (4) plate thermometers are installed to measure the temperature in the furnace. These temperatures are used to control the fuel supply to the burners to follow the required time-temperature curve. As required by ASTM E119 and CAN/ULC S-101 Standards, the shielded thermocouples were made of No. 18 gauge type K thermocouple wires enclosed in porcelain protection tube. The thermocouple with the porcelain tube was then inserted into a 21-mm outer diameter steel pipe with a capped end. A schematic view of the shielded thermocouple is shown in Figure 3.2 as reproduced from Peng et al. (2010). The shielded thermocouples as required by the Standards, were symmetrically located as shown in Figure 3.3.

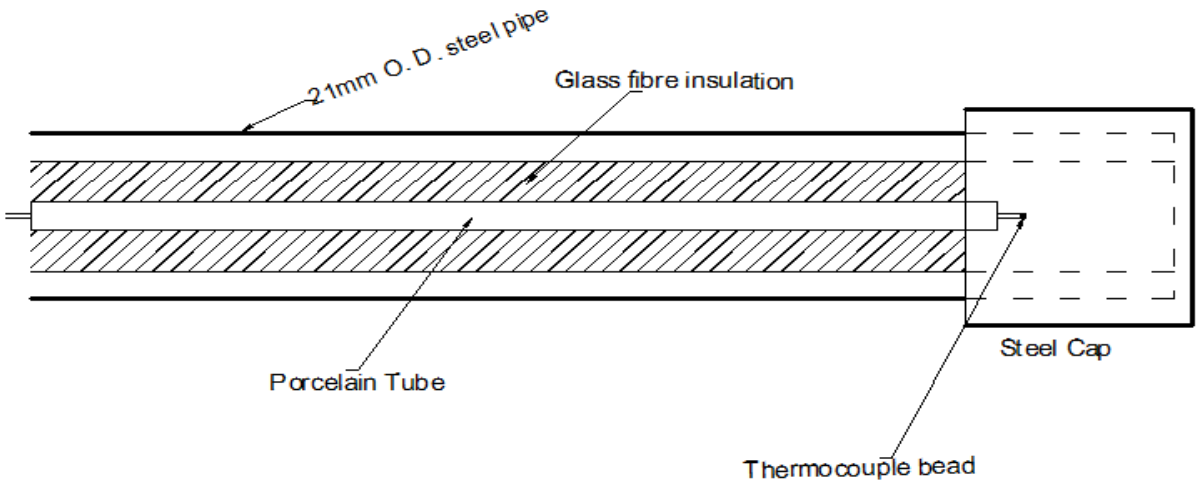

Figure 3.2 Schematic view of the shielded thermocouple, (Peng et al., 2010)

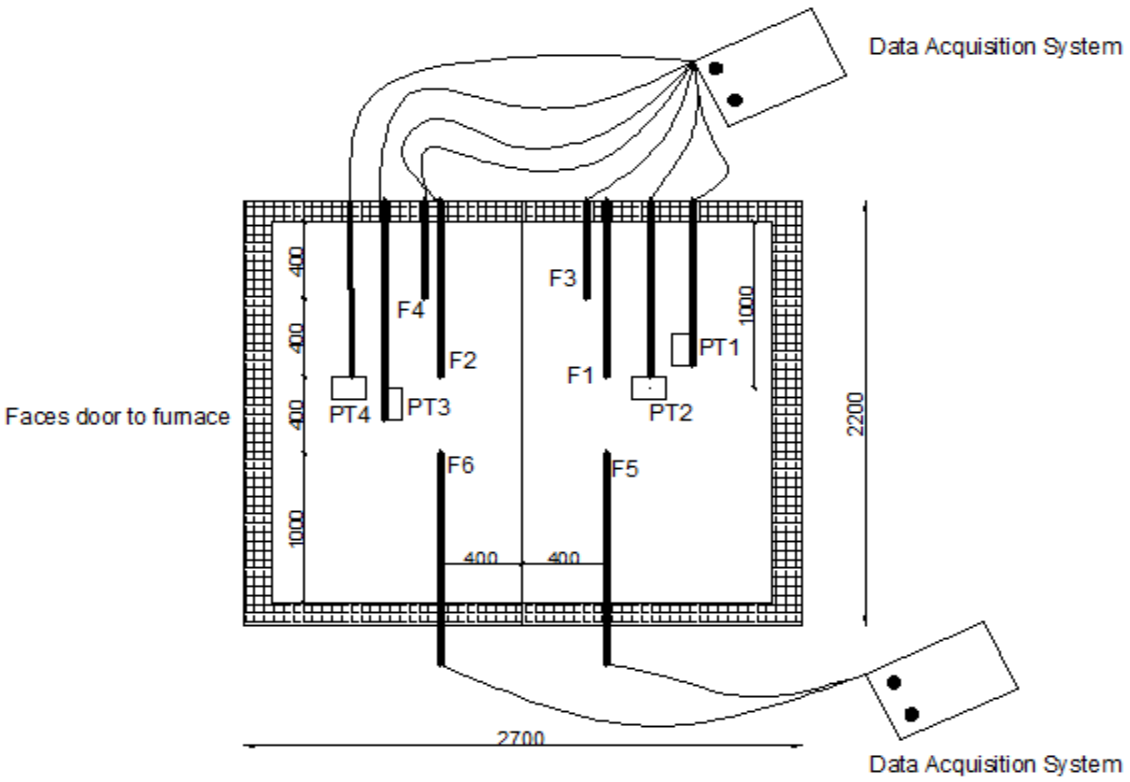

Figure 3.3 Schematic diagram showing an elevation view of the furnace with positions of plate thermometers (PTs) and Thermocouples (Fs)

The plate thermometers were installed close to the location of the connections to measure the heat load as experienced by the test specimens. The use of the plate thermometers in addition to the shielded ones was to obtain temperature data to be used in numerical finite element modelling of the tests.

3.1.3 Load Application system

A loading frame is available in the furnace to support the connection assembly and apply the desired load. The load is applied using a hydraulic cylinder, Model RD1610 from Enerpac®. A 250KN capacity load cell (MTS® 661.22D-01) is employed to measure the load.

3.1.4 LVDTs

As shown in Figure 3.4 (a), three Linear Variable Displacement Transducers (LVDTs) were installed to measure the deflections during testing. Two of the LVDTs were installed on top of the

beam to measure deflection at the connection ends. The other was placed underneath the beam at mid – span to measure the downward deflection. The total deflection of a connection was found as the difference between the bottom displacement and the top displacement as measured by the LVDTs.

3.1.5 Data Acquisition System

All the data from the furnace was channeled to a three 5000 – Series Ethernet IMP (Slartron Mobrey Limited®) set up as the data acquisition system. Each Ethernet IMP has 20 analog channels. The IMP devices were then connected to a computer through an Ethernet cable to record and store test data every second.

3.2 Specimen Details and Instrumentation

All tested glulam beams were obtained from Nordic Wood Engineering. The beams were 1880 mm long with two specifically selected cross–sectional dimensions of 140 mm wide x 191 mm deep and 137 mm wide x 222 mm deep. As shown in Figure 3.4 (b), the glulam beams were structurally connected to the two 3200 mm long pin-pin steel columns (W 150 x 37) by means of a 9.5 mm thick shear tab plate (grade 300W) with 4-12.7 mm A325 bolts. Shear tab plates are a common type of simply supported connections in structural steel framing. They are easy to fabricate and erect. The shear tab connectors were designed by Ali et al. (2014) per provisions in CAN/CSA S16-09 (2009) to ensure the connections have a better resistance in fire than the main members. Detailed design drawings of the shear tab plates are shown in the Appendices section.

To mimic the presence and the effect of a floor slab system on the beams, the top surface was insulated with a 25 mm thick layer of Fibrefrax® mineral blanket. As such, all beams were tested with three sides exposed to the extreme temperatures. The steel columns and loading frame in the furnace were heavily insulated as well. A typical specimen placed in the furnace for testing is

shown in the figure below. The heavily insulated steel columns and loading frame can be seen as well.

(a)

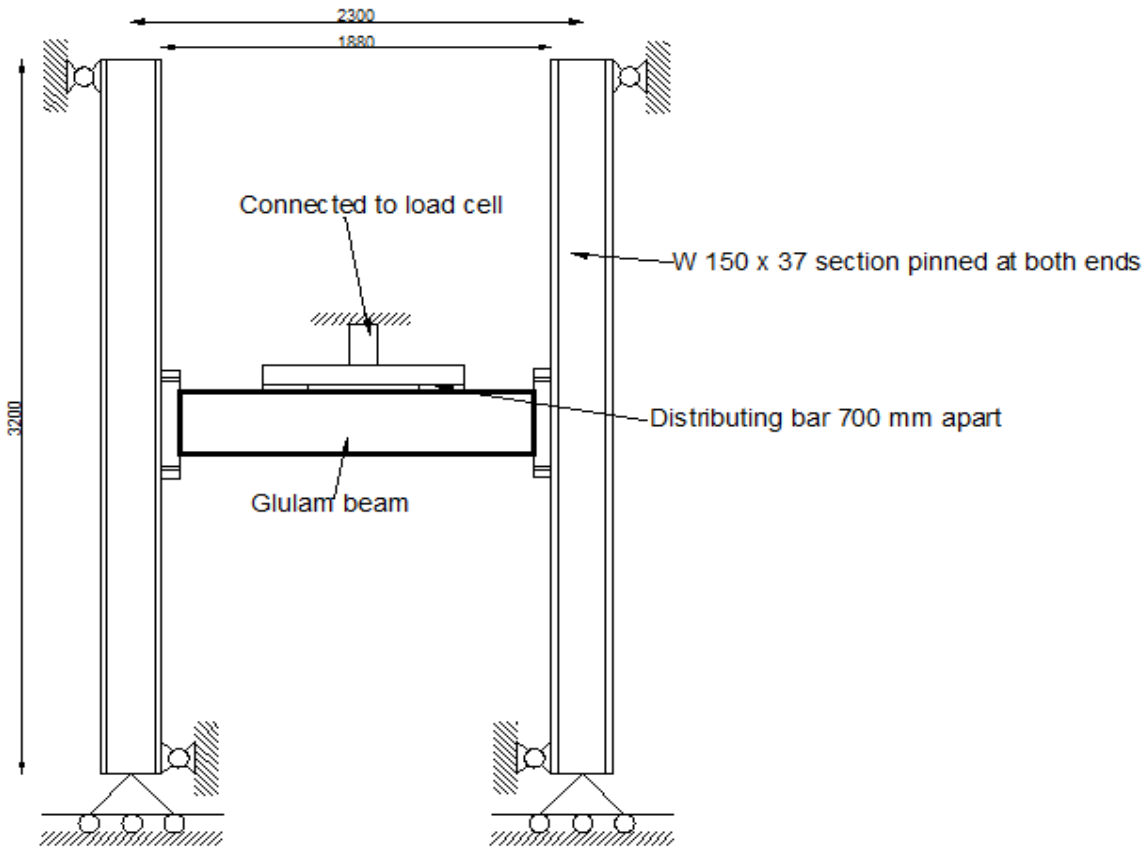

(b)

Figure 3.4 (a) Typical specimen set up for testing in the furnace (b) Configuration of the tested assembly

All the specimens were stored in the atrium of the research facility. Prior to the start of the fire resistance test, the moisture content of the specimen was taken. An average moisture content of 9.5% was recorded for all eight specimens tested. Details of each specimen is provided in Table 3.1 below.

Table 3.1 Details of each specimen tested.

DATA SHEET FOR TESTS										
SAMPLE NUMBER	SIZE OF BEAM				CONNECTION TYPE	LOAD		BOLT		
	WIDTH (mm)	DEPTH (mm)	LENGTH (mm)	MOISTURE CONTENT (%)		LR (%)	LOAD APPLIED (KN)	DIAMETER (mm)	LENGTH (mm)	GRADE
1 (F)	137	222	1880	9	Exposed	60	53	12.7	175	A307
2	137	222	1880	10	Exposed	100	98	12.7	175	5 (ASTM A325)
3 (F)	137	222	1880	9	Exposed	60	59	12.7	175	5 (ASTM A325)
4	137	222	1880	9	Exposed	60	59	12.7	175	5 (ASTM A325)
5	140	191	1880	10	Concealed	60	43	12.7	175	5(ASTM A325)
6	140	191	1880	9	Concealed	100	71.8	12.7	175	5 (ASTM A325)
7	137	222	1880	9	Seated	60	70	12.7	7	5(ASTM A325)
8	137	222	1880	11	Seated	100	118	12.7	7	5(ASTM A325)

(F) Refers to tests that were stopped due to few technical problems.

**Refer to the Appendices for information on the design of the connection assemblies.*

The beam specimens were instrumented with thin metal-sheathed and mineral-insulated (MSMI) type K thermocouples at various depths. These thermocouples measured the temperature profile change with time at the various depths. The thermocouples were installed from all faces of the beams as detailed in the figures below (Figures 3.5 to 3.11). The temperature profiles recorded are useful in calculating the char rate and the charring depth. Figure 3.5 shows typical beam with locations of installed thermocouples. Figures 3.5 to 3.9 detail the thermocouples' position and

depth, d in mm from all faces of the beam. The front face (F) of beam is deemed as the side adjacent to the burner close to the furnace door.

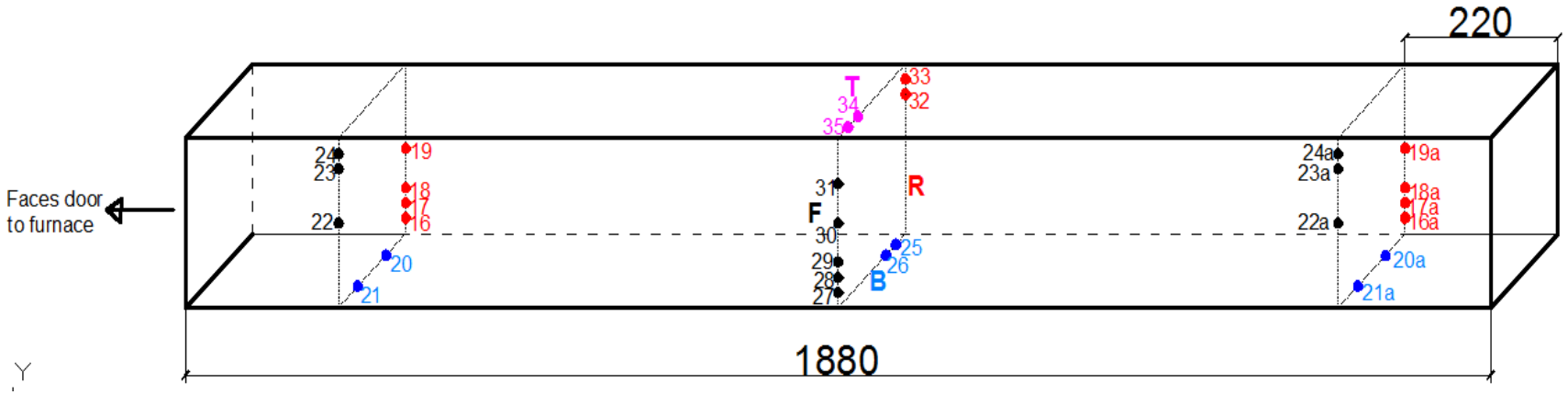

Figure 3.5 Instrumentation of a typical beam specimen showing position of installed thermocouples from faces of the beam

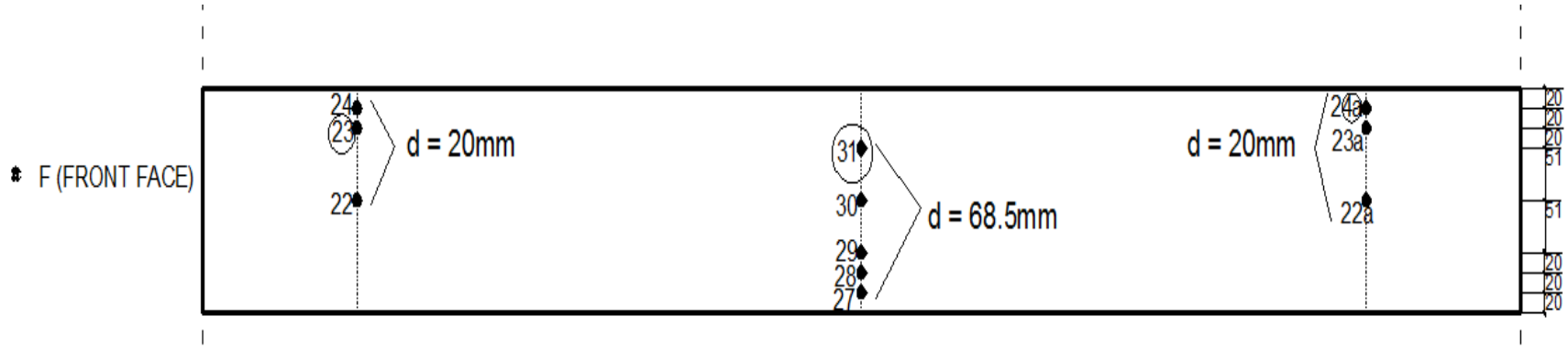

Figure 3.6 Position and depth of installation of thermocouples from the front face (F) of beam

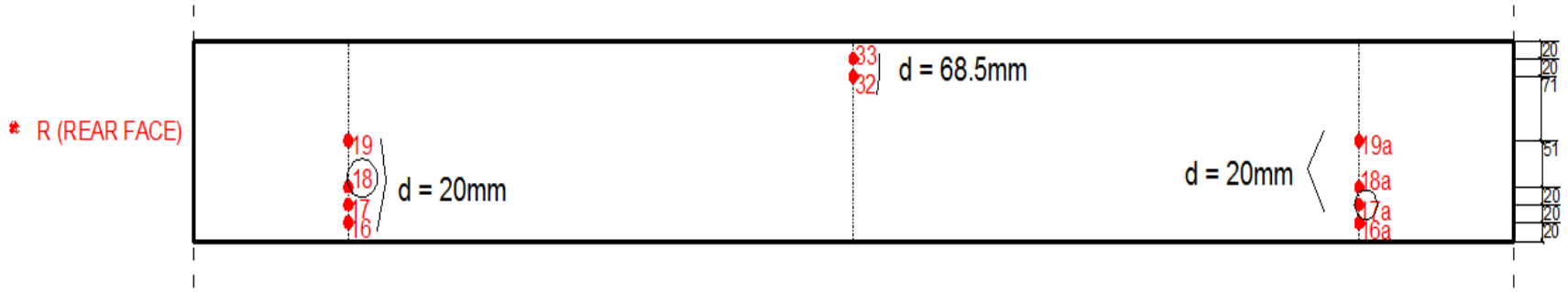

Figure 3.7 Position and depth of installation of thermocouples from the rear face (R) of beam

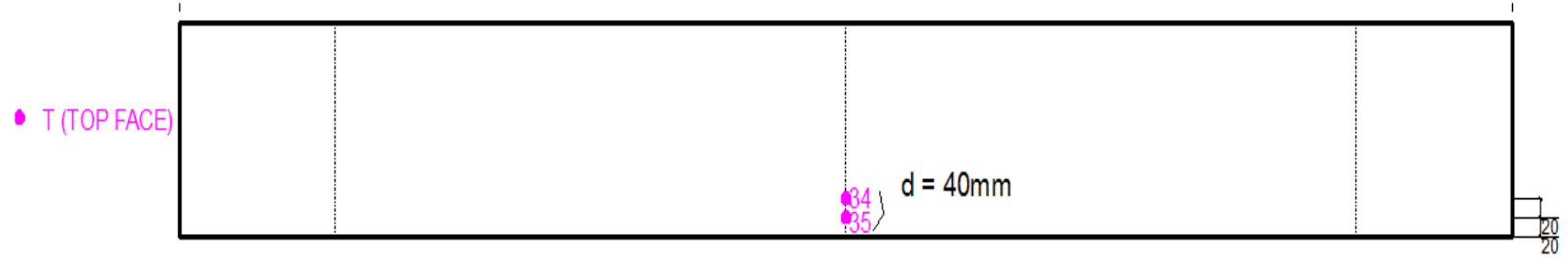

Figure 3.8 Position and depth of installation of thermocouples from the top face (T) of beam

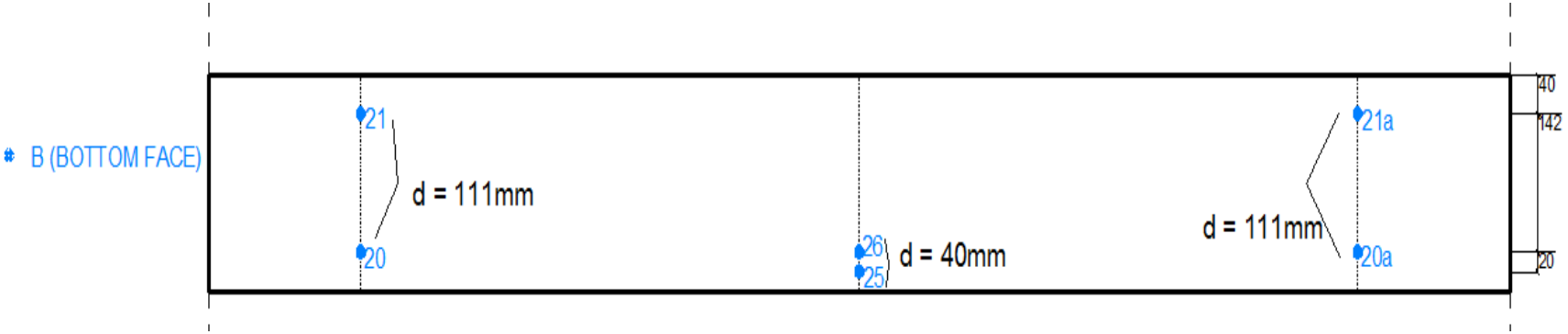

Figure 3.9 Position and depth of installation of thermocouples from the bottom face (B) of beam

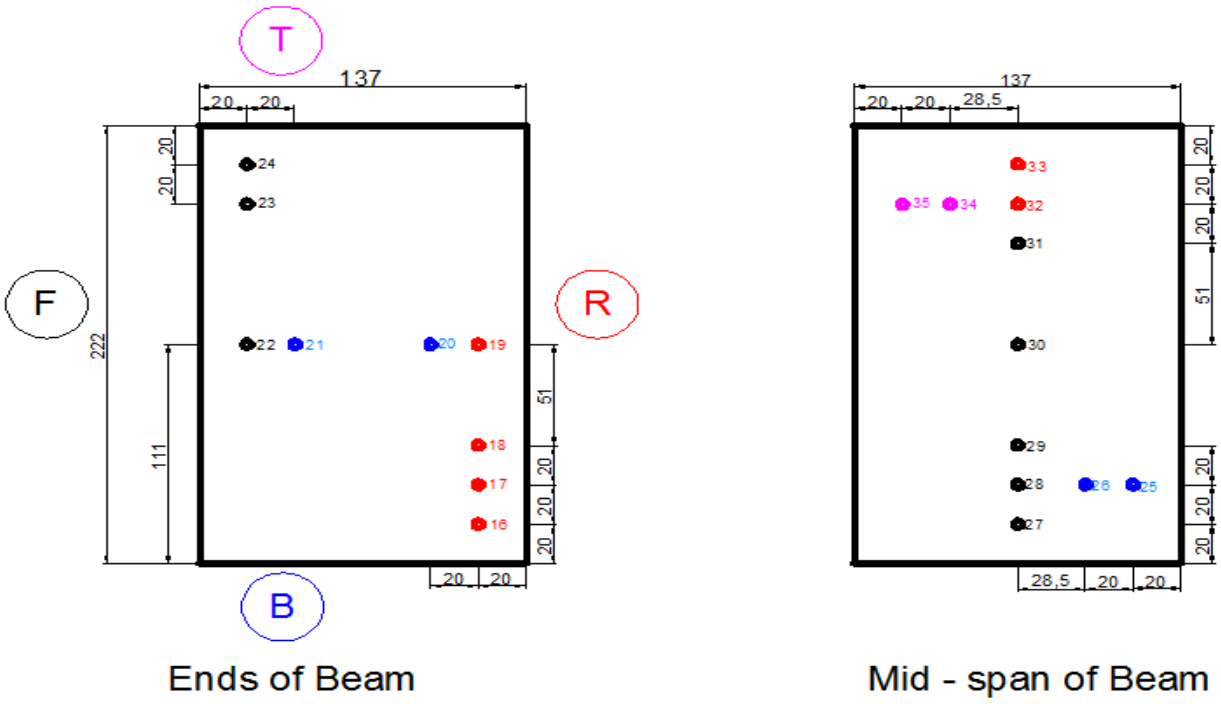

Figure 3.10 Typical plane in beam showing position of thermocouples in the 137 mm x 222 mm specimens

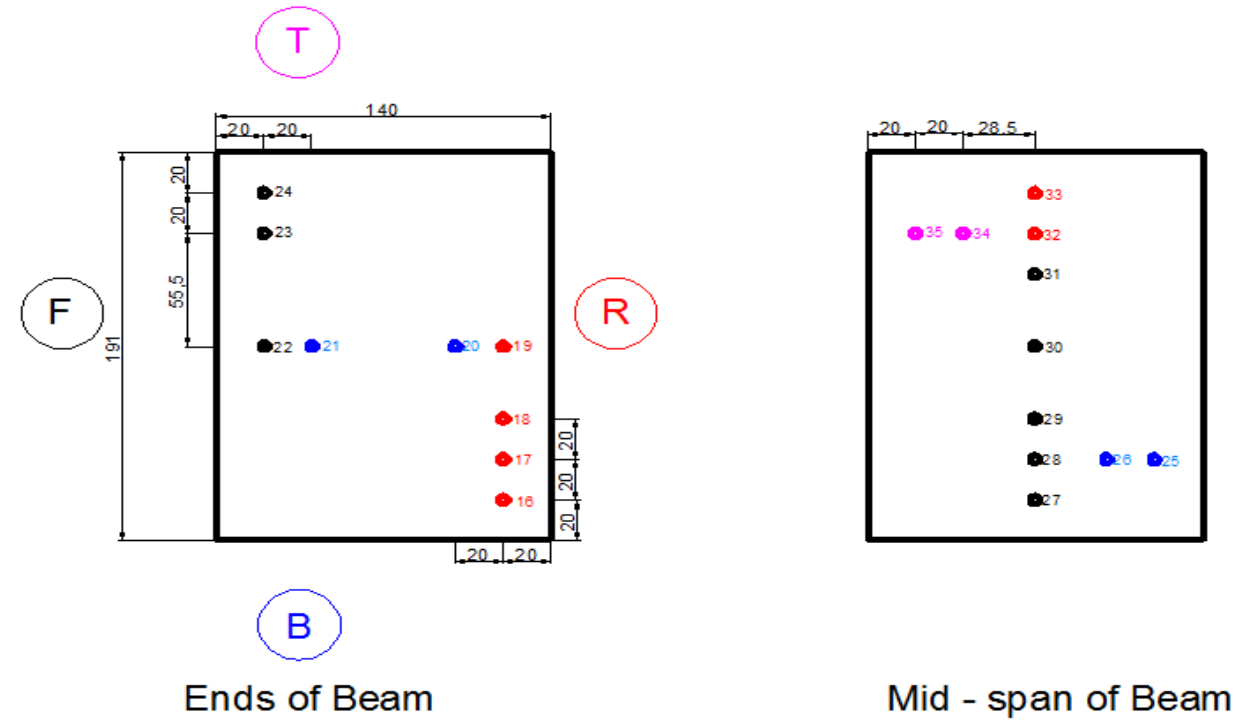

Figure 3.11 Typical plane in beam showing position of thermocouples in the 140 mm x 191 mm specimens

In the above figures, the dots and numbers represent the thermocouples installed. The four main faces of the beam comprising the front, rear, top and bottom faces are represented with the letters F, R, T and B respectively. Each face is also given a different color representation for clarity. To measure temperatures of sections as close as possible to the connection ends, thermocouples were installed at 220 mm from the ends of the beam. Others were also installed in the mid – span to measure and compare the difference in temperature distribution to that at the connection.

To get an estimate of the change in temperature profile with time at different depths within the wood, thermocouples were installed at depths of 20 mm from the front and back faces, and 40 mm from the bottom and top faces. Other thermocouples were also positioned 68.5 mm deep from the front and back faces to measure the temperature change within the inner core. From the bottom of the beams, thermocouples were also installed at a depth of 95.5 mm and 111 mm for the 140 mm x 191 mm and 137 mm x 222 mm sections respectively as shown in Figures 3.10 and 3.11.

The face of the beam, number and depth of installation of thermocouples are used to formulate names to represent each thermocouple in the various plots of temperature with time. For instance, a thermocouple with the name TF – 24 – 20mm means thermocouple number 24 installed at a depth of 20 mm from the front face of the beam. Similarly TB – 21 – 111mm thermocouple represents readings recorded by thermocouple 21 installed at a depth of 111 mm from the bottom face of the beam. As such all thermocouples are given the simple representation shown below;

T(face of beam) – Number – depth of installation from the face

Thermocouples were also welded to the bolts at 25 mm and 50 mm from the head to measure the temperature change with time of the bolts. Most of these attached thermocouples however failed in the course of the test.

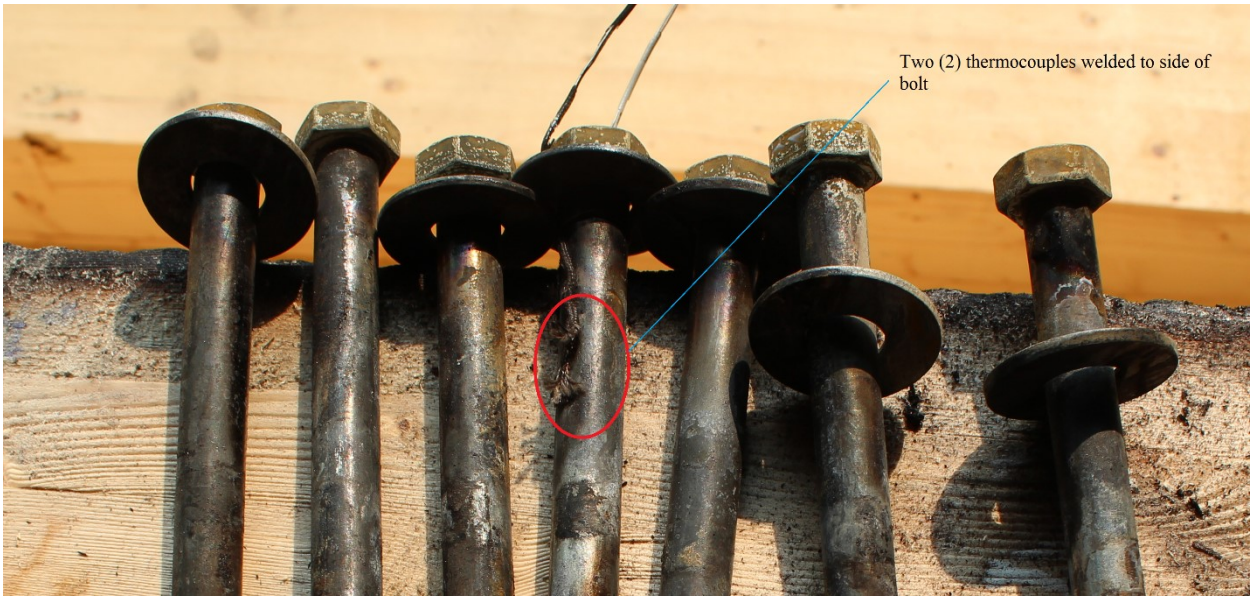

Figure 3.12 Thermocouples on bolts

3.3 Load Ratio

Load ratio (LR) is defined as the ratio of the anticipated loads on a structure in the event of a fire to the loads that would cause failure under ambient conditions. It significantly affects the fire resistance of structures. Structures with lower load ratios perform well in fire due to the reduced loss of load carrying capacity in fire (*Buchanan, 2002 and Peng et al., 2010*). Performing well in fire implies increased time of exposure, and increased charring resulting in more loss of cross-section. This ultimately leads to failure of connections due to loss of strength in the wood (*Peng et al., 2010*). Peng et al. (2010) reported higher load ratios increase stress on fasteners resulting in failure due to loss of stiffness and strength in the fasteners. As such failure is less dependent on charring of wood side members, but on the thermal effects on the fasteners when higher load ratios are used. He defined higher load ratios as being greater than 50% of the ultimate load capacity under ambient conditions. CAN/ULC S-101 (2007) recommends that loads applied in fire to a member are as close as possible to the factored resistance in accordance with the provisions made

in CAN/CSA O86 – 09 (2010) for the design of timber connections. However, the standard also allows lesser loads to be used as long as they are recorded and documented. For the series of tests conducted, two load ratios of 60% and 100%were applied to study the effect of load ratio on the time to failure of the specimens.

3.4 Fire Exposure Model

The Non-Standard Time Temperature Curve employed in this research was modelled by Aguanno (2013). It is based on a fire that would occur in a typical residential bedroom with CLT panels as the wall lining material. McGregor in 2012 conducted fire tests on two fully furnished CLT rooms of size 4.5 x 3.5 x 2.5 m high built in the Full – Scale Fire Research Facility of Carleton University in Almonte, Ontario. The rooms had a 1.07 x 2 m high doors as shown in Figure 3.13. The rooms were lined with 3-ply CLT panels with the floor made of hardwood on a cement board. The contents in the room (Fig. 3.13) included a bed, two night tables, two dressers and various linens and books, all contributing to a fuel load of 560 MJ/m^2. One of the rooms had the CLT panels exposed to the extreme heat, whilst the other had 2 layers of 12.7 mm (1/2") Type C gypsum board on the CLT panels.

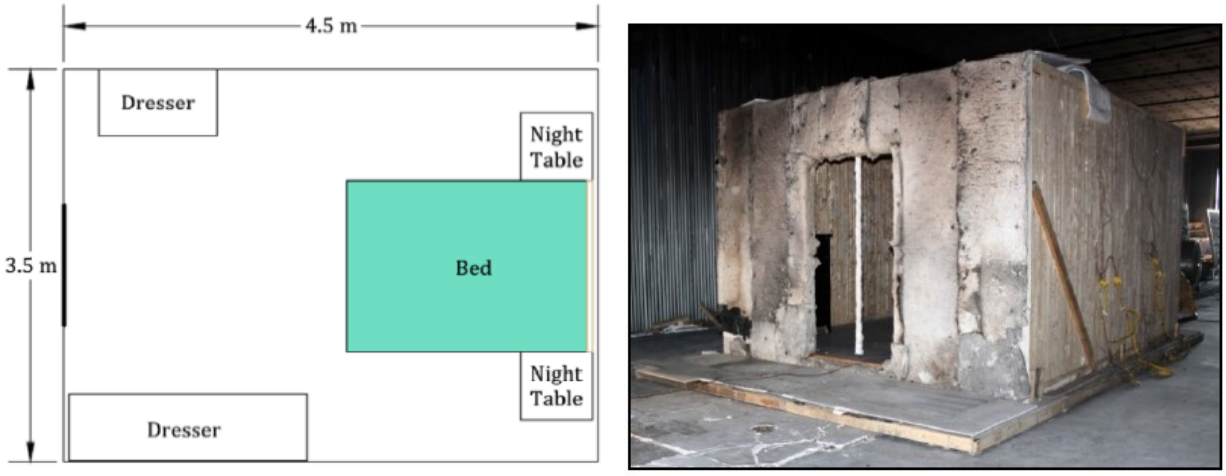

Figure 3.13 CLT Room test layout (Aguanno, 2013)

Temperature readings as recorded by plate thermometers installed in the room were used to design the Non-Standard Time Temperature Curve. As such subsequent fire tests involving this curve were to be controlled by plate thermometers (Aguano, 2013). Temperatures as recorded from both rooms by the plate thermometers are shown in Figure 3.14. As can be seen, the noticeable feature of both curves is the similarity in the growth phase up to a temperature of 700°C, and the significant difference after about 20 minutes of exposure. Temperature readings in the gypsum lined room started decaying after 20 minutes of exposure. That of the unlined room however continued burning incessantly as the CLT walls and ceiling contributed to the fire until it was manually extinguished.

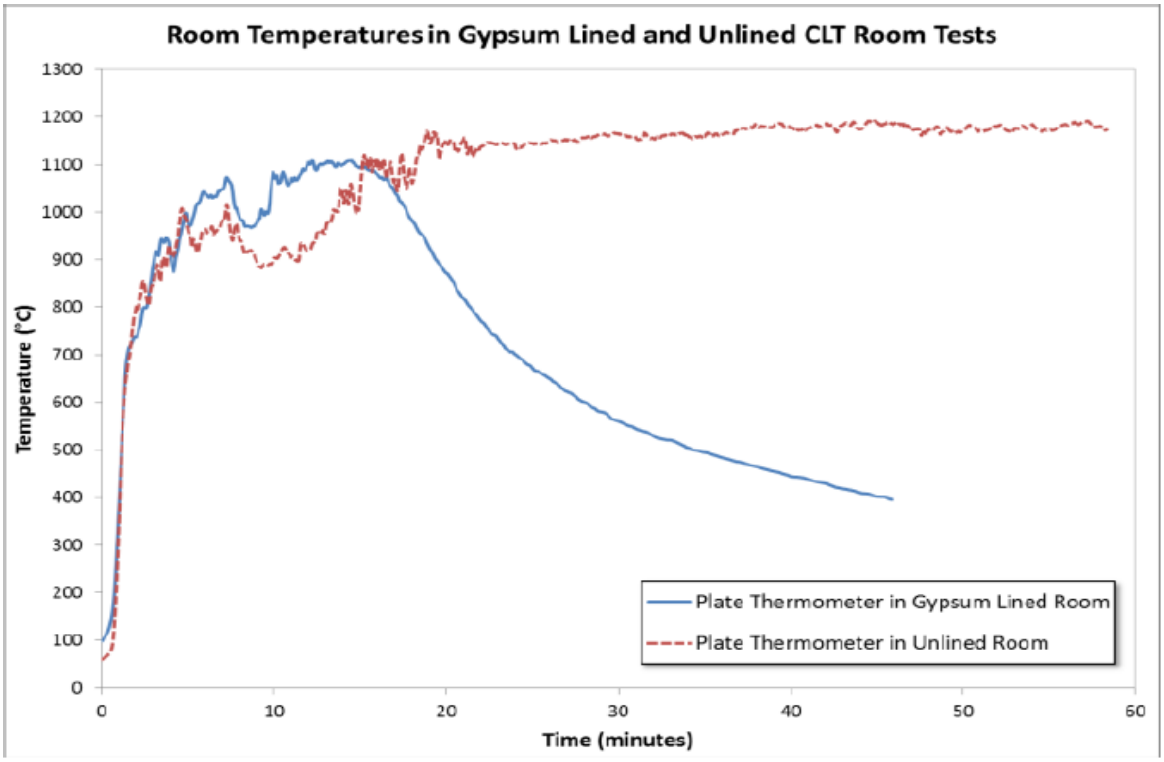

Figure 3.14 Fire Temperatures as observed in both protected and unprotected CLT room tests (Aguanno, 2013)

Therefore to model the Non-Standard Fire Curve, Aguanno (2013) considered a blend of steady burning for some time and a decay phase. As most residential CLT buildings have gypsum board protection, a never ending steady phase as seen in the unlined fire test would be unrealistic. Moreover, the decaying phase observed in the gypsum lined room was deemed too fast to simulate severity in the cooling phase under real fires. As such, the author adopted a slower decay phase from 1100°C to 300°C over a time range of 2 hours to simulate possible continuous charring of wood in the cooling phase.

From these feasible observations and assumptions, an exposure model using the equations below was developed (Figs. 3.15 and 3.16). This model was deemed capable of simulating real fires as seen in CLT room tests with a decay phase long enough to cause significant charring leading to structural failure. As such employing this fire curve for structural assemblies involving glulam beams is justifiable as both CLT and glulam beams are combustible, and likely to be found together in a typical residential building.

$$T = 126.446t^2 + 18 \qquad for\ 0 \le t < 2.2min \qquad \textbf{Equation 3.1}$$

$$T = 1100 - \left(\frac{t - 24}{1.005559}\right)^2 \qquad for\ 2.2 \le t < 24min$$

$$T = 1100 \qquad for\ 24 \le t < 36min$$

$$T = 1881.12 - 130.186\sqrt{t} \qquad for\ 36 \le t \le 200min$$

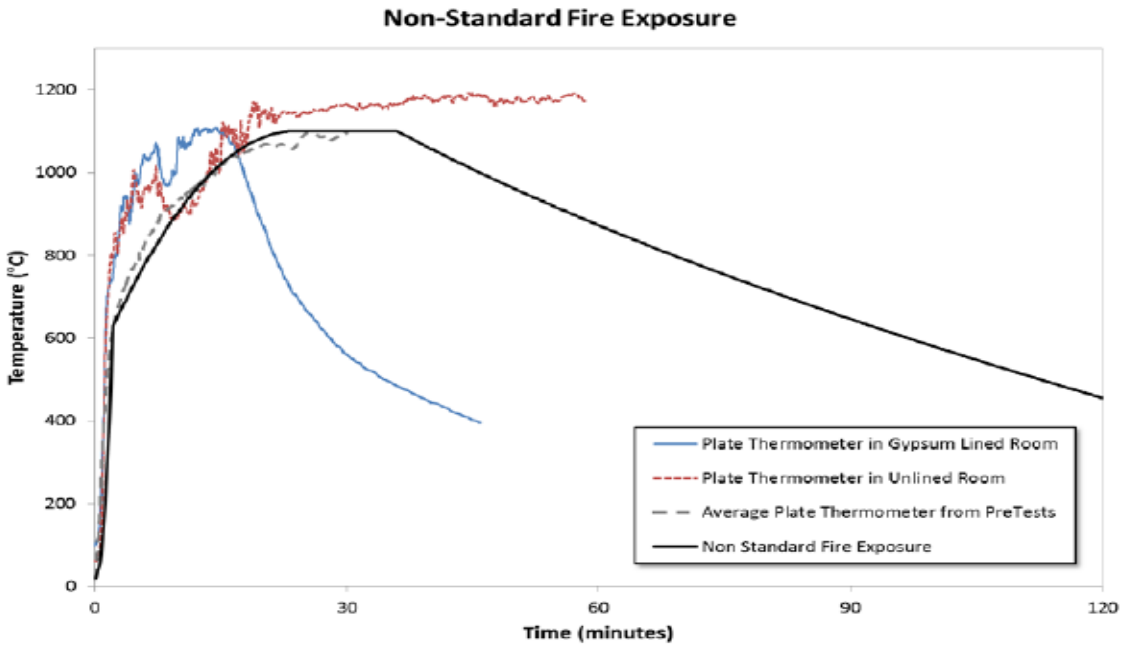

Figure 3.15 Non-Standard Time Temperature Curve developed from CLT tests (Aguanno, 2013)

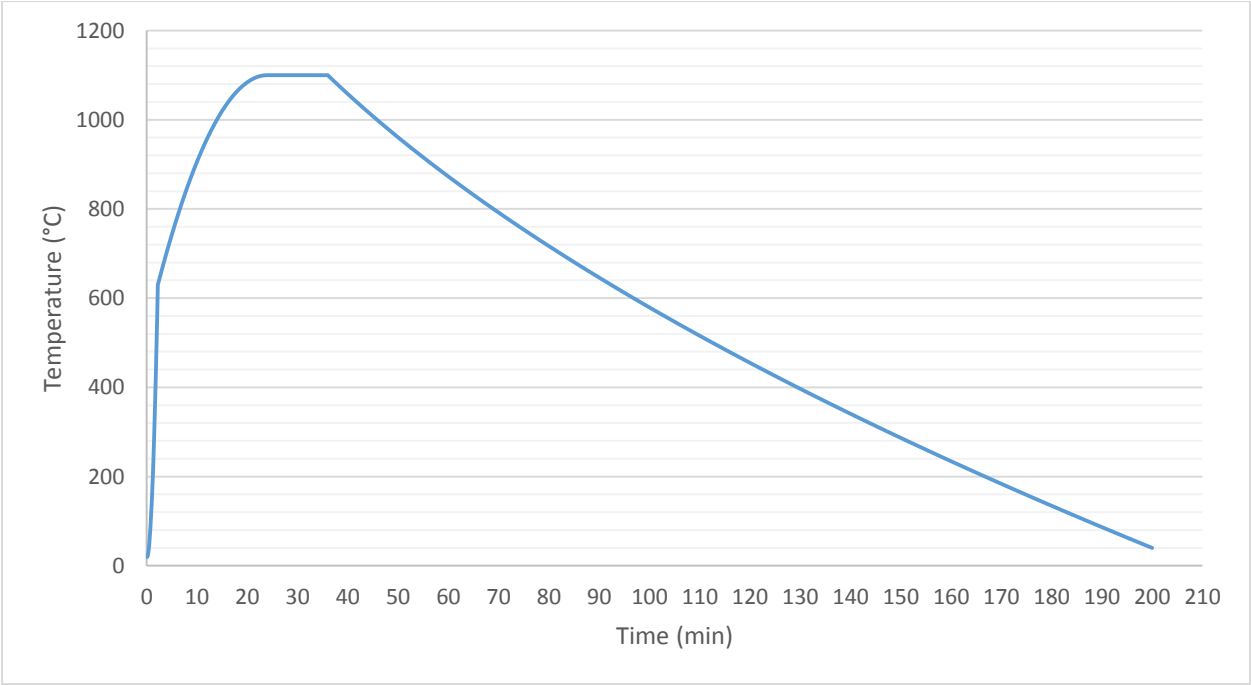

Figure 3.16 Non-Standard Time Temperature Curve used as exposure model for the series of tests conducted

3.5 Testing procedure

All eight glulam beams and connection types were fabricated in the atrium of the Carleton University Research Facility in Almonte, Carleton Place. The connections were then bolted to the steel columns by means of 3/8" shear tab plate with four ½ inch bolts.

The fabricated beam to be tested was then placed in the furnace and bolted to the steel columns at the ends. Following that, the thermocouples on the specimen, and LVDTs were hooked to the data acquisition system. Prior to igniting the burners, the beam was subjected to two – point constant gravity load at 1/3 points along its length. Ideally, this load was applied 30 minutes before the fire resistance test and maintained until failure of the specimen. A hydraulic jack connected to the load cell was used to apply and maintain the constant load. The load was transmitted through two distributing bars 700 mm apart attached to a vertical steel post and placed on the beam. Afterwards, the burners were ignited and the assembly was subjected to the modelled non-standard time – temperature curve until failure. Failure is characterised by a sudden drop in the applied constant load, and the inability of the specimen to sustain the desired load. Temperature readings in the furnace and within the specimen, as well as the mid-span and end deflections were monitored through the data acquisition system. The propane burners and blowers were then shut down after failure. To prevent further charring and smouldering combustion of the specimen, enough water was sprayed on the specimen immediately after shut down of the burners and blowers.

After the fire test, the layer of char was brushed off. Measurements of the residual width and height were then taken at various cross-sections along the length of the member for charring rate calculations.

4 RESULTS AND DISCUSSION

4.1 Introduction

Hybrid connections are employed in many structural applications involving structural steel, wood and concrete materials. In this research, the performance of hybrid connections involving glulam beams and steel columns are evaluated in real or non – standard fires.

In this experimental research, Exposed (EX), Concealed (CN) and Seated (SN) Connection types connecting structural members of glulam beam and steel columns were subjected to two point loading in bending, with load ratios of 60% and 100% under a non-standard/real time-temperature curve. As indicated in Chapter 3, Section 3.2 (Table 3.1), Tests 1 and 3 were stopped due to technical problems that were encountered. Presentation of the results therefore begins with Test 2.

4.2 Test 2 – Exposed Shear Tab Connection

Test 2 was conducted on the 8th of July, 2014 with the objective of evaluating the structural performance of an Exposed Shear Tab Connection System under 100% load ratio. The size of the glulam beam tested was 137 x 222 mm high. After the specimen fabrication, the beam was connected to the insulated steel column by means of the Exposed Shear Tab Connection as shown in Figure 4.1 using 4-1/2" (12.7 mm) diameter Grade 5 (ASTM A325) bolts. The measured average moisture content of the glulam beam was 10%.

Figure 4.1 Test 2 set up involving EX Connection system under 100% load ratio

4.2.1 Loading

Prior to igniting the burners, a load of 98 KN corresponding to 100% load ratio was applied to the beam at 10:40 am. This was done to induce internal stresses in the member as it is the case in structural members in real buildings before being engulfed by fire. This applied load was kept constant throughout the test until failure. As stated in the literature review, failure of the specimen is characterised by its inability to sustain the applied constant load. This is manifested by the sudden drop in the applied constant load on the load curve (Fig 4.2).

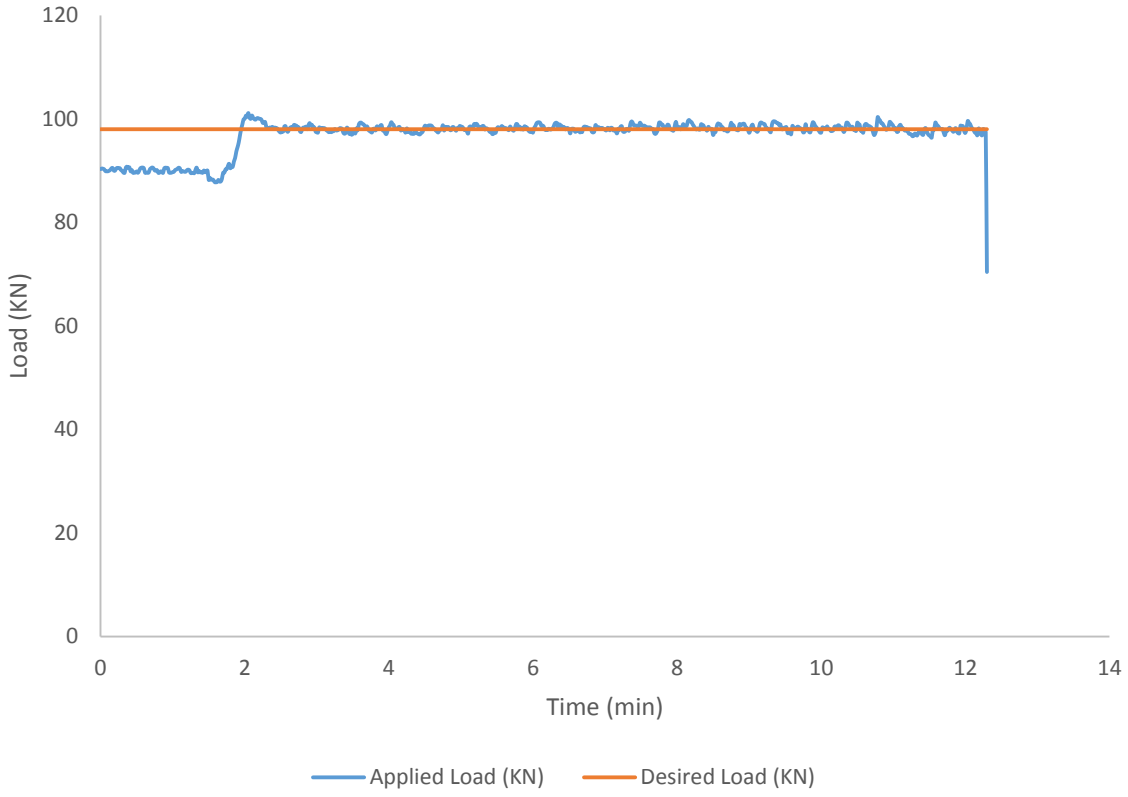

Figure 4.2 Graph of Desired and Applied Load vs Time (EX - 100%)

4.2.2 Furnace Temperature

The propane burners were ignited at 11:20 am to commence exposure of the loaded member to the non-standard time temperature curve. In order to control the temperature in the furnace to follow the modelled real time-temperature curve, thermocouples and plate thermometers connected to the data acquisition system were monitored to adjust the flow of propane gas into the furnace after ignition. This process was continued until failure of the beam.

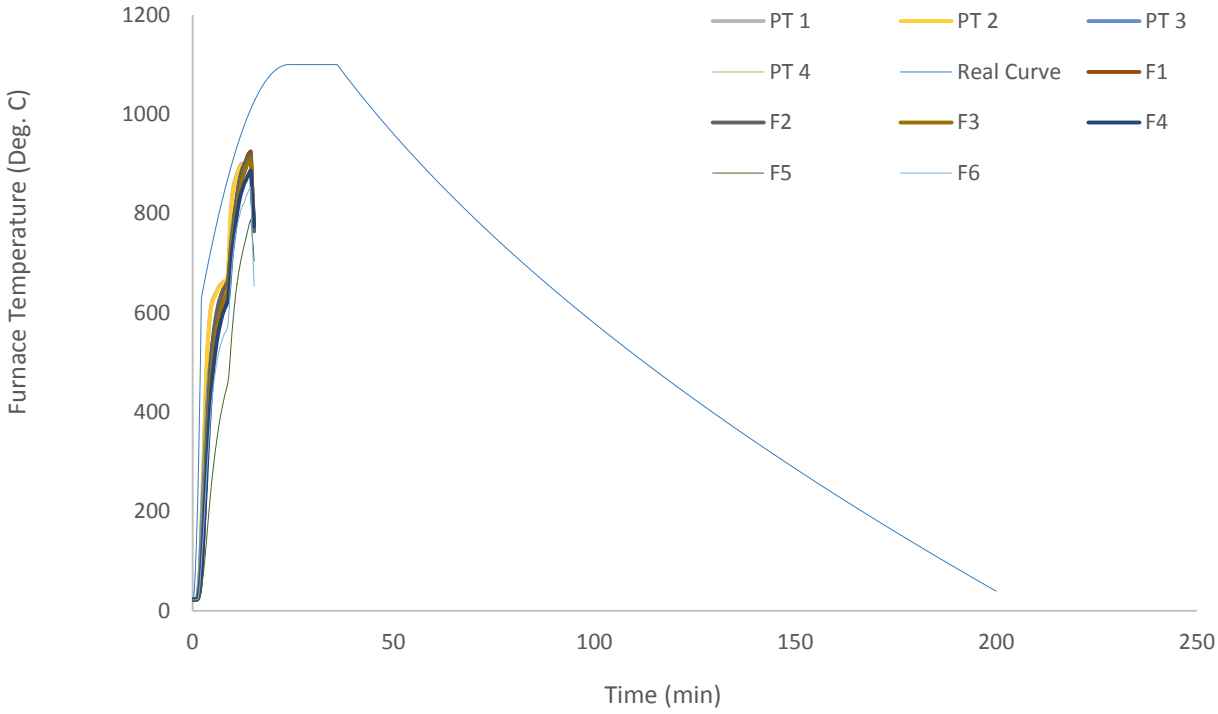

Figure 4.3 Furnace temperature as recorded by all thermometers

Figure 4.3 above shows the evolution of temperature within the furnace as recorded by installed thermocouples and plate thermometers. These temperature readings follow closely the desired real time-temperature curve. As shown in Figure 4.4, the average temperature readings of the plate thermometers are very close to the real-time temperature curve. The difference between that and the readings from the thermocouples is however insignificant. As can be seen from Figure 4.4, temperature in the furnace went as high as 825°C before failure of the beam and shut down of the burners.

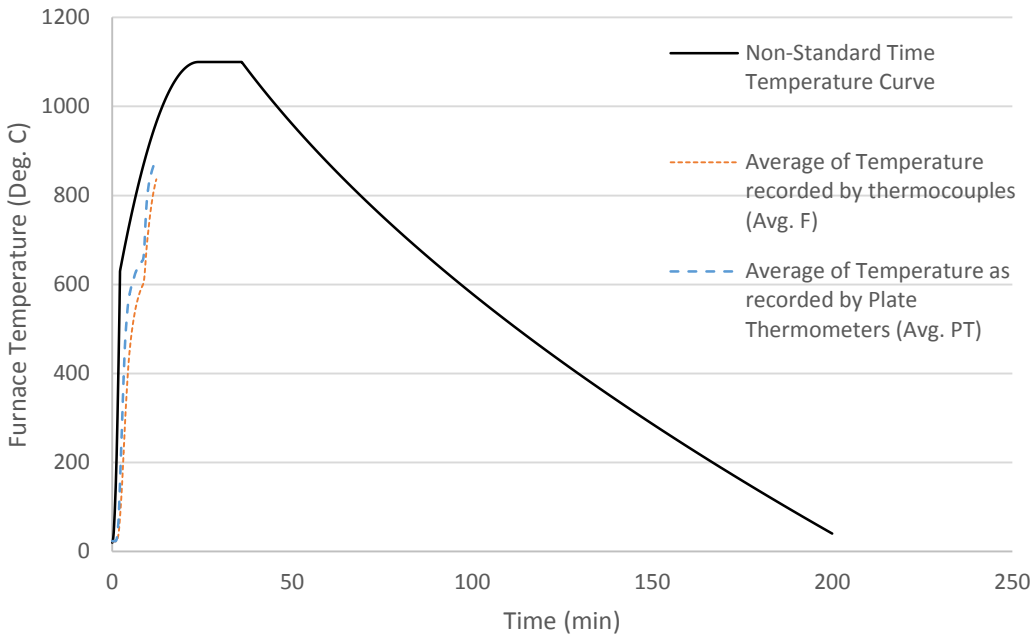

Figure 4.4 Average Furnace Temperature (EX - 100%)

4.2.3 Failure Mode and Failure Time

All beams were designed to fail at the connection end either by splitting along the grain or yielding of the bolts. The specimen in Test 2 endured the fire load and applied constant load for 12 minutes. Failure of the specimen was sudden and brittle. Though predicted to fail in splitting at the connection end, failure of the specimen was due to a combination of both splitting at the left connection end and bending failure directly under one of the loading plates. After the sudden drop in the applied constant load, and shutting down of the burners, it appeared that the specimen had failed in bending (Fig. 4.5). However, after taking out the bolts and brackets, the anticipated splitting failure which was hidden by the side plates and char was observed (Fig. 4.5 right). Splitting along the grain of the wood occurred just above the upper row of bolt holes (Fig. 4.6). The splitting failure was slightly above the glue line of one of the laminates. It was also observed that embedding of the bolts in the bolt holes was not severe (Fig. 4.6).

Figure 4.5 Failure mode of specimen in Test 2 (EX - 100%)

The accompanying bending failure at the tension side of the glulam beam manifested in the form of a rupture at the finger joint between laminates (Fig. 4.7 and 4.8).

Figure 4.6 Splitting along the grain at connection end (EX - 100%)

Figure 4.7 Fracture of beam at the tension side (EX - 100%)

Figure 4.8 Detailed view of fracture at the finger joint of glulam beam (EX - 100%)

4.2.4 Heat Transfer and Temperature Profile

In this section, the temperature distribution within the beam at sections close to the connection and at the mid-span is presented. These temperature profiles were recorded by various thin-wire thermocouples installed at various depths within the beam. As it can be seen in Figures 4.9 and 4.10, the temperature at sections of the beam close to the connection remained at ambient for the first 1-2 minutes of exposure. Thermocouples installed at 20 mm depth from the faces of the beam recorded very high temperatures at the time of failure of the specimen. As already discussed, failure of the specimen occurred at the left connection end. It is therefore expected that the

temperature readings at this connection were relatively higher compared to those at the right connection (Figs. 4.9 and 4.10). Figure 4.9 shows that temperatures near the front face of the beam ranged from 600°C to 800°C as recorded by thermocouples TF-22-20mm and TF-24-20mm, whilst temperatures close to the rear face ranged from 280°C to 380°C (TR-16-20mm and TR-17-20mm) at failure. Splitting of the beam at the left end was initiated at the front face of the beam.

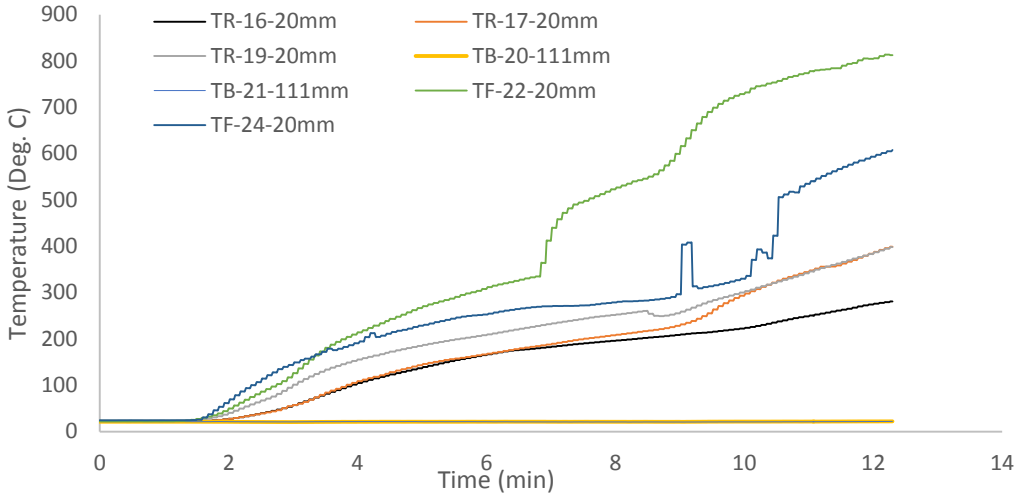

Figure 4.9 Temperature distribution at the left connection end of beam (EX - 100%)

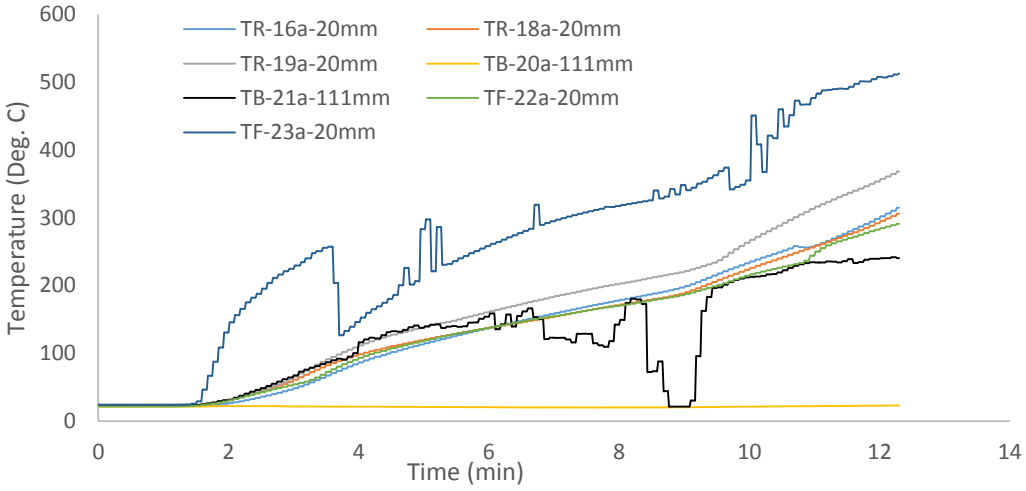

Figure 4.10 Temperature distribution at the right connection end of beam (EX - 100%)

Temperatures within the inner core of the beam remained at the initial temperatures throughout the test. There were significant fluctuations in temperature readings by thermocouples TF-23a-20mm and TB-21a-111mm at the right connection end at failure (Fig. 4.10). At failure temperatures near the right connection end ranged between 200°C to 300°C, with TF-23a-20mm recording as high as 500°C.

A graph of average temperature-depth with time at the connections is presented in figure 4.11. At 20 mm depth from the sides of the beam at the connection end, the temperature ranges from 360 to710°C immediately after time to failure of approximately 12 minutes. Within the core of the beam, no significant changes in the measured temperatures were recorded from the onset of testing to failure.

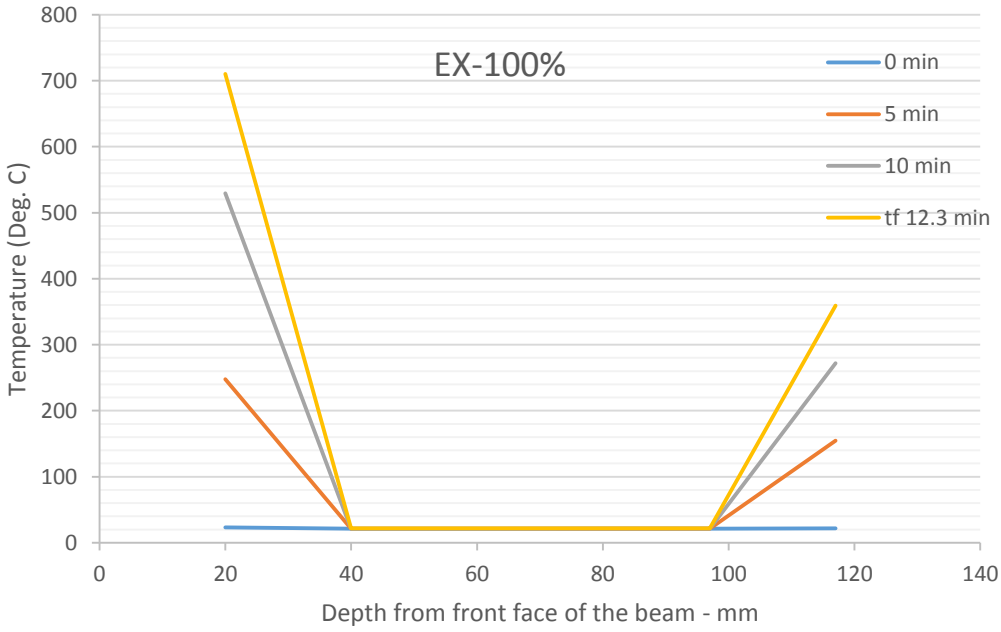

Figure 4.11 Temperature-depth distribution against time (EX-100%)

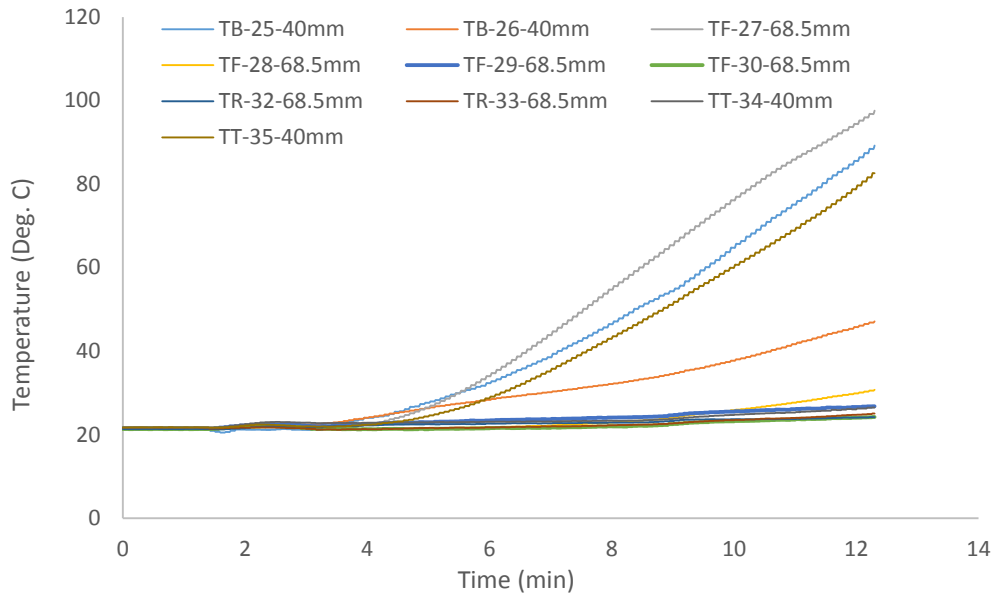

Figure 4.12 Temperature distribution at the mid-span of beam (EX - 100%)

Unlike the temperatures at the connection ends, temperatures at the mid-span of the beams were relatively lower, not exceeding 100°C at failure (Fig. 4.12). Thermocouples installed at mid-section, 68.5 mm, of the beam from the outer surface remained at ambient.

4.2.5 Charring Rate

Charring rate is an important parameter in evaluating the reserve strength of timber members after exposure to fire. In this research, the charring rate was calculated by two main ways:

- Temperature profile within beams: The time (min) taken for the char isotherm (300°C) to reach the depth at the tip of thermocouples was divided by the depth (mm). This provided the distance traveled by the char front to the particular depth of installed thermocouple per minute. The average of all such values is then taken as the average char rate (mm/min). The second method, often referred to as the real charring rate (mm/min) computes the charring rate from the reduced cross-section of the specimens and the time to failure. The

beam was divided into three sections involving the two connection ends and the mid-span. The residual width, and char depth was measured for each cut section, and the ratio between that and the time to failure gives the charring rate. The average of the three values is found as the real charring rate of the beam.

Table 4.1 Average charring rate of beam as computed from the Temperature Profile plots (EX-100%)

Section of beam	Depth (mm)	Thermocouple	Time to 300°C (min)	Charring Rate (mm/min)
Connection End (Close to furnace door)	20	*TR-16-20mm*	12.3	1.63
		TR-17-20mm	10.2	1.96
		TR-19-20mm	10	2.00
		TF-22-20mm	6	3.33
		TF-24-20mm	9	2.22
	111	*TB-20-111mm*	n/a	n/a
		TB-21-111mm	n/a	n/a
Mid-Span	40	*TB-25-40mm*	n/a	n/a
		TB-26-40mm	n/a	n/a
		TT-34-40mm	n/a	n/a
		TT-35-40mm	n/a	n/a
	68.5	*TF-27-68.5mm*	n/a	n/a
		TF-28-68.5mm	n/a	n/a
		TF-29-68.5mm	n/a	n/a
		TF-30-68.5mm	n/a	n/a
		TR-32-68.5mm	n/a	n/a
		TR-33-68.5mm	n/a	n/a
Connection End	20	*TR-16a-20mm*	12	1.67
		TR-18a-20mm	12.2	1.64
		TR-19a-20mm	11	1.82
		TF-22a-20mm	12.2	1.64
		TF-23a-20mm	7.2	2.78
	111	*TB-20a-111mm*	n/a	n/a
		TB-21a-111mm	n/a	n/a
			Average char rate =	**2.07**

Table 4.1 presents the average charring rate as computed from the time taken for the installed thermocouples to record a temperature value of 300°C. The average charring rate for the Exposed Connection System under 100% load ratio was found to be 2.07 mm/min.

Figure 4.13 Measurement of residual cross-section for charring rate computations (EX - 100%)

After clearing off the char from the burnt wood, measurements of the residual cross-section at each cut section was taken (Fig. 4.13). Based on these, the real charring rate at both connection ends and the mid-span of beam were computed (Table 4.2).

Table 4.2 Real charring rate (mm/min) as measured from the reduced cross-section of beams (EX-100%)

Length	1880	mm	
thickness	137	mm	
Height	222	mm	
t_f	12.3	min	
LR	100%		
Calculating char rate			
	Connection End	**Mid-span**	**Connection End (Close to furnace door)**
Thickness of residual section	108.7	109.3	108.3
Char depth, c (mm)	14.1	13.8	14.3
Char rate (mm/min) at different sections	1.15	1.12	1.17
Average Thickness of residual section(mm)	108.8		
Average char depth, c (mm)	14.10		
Real Char Rate β (mm/min)	**1.15**		

The char rate at the connection averaged at 1.16 mm/min whilst that at the mid-span of the beam was 1.12 mm/min. This demonstrates that the exposed steel plates do not affect the char rate. Thermo-hydric reaction at the interface between steel and wood at the temperature close to that at which bound water in wood evaporates delays transfer of heat from the exposed plate to the wood. This phenomenon delays the travel rate of the char front from the exposed surface of wood to the inner core at the connection end, and could be responsible for the relatively smaller difference between the char rates at the connection ends and that at the mid-span. Transfer of heat flux from the exposed steel side plates and bolts account for the high charring rate at the connections. An average char layer of 14.10 mm was recorded for the beam which corresponds to charring rate of 1.15 mm/min. About 21% of the cross-section width was converted to char.

4.3 Test 4 – Exposed Shear Tab Connection

On the 18th of July, 2014, Test 4 was conducted on a 137 x 222 mm glulam beam to evaluate the performance of the Exposed Shear Tab Connection System under a 60% load ratio. After setting up the beam in the furnace, a moisture content of 9% was measured.

Figure 4.14 Test 4 set up before and after testing (EX-60%)

4.3.1 Loading

At 10:35 am, a static load of 59 KN corresponding to 60% load ratio was applied on the test assembly. The assembly was subjected to this constant load for almost 2 hours 30 minutes before starting the test. This applied load was kept constant throughout the test until failure. (Fig 4.15).

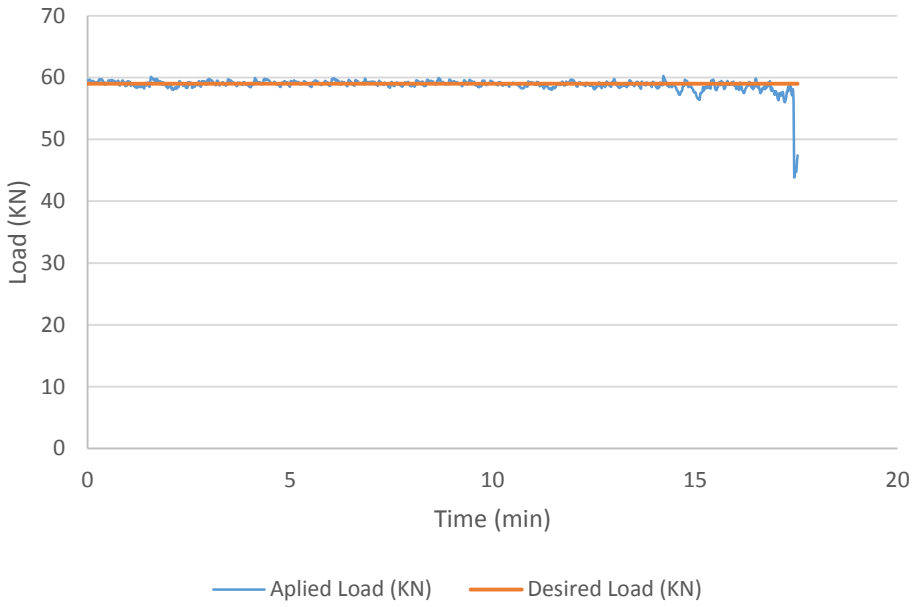

Figure 4.15 Graph of Desired and Applied Load vs Time (EX - 60%)

4.3.2 Furnace Temperature

At 1:00 pm, the propane burners were ignited. Figures 4.16 and 4.17 show the measured furnace temperatures as recorded by the thermocouples and the plate thermometers. As it can be seen from both curves, the initial growth stages of the fire curve are accurately reproduced in the furnace. Slight deviations from the non-standard time temperature curve were observed after approximately 400°C (Fig. 4.18). After flashover temperature, the plate thermometers were more accurate in reproducing the desired fire curve compared to the thermocouples. Temperatures in the furnace measured by the plate thermometers reached to above 1000°C before failure of the specimen.

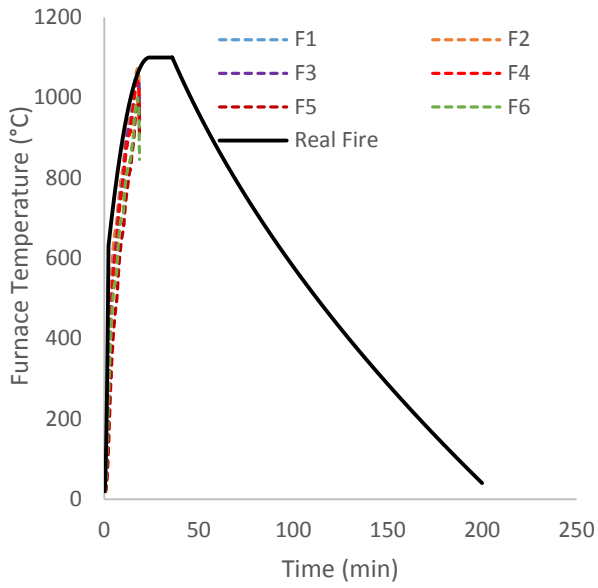

Figure 4.16 Furnace temperature as recorded by thermocouples (EX-60%)

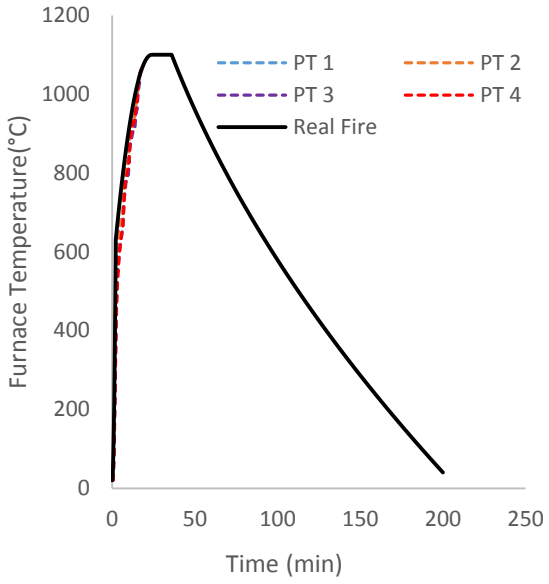

Figure 4.17 Furnace temperature as recorded by plate thermometers (EX-60%)

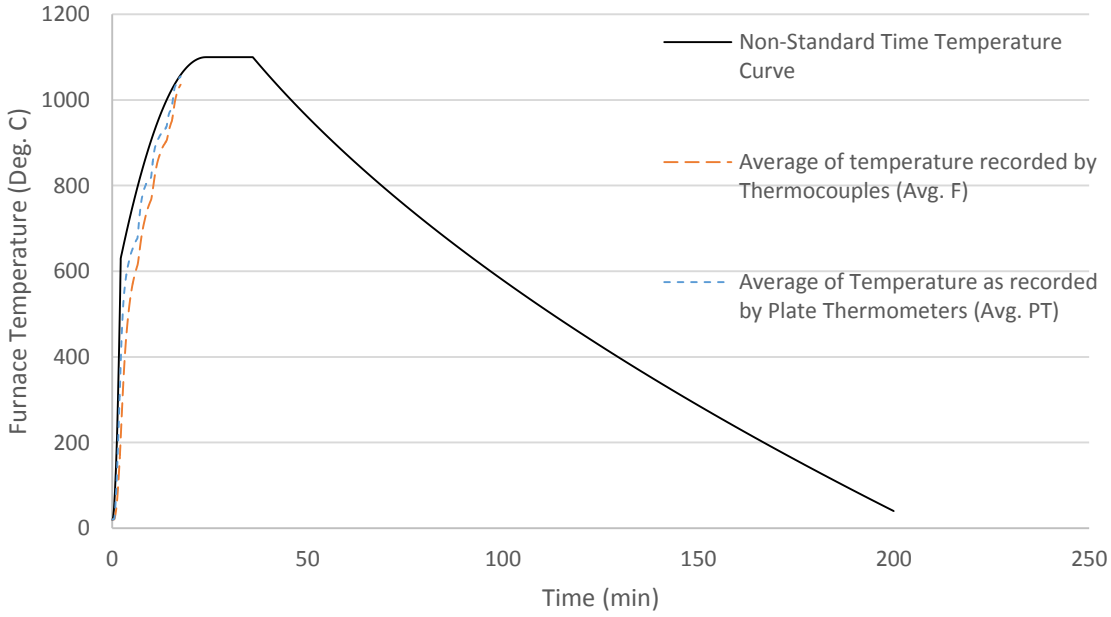

Figure 4.18 Average Furnace Temperature (EX - 60%)

4.3.3 Failure Mode and Failure Time

The specimen of test 4 was predicted to fail by splitting along the grain at the connection end. Test 4 sustained the fire load for 18 minutes. Reduction of the load ratio by 40% had resulted in an increase of the time to failure by 50%. Failure of the specimen was sudden and brittle, as the left connection end of wood split at sections just below the bottom row of bolts (Fig. 4.20). This longitudinal split stretched almost half the span of the beam. It was wide enough to expose the interior sections in the split to the high furnace temperature (Fig. 4.19).

Figure 4.19 Extent of splitting failure of beam (EX-60%)

Figure 4.20 Splitting of wood below bottom row of bolts (EX-60%)

The brackets experienced quite an amount of deformation as it can be seen in Figure 4.20. Embedment of bolts were quite severe at the splitting end of the beam (Fig. 4.21).

Figure 4.21 Embedding of bolts at connection ends of beam (EX - 60%)

4.3.4 Heat Transfer and Temperature Profile

The temperature distribution within the beam was measured at the two connection ends and at the mid-span. At the connections, temperatures in the interior of the beam remained at ambient, as shown by the readings of thermocouples TB-20, TB-21, TB-20a and TB-21a in Figures 4.22 and 4.23. These thermocouples were installed at 111 mm deep from the bottom face of the beam. Thermocouples installed close to the exposed surface of the beam (TF-22-20mm and TR-19a-20mm) recorded temperatures as high as 800 and 900°C at the left and right connections respectively. The temperatures close to the top face of the beam were as low as 200°C (TF-24-20mm and TF-23a-20mm). The exposed sides and bottom of the beam is exposed to radiative heat flux from all corners of the furnace room, as well as heat transfer from the brackets and bolts. This accounts for the significant difference in temperature readings between the exposed sides and the top face which was covered with a layer of insulating material. The temperatures recorded by thermocouples at both connection ends show similar trends.

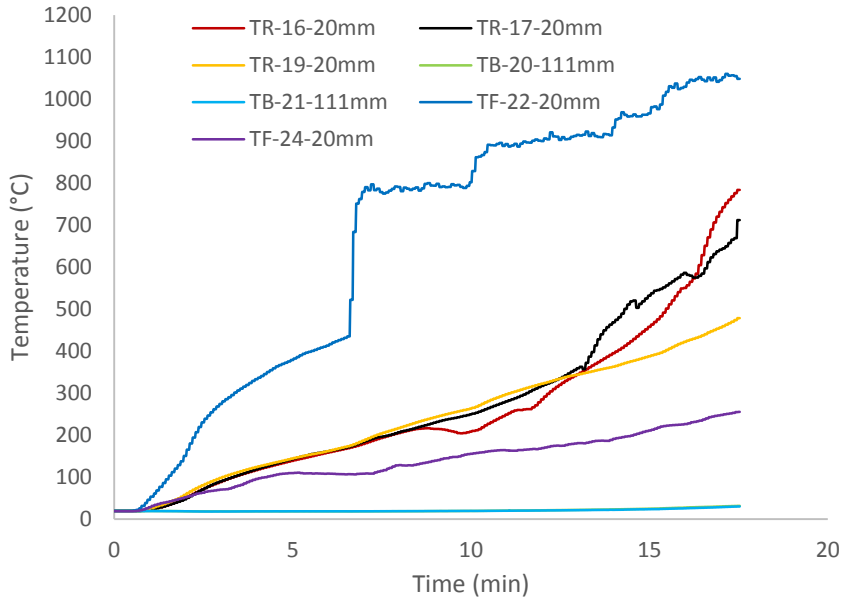

Figure 4.22 Temperature profiles at the left connection end of beam (EX - 60%)

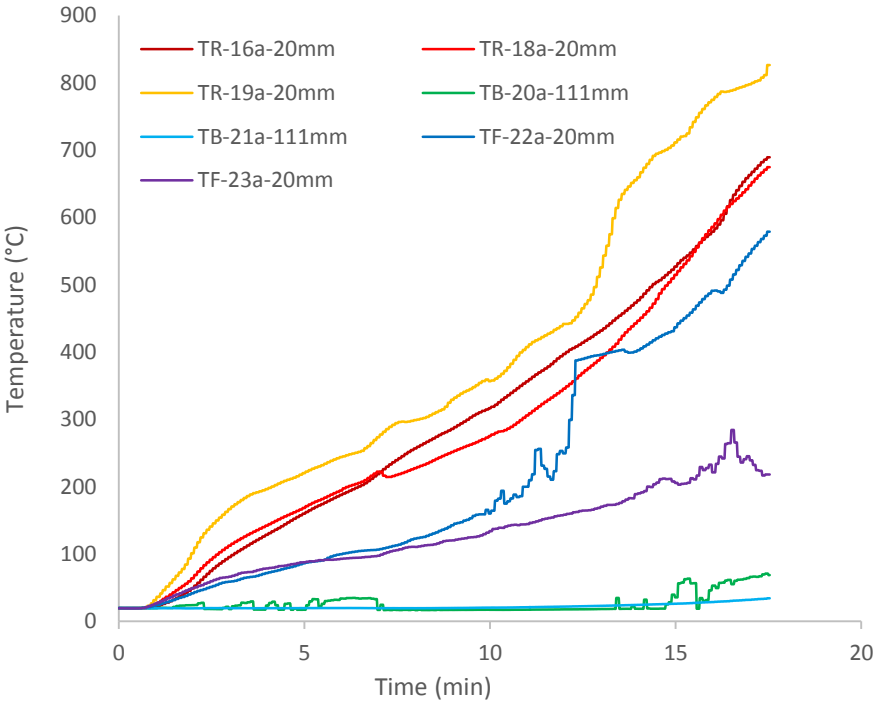

Figure 4.23 Temperature profiles at the right connection end of beam (EX - 60%)

Compared to the connection ends, temperatures at the mid-span were much lower peaking at 250°C (TB-25-40mm) at failure at 40 mm depth from the bottom face and 20 mm depth from the front face (Fig. 4.24). At the mid-span of the beam, TT-35-40mm installed 20 mm from the front face of the beam recorded a temperature of about 230°C at failure. This value is similar to that recorded by TF-23a-20mm which was located at the connection end at 20 mm from the front face and 40 mm from the top face. Temperature within the inner core at 68.5 mm depth from the sides remained at ambient.

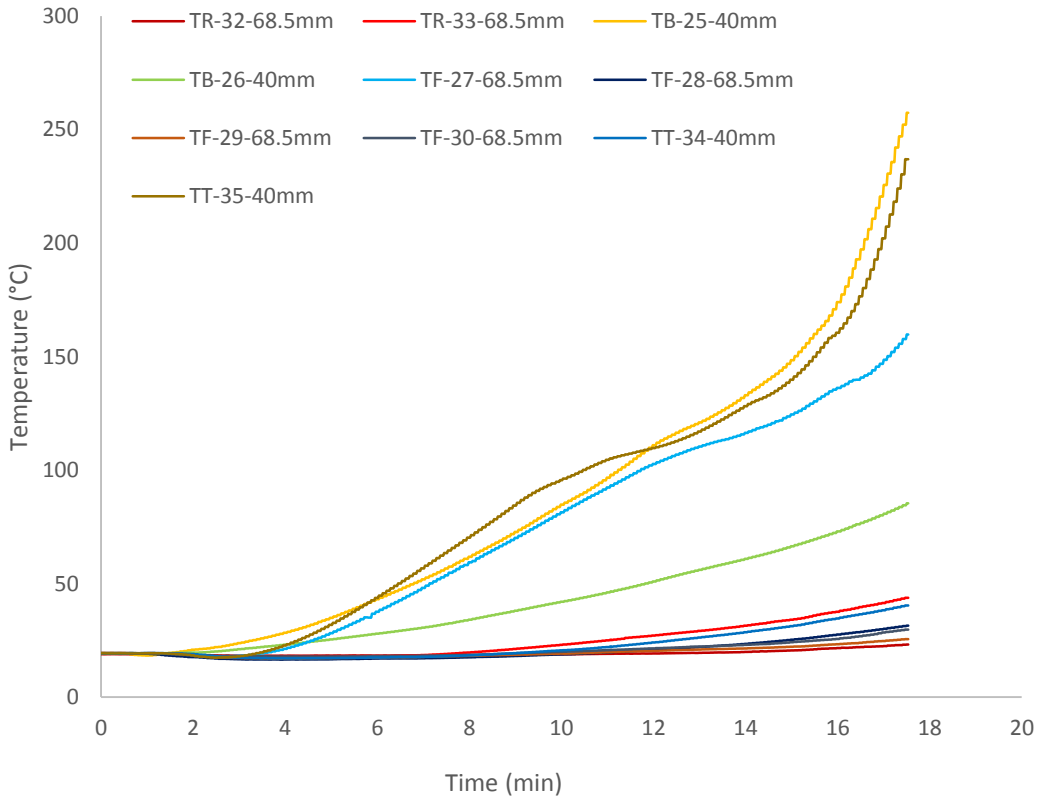

Figure 4.24 Temperature distribution at the mid-span of beam (EX - 60%)

A graph of average temperature-depth with time at the connection ends is presented in Figure 4.25. At failure, an average temperature of 650°C was recorded at 20 mm depth from the face of the beam at the connections. Temperature distribution at depths within the cross-section ranging from 40 – 100 mm stayed at almost ambient.

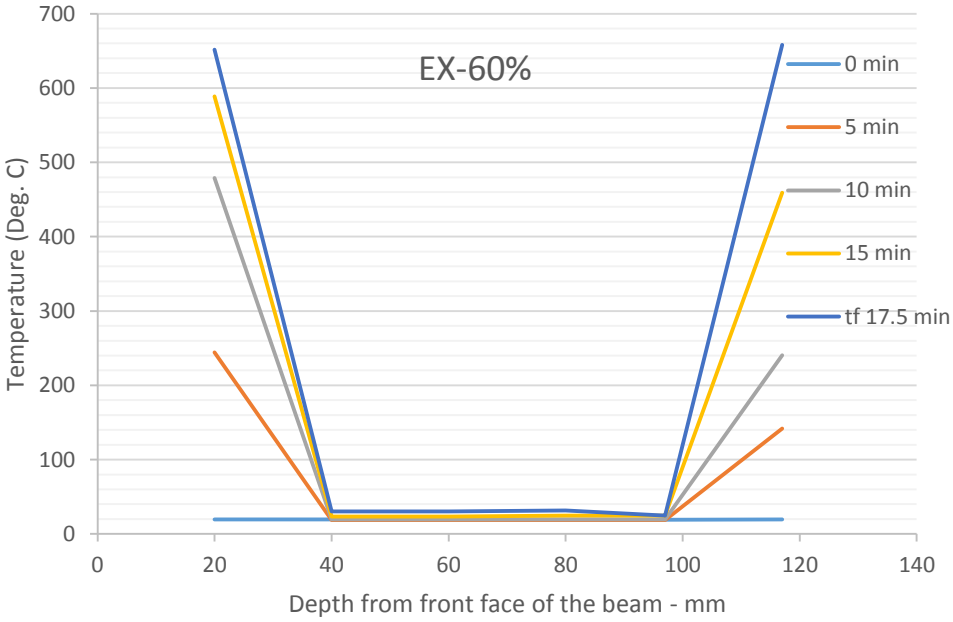

Figure 4.25 Temperature-depth distribution against time (EX-60%)

4.3.5 Charring Rate

The char rates were computed from the plots of temperature distribution and residual cross-section measurements. From Table 4.3, an average char rate of 2.96 mm/min and 1.14 mm/min was found for the right and left connection ends of the beam respectively. The unusual higher value recorded at the right connection end close to the furnace door is as a result of thermocouple TF-22-20mm reading 300°C at quite an early time of exposure of 3 minutes. (Fig. 4.22). Thermocouples installed at depths in mid-span of the beam recorded temperatures less than 300°C. As such the average

char rate at the mid-span could not be calculated by this method. The average char rate of the exposed assembly beam under 60% load ratio was calculated to be 2.50 mm/min.

Table 4.3 Average charring rate of beam as computed from Temperature Profile plots (EX-60%)

Specimen	Section of beam	Depth (mm)	Thermocouple	Time to 300°C (min)	Charring Rate (mm/min)
4	Connection End (Close to furnace door)	20	*TR-16-20mm*	12	1.67
			TR-17-20mm	12	1.67
			TR-19-20mm	11	1.82
			TF-22-20mm	3	6.67
			TF-24-20mm	n/a	n/a
		111	*TB-20-111mm*	n/a	n/a
			TB-21-111mm	n/a	n/a
	Mid-span	40	*TB-25-40mm*	n/a	n/a
			TB-26-40mm	n/a	n/a
			TT-34-40mm	n/a	n/a
			TT-35-40mm	n/a	n/a
		68.5	*TF-27-68.5mm*	n/a	n/a
			TF-28-68.5mm	n/a	n/a
			TF-29-68.5mm	n/a	n/a
			TF-30-68.5mm	n/a	n/a
			TR-32-68.5mm	n/a	n/a
			TR-33-68.5mm	n/a	n/a
	Connection End	20	*TR-16a-20mm*	9	2.22
			TR-18a-20mm	11	1.82
			TR-19a-20mm	8	2.50
			TF-22a-20mm	12	1.67
			TF-23a-20mm	n/a	n/a
		111	*TB-20a-111mm*	n/a	n/a
			TB-21a-111mm	n/a	n/a
				Average char rate =	**2.50**

The real charring rate at the connection ends as computed from the reduced cross-section dimensions (Fig. 4.26) was found to be 1.04 mm/min (Table 4.4). At the mid-span the charring rate was computed to be 1.08 mm/min. An average char depth of 18.4 mm and a corresponding

average real charring rate of 1.05 mm/min was estimated for the Exposed Shear Tab Connection under 60% load ratio. About 27% of the cross-section width was converted to char. The sensitivity of the thermocouples in measuring the temperature profiles can have a significant effect on the calculated char rates. As it can be seen in Figure 4.22, the sudden rise in the temperature profile of thermocouple TF-22-20mm resulted in a computed high charring rate of 6.67 mm/min (Table 4.3), accounting for the big difference between the two char rate values reported earlier.

Figure 4.26 Typical residual cross-section been prepared for real charring rate computations (EX - 60%)

Table 4.4 Real charring rate (mm/min) as measured from the reduced cross-section of beams (EX-60%)

Length	1880	mm	
thickness	137	mm	
Height	222	mm	
t_f	17.53	min	
LR	60%		
Calculating char rate			
	Connection End	**Mid-span**	**Connection End (Close to furnace door)**
Thickness of residual section	99.5	99.1	101.8
Char depth, c (mm)	18.7	18.9	17.5
Char rate (mm/min) at different sections	1.07	1.08	1.00
Average Thickness of residual section(mm)	100.15		
Average char depth, c (mm)	18.42		
Real Char Rate β (mm/min)	**1.05**		

4.4 Test 5 – Concealed Shear Tab Connection

In Test 5, the fire performance of the Concealed Shear Tab connection under 60% load ratio was investigated. A 140 x 191 mm glulam beam was set-up in the furnace and tested on the 23rd of July, 2014. A moisture content of 10% was measured for the specimen. Figure 4.27 shows the test assembly in the furnace before testing.

Figure 4.27 Test 5 set up before testing (CN-60%)

4.4.1 Loading

A static constant load of 43 KN corresponding to 60% of the splitting capacity (Refer to Appendix B) of the beam was applied at noon. This load was applied for an hour and twenty minutes before commencement of the furnace test. Figure 4.28 presents the accuracy of the applied load curve as compared to the desired one.

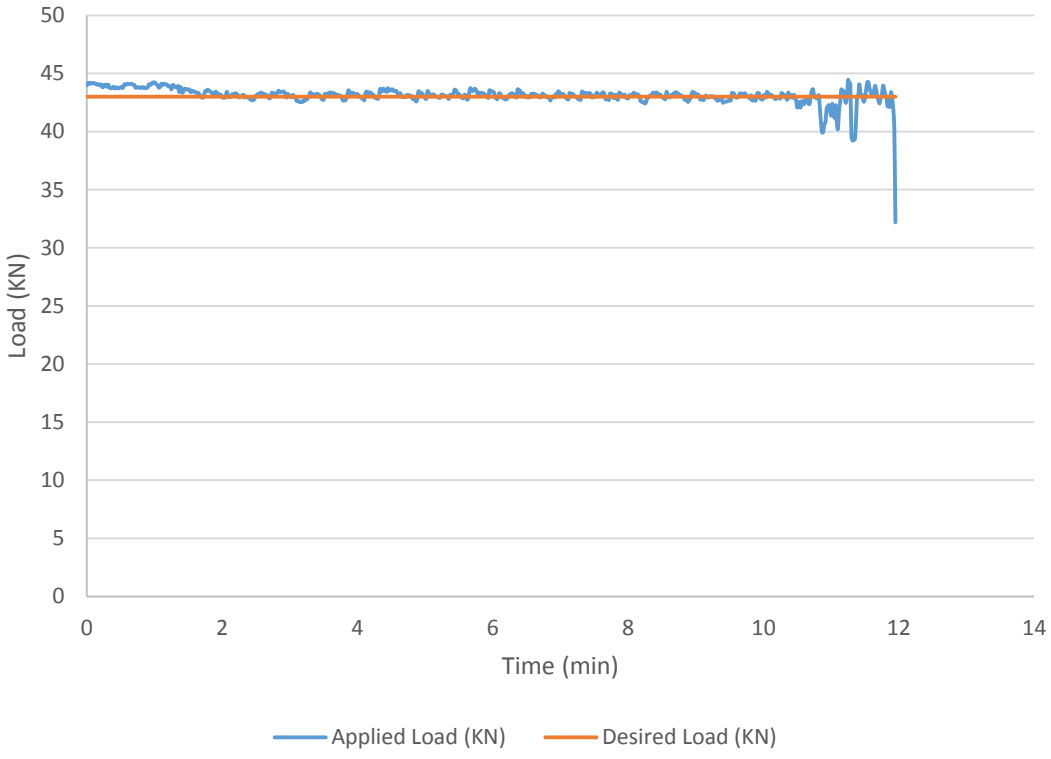

Figure 4.28 Graph of Desired and Applied Load vs Time (CN - 60%)

4.4.2 Furnace Temperature

The furnace test began an hour and twenty minutes after applying the constant static load. The furnace temperature was measured by the thermocouples and plate thermometers as shown in Figures 4.29 and 4.30.

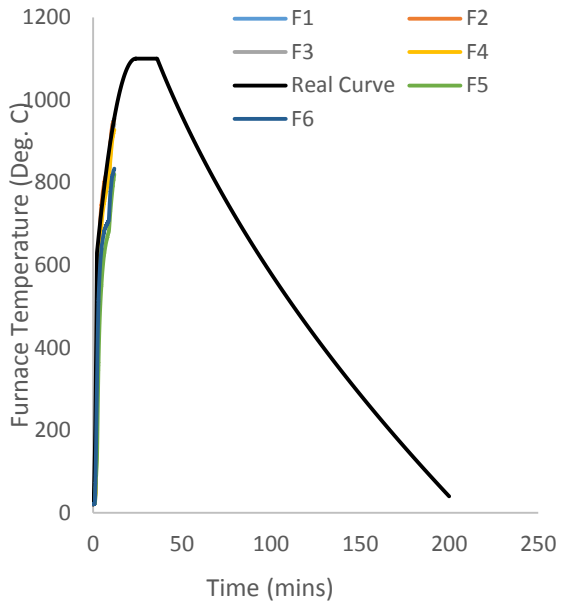

Figure 4.29 Furnace temperature as recorded by the thermocouples (CN-60%)

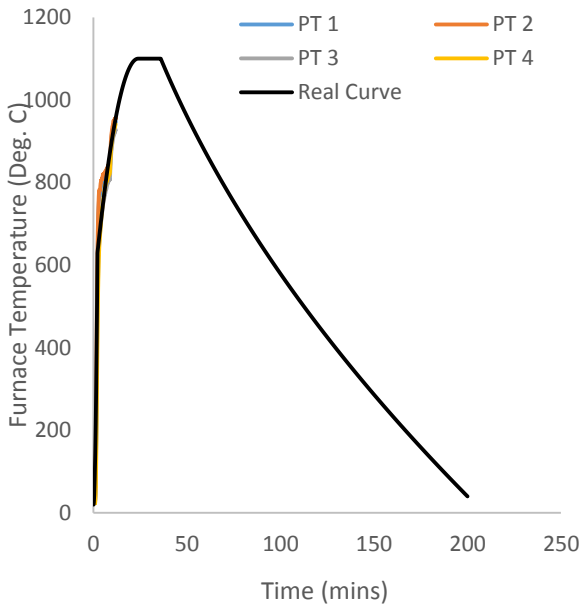

Figure 4.30 Furnace temperature as recorded by the plate thermometers (CN-60%)

From the readings of the thermocouple and the plate thermometer depicted in Figures 4.29 and 4.30 as well as the average temperature shown in Figure 4.31, it can be seen that the non-standard time temperature curve was followed closely. Furnace temperatures went as high as 930°C before the failure of the specimen.

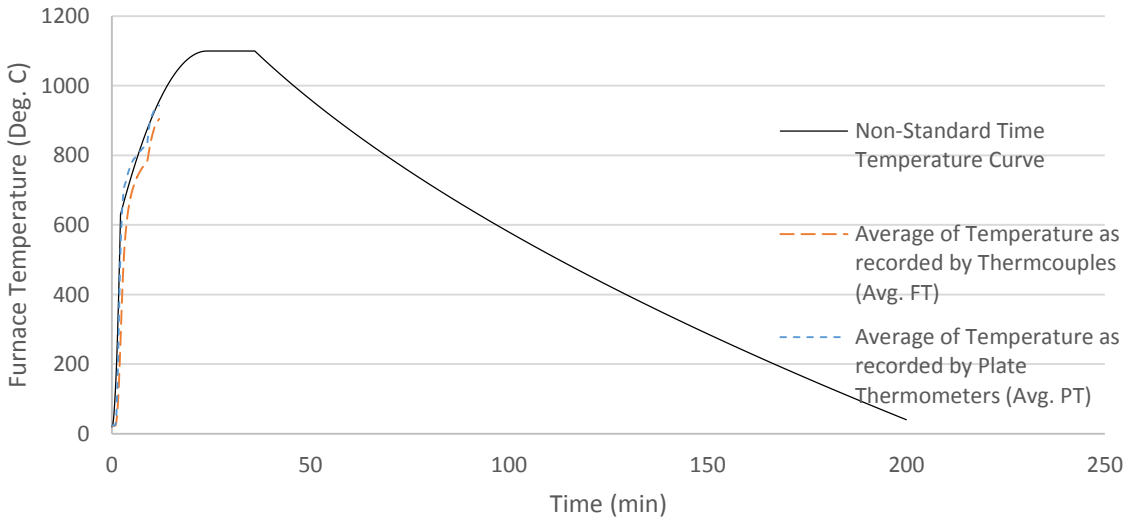

Figure 4.31 Average Furnace Temperature (CN - 60%)

4.4.3 Failure Mode and Failure Time

The specimen of Test 5 was predicted to fail by splitting along the grain at the joint. As expected, sudden splitting failure of the beam occurred after an exposure time of 12 minutes. This failure mode was prevalent at the left connection just underneath the bottom row of bolts (Fig. 4.32).

Figure 4.32 Splitting failure prevalent at left joint (CN-60%)

Figure 4.33 Splitting failure exposing inner core of beam (CN-60%)

After splitting, the inner core of the beam joint, within the notch was exposed to the heat fluxes from the still burning flames (Fig. 4.33), which would affect charring of sections close to the

connection. After clearing the char layer, it was realised that splitting of the beam had also commenced at the right connection end (Fig. 4.34 and 4.35). Splitting was initiated above the top row of bolt holes. Splitting failure did not initiate at the glue line of the laminates.

Figure 4.34 Splitting failure of beam with char on (CN-60%)

Figure 4.35 Splitting failure as seen after clearing off char layer (CN-60%)

4.4.4 Heat Transfer and Temperature Profiles

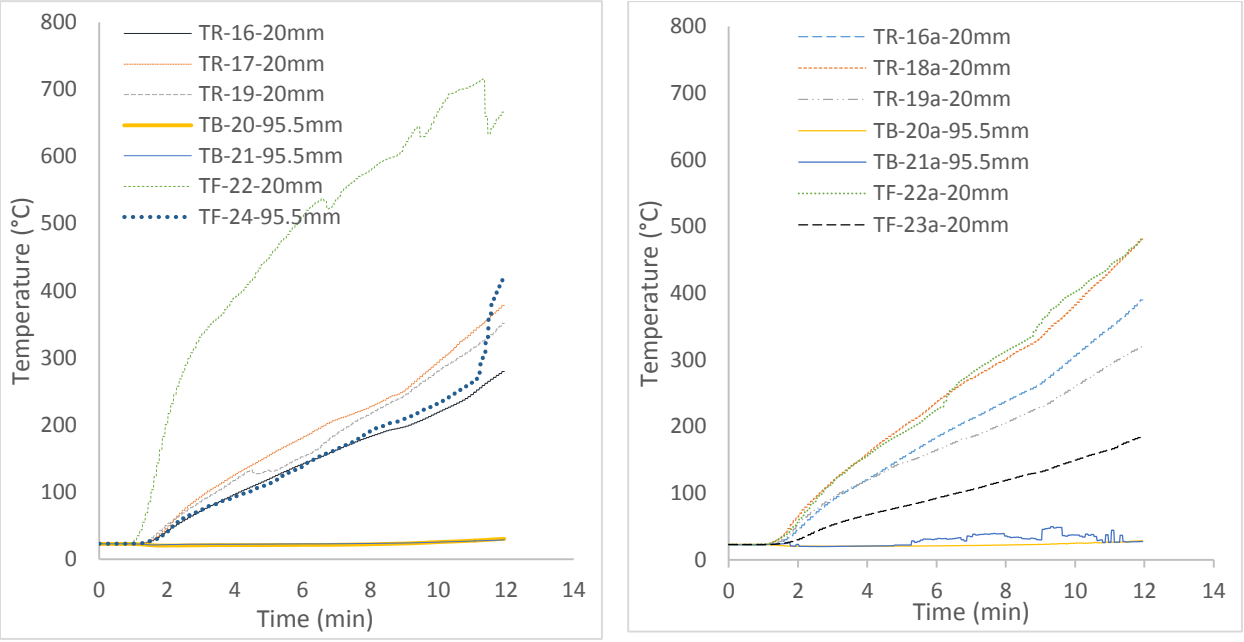

(a) (b)

Figure 4.36 Temperature distribution at (a) the left connection (b) right connection end of beam (CN- 60%)

In Figure 4.36, temperature profiles close to the connection is presented. Temperatures started to rise a minute after igniting the burners. At failure, the temperatures at 20 mm depth from the exposed surface ranged from 185°C to 700°C. With the exception of TF-22-20mm which recorded very high temperatures, temperatures at both connection ends were similar.

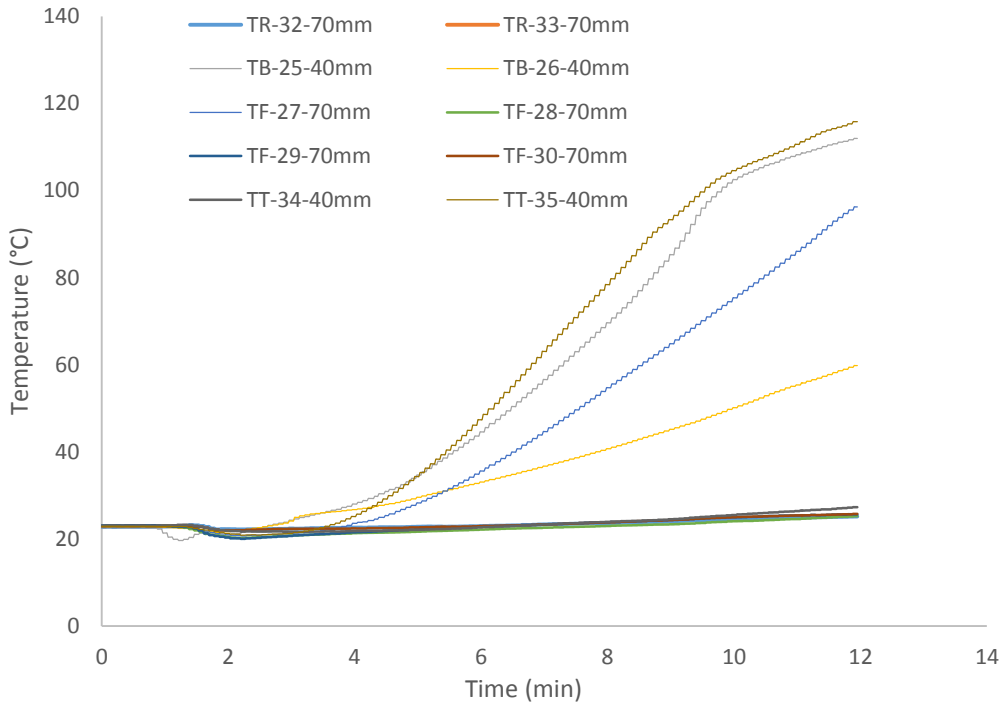

Figure 4.37 Temperature distribution at the mid-span of beam (CN - 60%)

At the mid-span of the beam, temperatures at 20 mm from the exposed sides peaked at 115°C at failure (Fig. 4.37). TB-25-40mm installed close to the bottom face of the beam at 20 mm depth from the rear face recorded a temperature of 115°C at failure. Compared to the temperatures at the connections, temperatures at the mid-span were much lower, and started to rise after almost 4 minutes of exposure.

Figure 4.38 shows the average temperature-depth distribution with time at the connection ends. At failure, an average temperature range of 350 - 450°C was measured 20 mm from the exposed sides. Temperature within the inner core from 40 mm to 100 mm depth from the front face rose slightly above ambient at the failure time of 12 minutes.

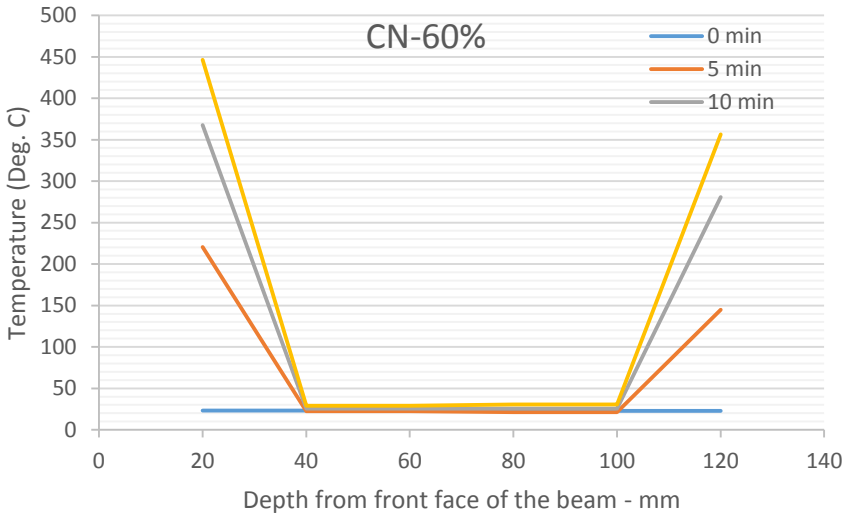

Figure 4.38 Temperature-depth distribution against time (CN-60%)

4.4.5 Charring Rate

An average charring rate of 3.01 mm/min was found for the connection end close to the furnace door as compared to 2.21 mm/min for the right connection end of the beam. An overall average charring rate of 2.64 mm/min was recorded for the beam connected to the steel columns using Concealed Shear Tab Connection under 60% load ratio (Table 4.5).

The thickness of char layer at sections close to the connection averaged 16.5 mm (Table 4.6), while the thickness at the mid-span was 15.3 mm. The real charring rate at the split end of beam was estimated to be 1.43 mm/min, and 1.34 mm/min at the other connection. An average real charring rate of 1.28 mm/min was measured for the mid-span. The average char rate at the connection was found to be 1.39 mm/min. From Table 4.6, the average thickness of the residual cross-section was 108 mm with a corresponding char rate of 1.35 mm/min at failure. The sensitivity of thermocouple TF-22-20mm could be responsible for the big difference in char rates measured from the temperature profiles and the reduced cross-section (Fig. 4.36 (a) and Table 4.5).

Table 4.5 Average charring rate of beam as computed from Temperature Profile plots (CN-60%)

Specimen	Section of beam	Depth (mm)	Thermocouple	Time to 300°C (min)	Charring Rate (mm/min)
5	Connection End (close to furnace door)	20	*TR-16-20mm*	n/a	n/a
			TR-17-20mm	10	2.00
			TR-19-20mm	11	1.82
			TF-22-20mm	3	6.67
			TF-24-20mm	11	1.82
		95.5	*TB-20-111mm*	n/a	n/a
			TB-21-111mm	n/a	n/a
	Mid-span	40	*TB-25-40mm*	n/a	n/a
			TB-26-40mm	n/a	n/a
			TT-34-40mm	n/a	n/a
			TT-35-40mm	n/a	n/a
		70	*TF-27-68.5mm*	n/a	n/a
			TF-28-68.5mm	n/a	n/a
			TF-29-68.5mm	n/a	n/a
			TF-30-68.5mm	n/a	n/a
			TR-32-68.5mm	n/a	n/a
			TR-33-68.5mm	n/a	n/a
	Connection End	20	*TR-16a-20mm*	10	2.00
			TR-18a-20mm	8	2.50
			TR-19a-20mm	11	1.82
			TF-22a-20mm	8	2.50
			TF-23a-20mm	n/a	n/a
		111	*TB-20a-111mm*	n/a	n/a
			TB-21a-111mm	n/a	n/a
				Average char rate =	**2.64**

Table 4.6 Real charring rate (mm/min) as measured from the reduced cross-section of beams (CN-60%)

Length	1880	mm
thickness	140	mm
Height	191	mm
t_f	11.95	min
LR	60%	

Calculating char rate			
	Connection End	**Mid-span**	**Connection End (Close to furnace door)**
Thickness of residual section	105.8	109.3	108
Char depth, c (mm)	17.08	15.3	16.00
Char rate (mm/min) at different sections	1.43	1.28	1.34
Average Thickness of residual section(mm)	107.72		
Average char depth, c (mm)	16.14		
Real Char Rate β (mm/min)	**1.35**		

4.5 Test 6 – Concealed Shear Tab Connection

On the 29th of July, 2014, Test 6 was conducted to investigate the fire performance of the Concealed Shear Tab Connection Assembly under the full ultimate load. The glulam sample tested had a dimension of 140 x 191 mm. The moisture content of the specimen was 9%.

4.5.1 Loading

A static constant load of 71.8 KN corresponding to 100% of the splitting capacity of the beam was applied at 10:40 am, 66 minutes prior to starting the furnace test. Figure 4.39 presents a graph of the desired load and the applied constant load with time.

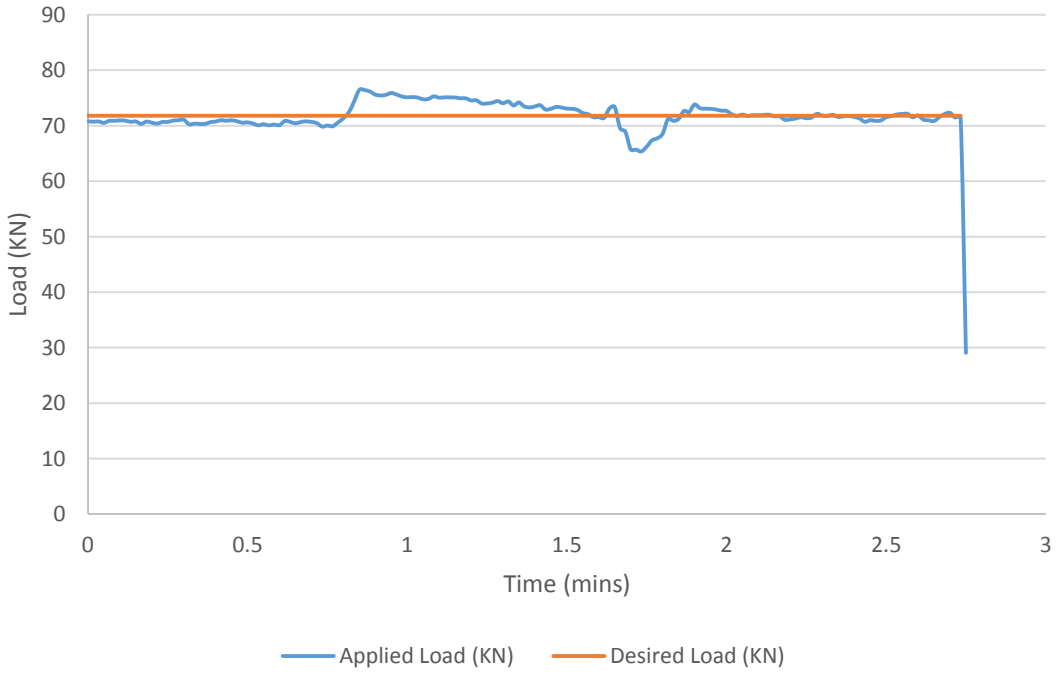

Figure 4.39 Graph of Desired and Applied Load vs Time (CN - 100%)

4.5.2 Furnace Temperature

The burners were ignited at 11:46 am to commence exposure of the connection assembly to the modeled real fire curve. The temperature in the furnace was controlled to follow the non-standard

time temperature curve as shown in the Figures 4.40 and 4.41. Figure 4.42 presents the average furnace temperature as recorded by the thermocouples and the plate thermometers.

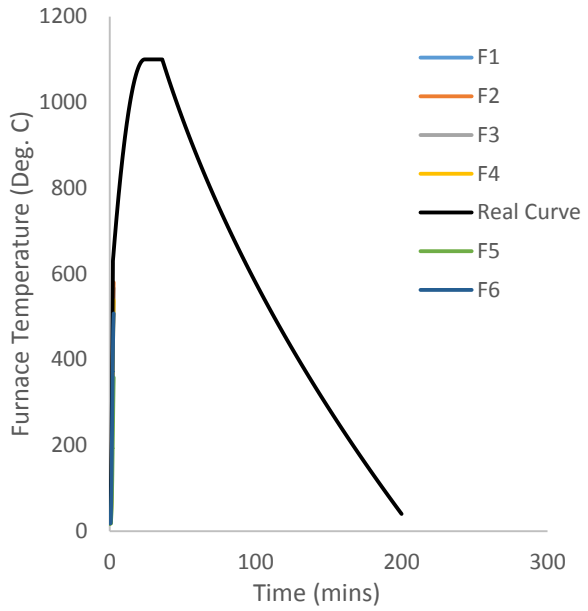

Figure 4.40 Furnace temperature as recorded by the thermocouples (CN-100%)

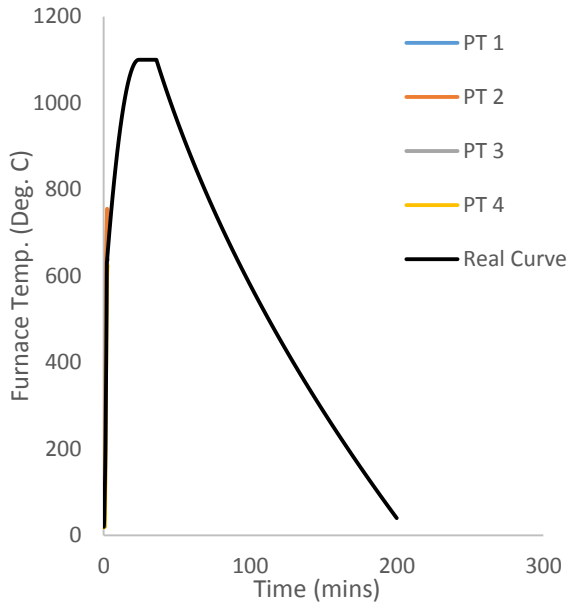

Figure 4.41 Furnace temperature as recorded by the plate thermometers (CN-100%)

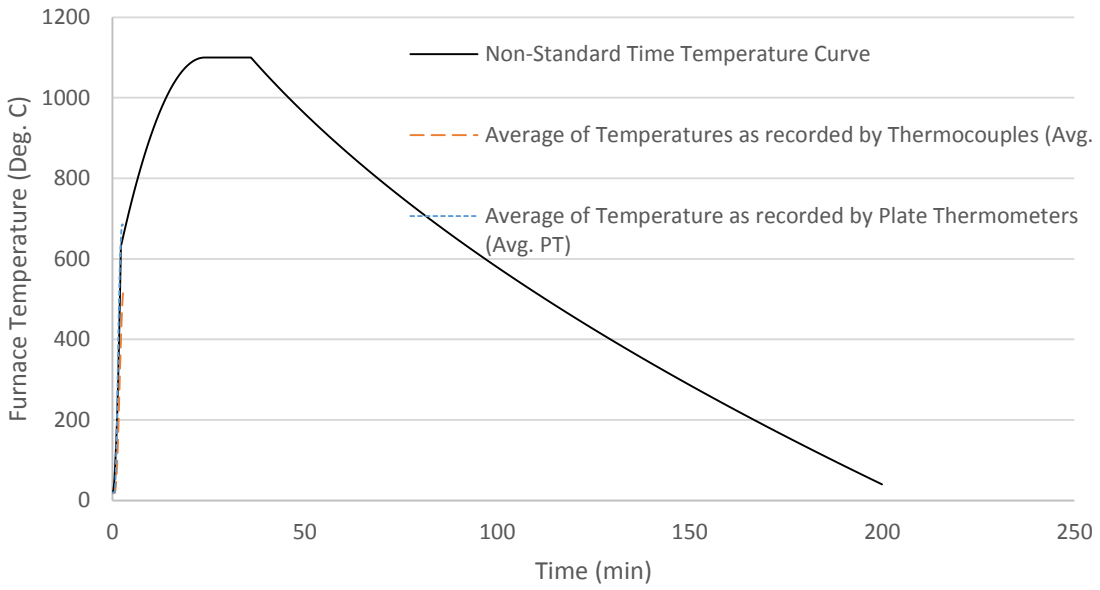

Figure 4.42 Average Furnace Temperature (CN - 100%)

4.5.3 Failure Mode and Failure Time

Specimen 6 lasted 3 minutes under exposure to the real fire curve. Failure was characterised by sudden longitudinal split at the left joint under the bottom row of bolts. This particular split profile was a bit unusual and irregular, unlike the previous splits observed in the other specimens.

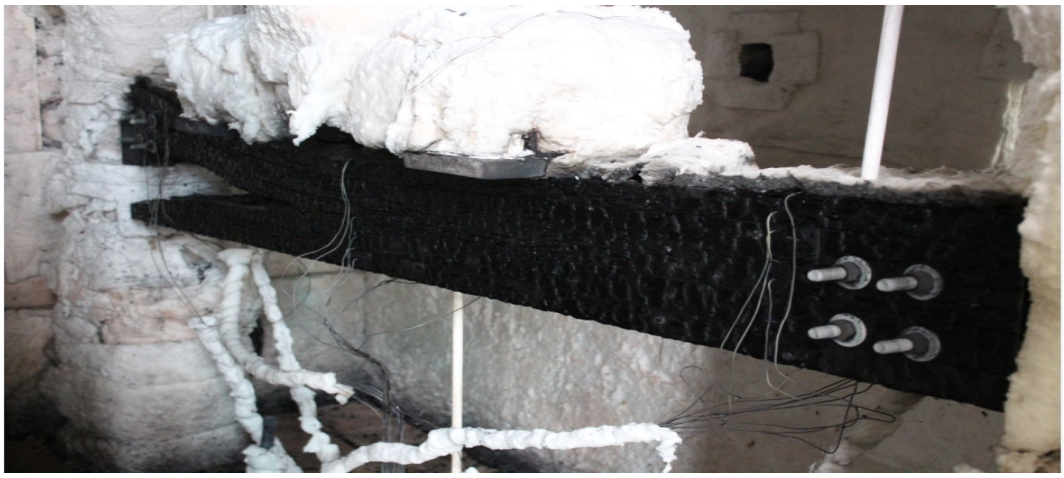

Figure 4.43 Splitting failure of beam (CN-100%)

The right connection end remained intact. There were no embedding in bolt holes at both joints (Fig. 4.44).

Figure 4.44 Left and right connection ends of beam at failure (CN-100%)

It was observed that splitting along the grain initiated at a knot (Fig. 4.45) on the wood at the left connection end, just above one row of bolt holes. This might be a possible trigger for early failure of the specimen as knots are known to weaken the strength of wood.

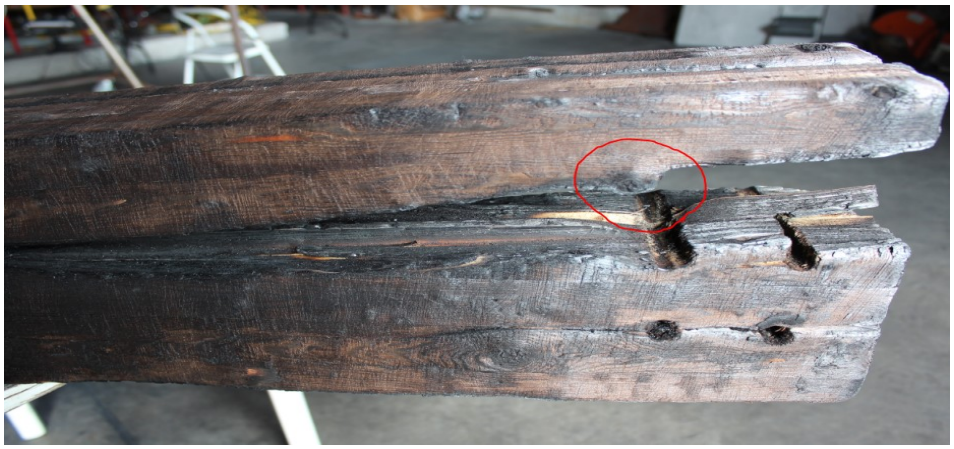

Figure 4.45 Knot along split profile (CN-100%)

4.5.4 Heat Transfer and Temperature Profile

In figures 4.46 and 4.47, the temperatures at sections close to the joint and the mid-span are presented. Sections within the mid-span rose a little above room temperature at failure (Fig. 4.47). The connection sections had higher temperatures, but did not exceed 300°C at the thermocouple installed depths.

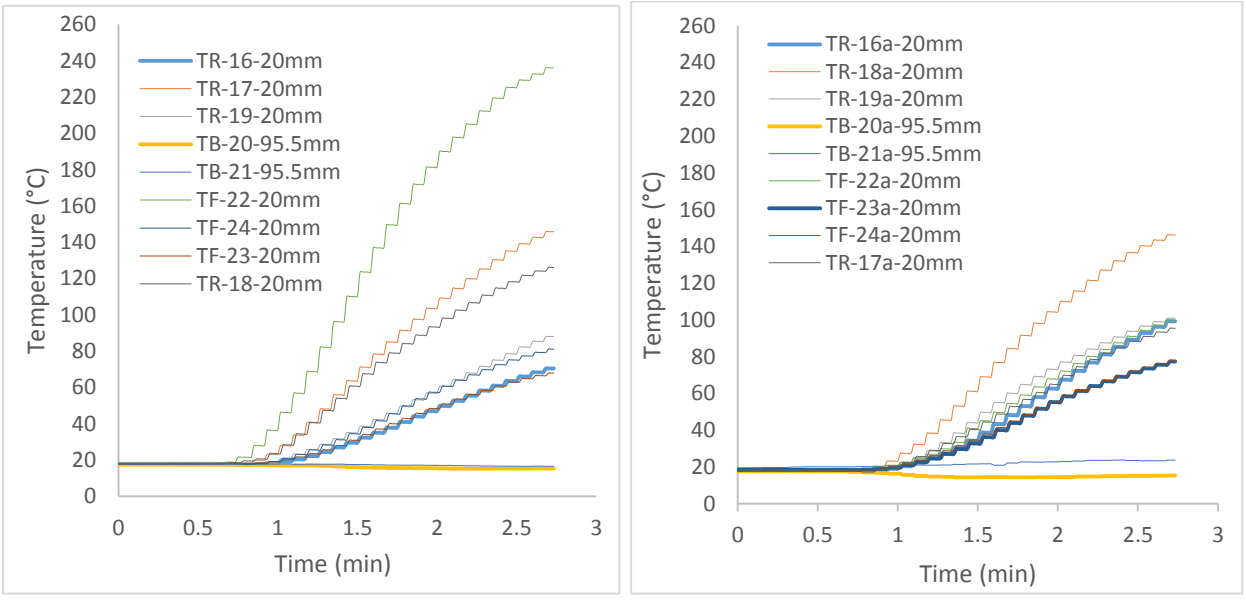

Figure 4.46 Temperature distribution at (a) the left connection (b) right connection end of beam (CN- 100%)

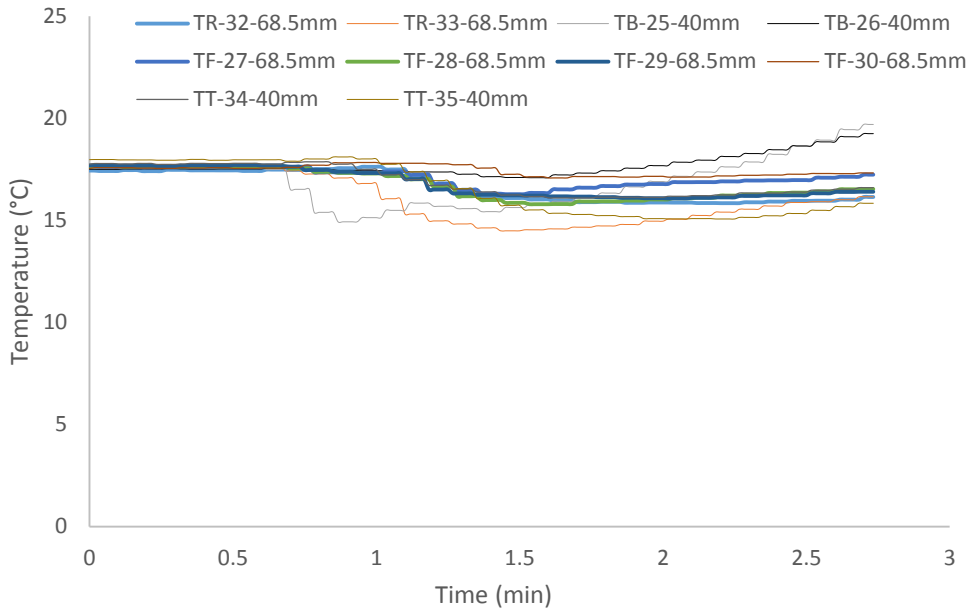

Figure 4.47 Temperature distribution at the mid-span of beam (CN - 100%)

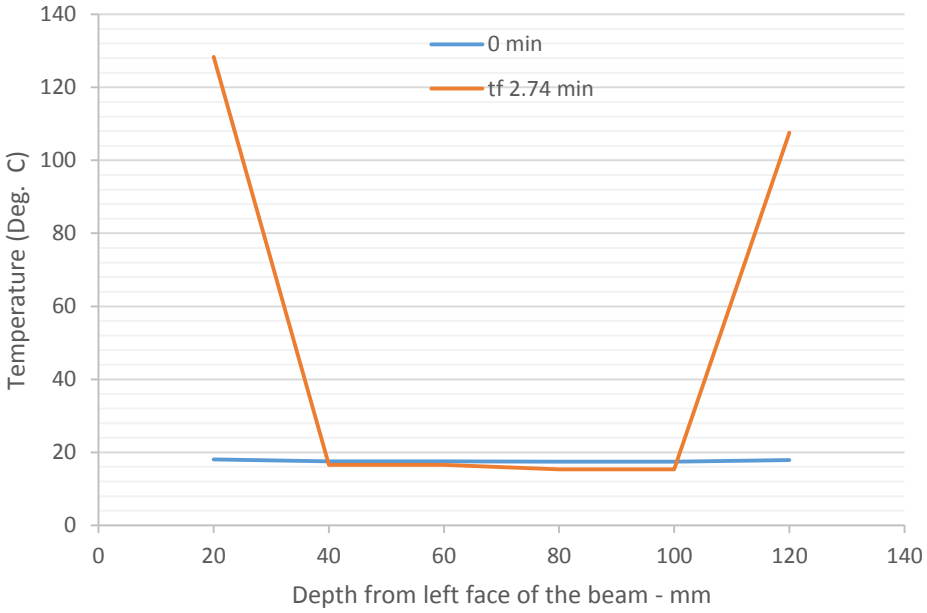

Figure 4.48 Temperature-depth distribution against time (CN-100%)

From Figure 4.48, the average temperature at 20 mm depth from the exposed sides at the connection end lied within the range of 108 - 128°C. The inner core remained unaffected by the furnace temperature.

4.5.5 Charring Rate

Charring computations are based on measurements from the residual cross-section. As can be seen from figure 4.49, the beam almost retained its original cross-section at failure. An average char layer depth of 7mm was recorded (Table 4.7) giving an average real charring rate of 2.59 mm/min for the beam.

Figure 4.49 Reduced section of beam after clearing off char layer (CN-100%)

Table 4.7 Real charring rate (mm/min) as measured from the reduced cross-section of beams (CN-100%)

Length	1880	mm
thickness	140	mm
Height	191	mm
t_f	2.74	min
LR	100%	

Calculating char rate			
	Connection End	**Mid-span**	**Connection End (Close to furnace door)**
Thickness of residual section	126.25	126.00	125.25
Char depth, c (mm)	6.87	7.00	7.38
Char rate (mm/min) at different sections	2.51	2.55	2.69
Average Thickness of residual section(mm)	125.83		
Average char depth, c (mm)	7.08		
Real Char Rate β (mm/min)	**2.59**		

4.6 Test 7 – Seated Shear Tab Connection

Test 7 involving the Seated Shear Tab Connection Assembly under a 60% load ratio was tested on the 9th of September, 2014. The glulam beam used had dimensions of 137 mm x 222 mm with a measured moisture content of 9%. The beam rested in the seated connection with one 12.7 mm A325 bolt to hold it in place.

Figure 4.50 Specimen for Test 7 before exposure to modelled real fire curve (SE-60%)

4.6.1 Loading

A static constant load of 70 KN corresponding to 60% of the bending capacity of the beam was applied at 11:20 am. The graph of applied and desired constant load with time after igniting the burners is shown in figure 4.51.

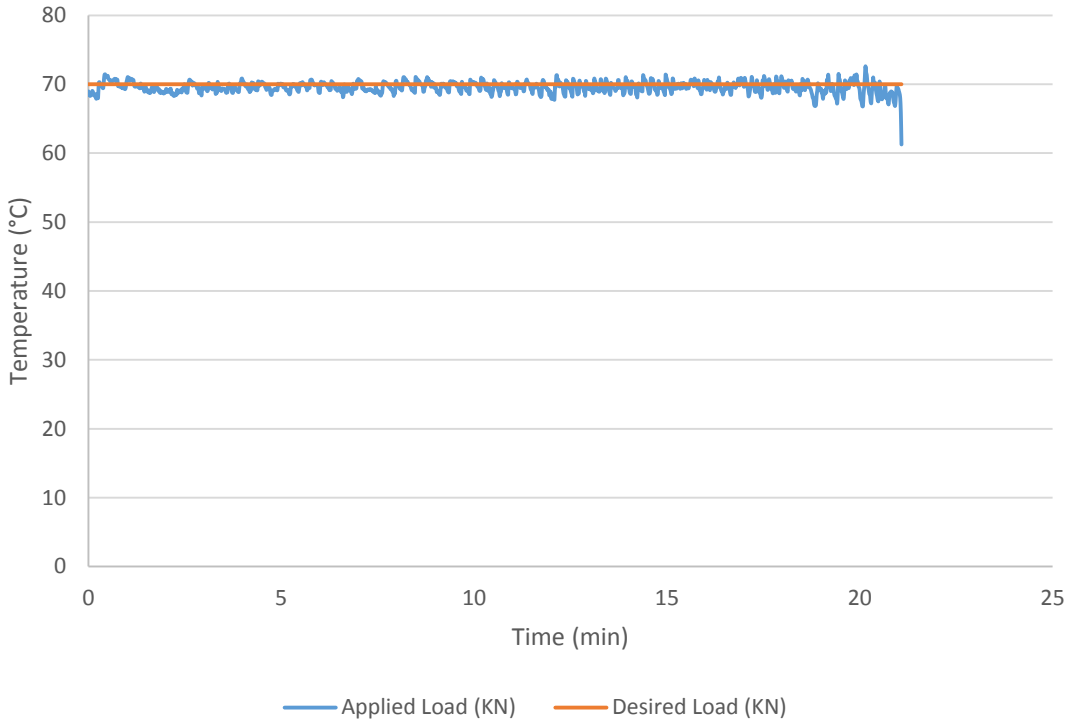

Figure 4.51 Graph of Desired and Applied Load vs Time (SE - 60%)

4.6.2 Furnace Temperature

At 1:00 pm, the propane burners were ignited. Figures 4.52 and 4.53 show the temperature in the furnace with time. The plate thermometer readings show that the furnace temperature followed closely the non-standard time temperature curve. This is further confirmed from Figure 4.54. Temperature in the furnace went as high as 1100°C prior to failure of the specimen. Thermocouple F5 failed after reaching the peak temperature (Fig. 4.52).

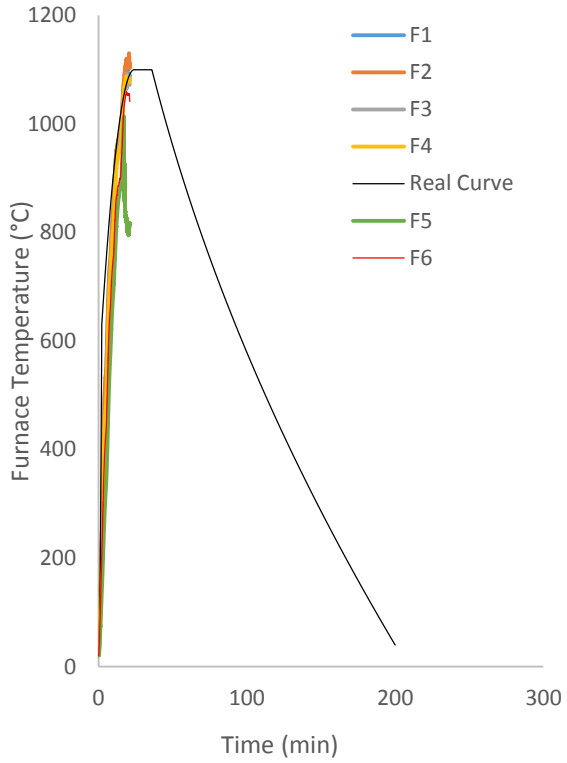

Figure 4.52 Furnace temperature as recorded by the thermocouples (SE-60%)

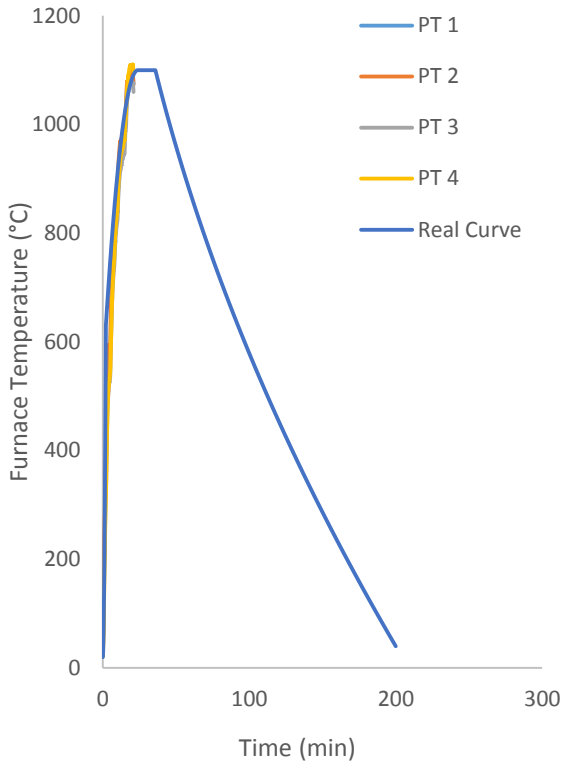

Figure 4.53 Furnace temperature as recorded by the plate thermometers (SE-60%)

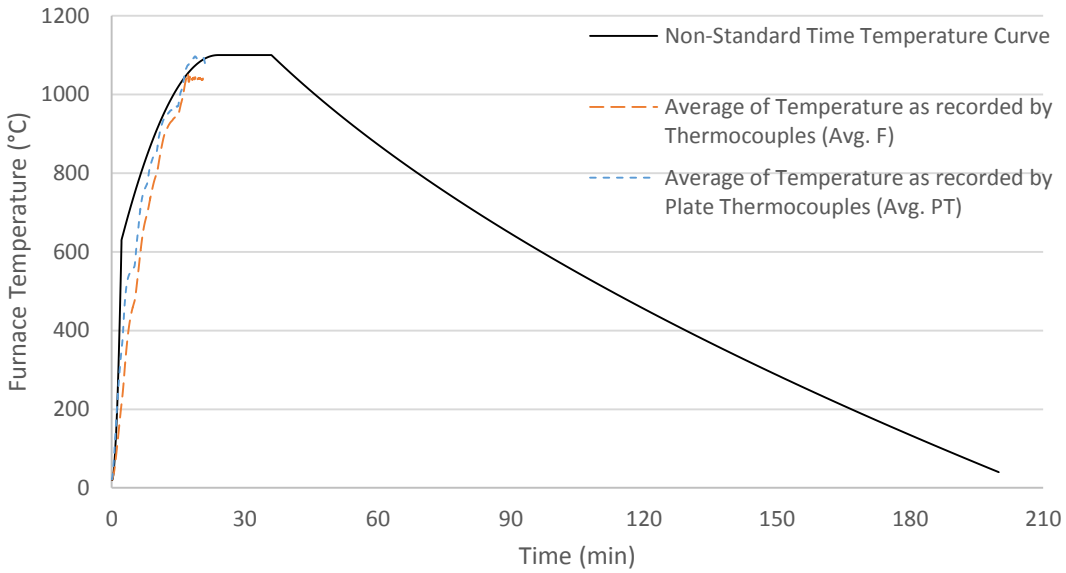

Figure 4.54 Average Furnace Temperature (SE - 60%)

4.6.3 Failure Mode and Failure Time

The specimen for Test 7 was designed to fail in bending at the mid-span. The specimen failed after 21 minutes of exposure to the furnace temperature. Failure as observed during the test involved a combination of bending and torsion under the load. Bending failure was initiated first with a significant amount of deformation at the mid-span. As the beam lost most of its cross-section width to char, the torsional rigidity of the beam was reduced. Twisting of the specimen commenced at the left joint 20 minutes after exposure. There were no observed significant fractures in the tension side of the beam (Fig. 4.56).

Figure 4.55 Sample for Test 7 after test (SE-60%)

Figure 4.56 Sample for Test 7 after clearing off char layer (SE-60%)

4.6.4 Heat Transfer and Temperature Profile

With the joints of the member remaining intact after the test, similar temperature profile was measured at both ends of the member (Figs. 4.58 and 4.59). TR-17 installed 20mm from the rear face and close to the bottom edge of the beam recorded temperatures in the range of 800-900°C at failure. The temperature range at immediate depths at the joints ranged from 600 to 925°C.

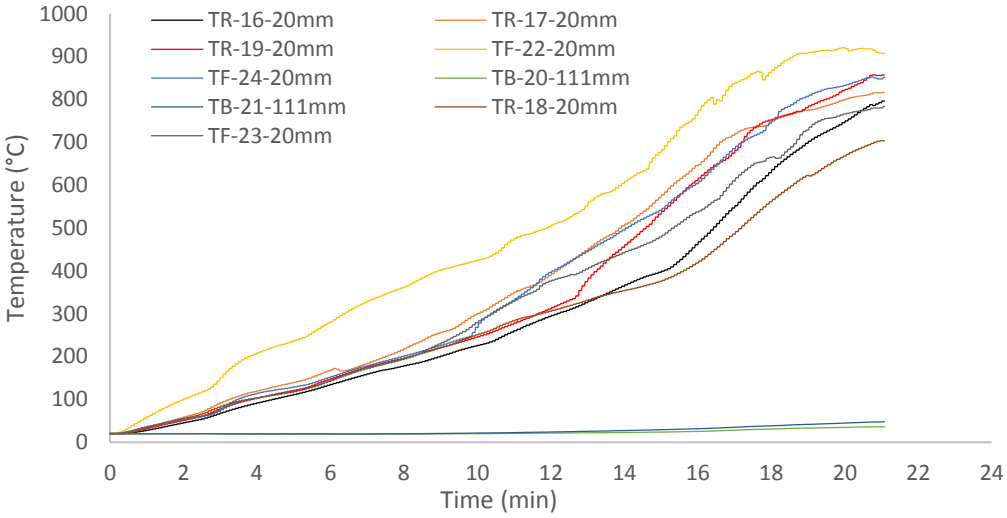

Figure 4.57 Temperature distribution at the left connection end of beam (SE-60%)

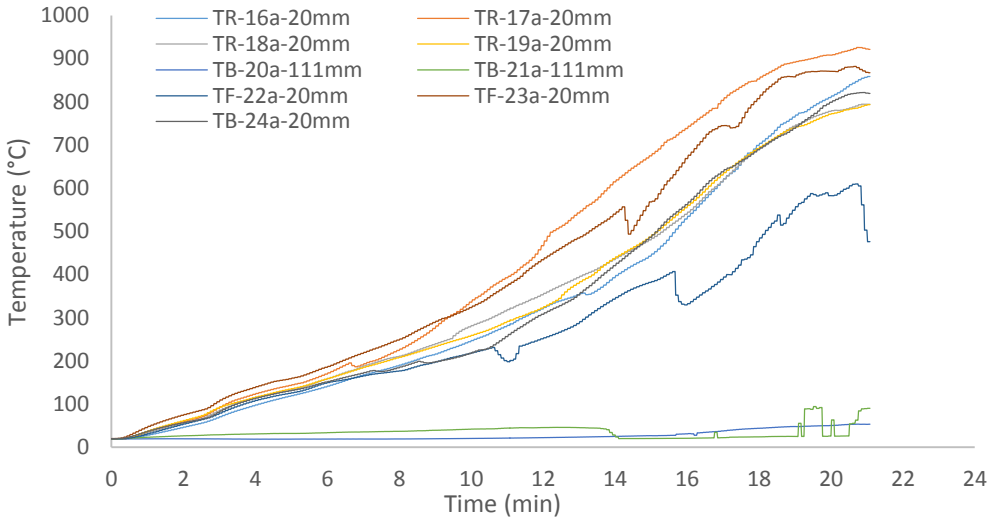

Figure 4.58 Temperature distribution at the right connection end of beam (SE - 60%)

In Figure 4.59, the temperature variation at the mid-span of the beam is presented. At failure, TB-25-40 mm installed 20 mm from the sides and 40 mm from the bottom measured a temperature of 370°C which is much lower than the temperatures at the joints which exceeded 600°C.

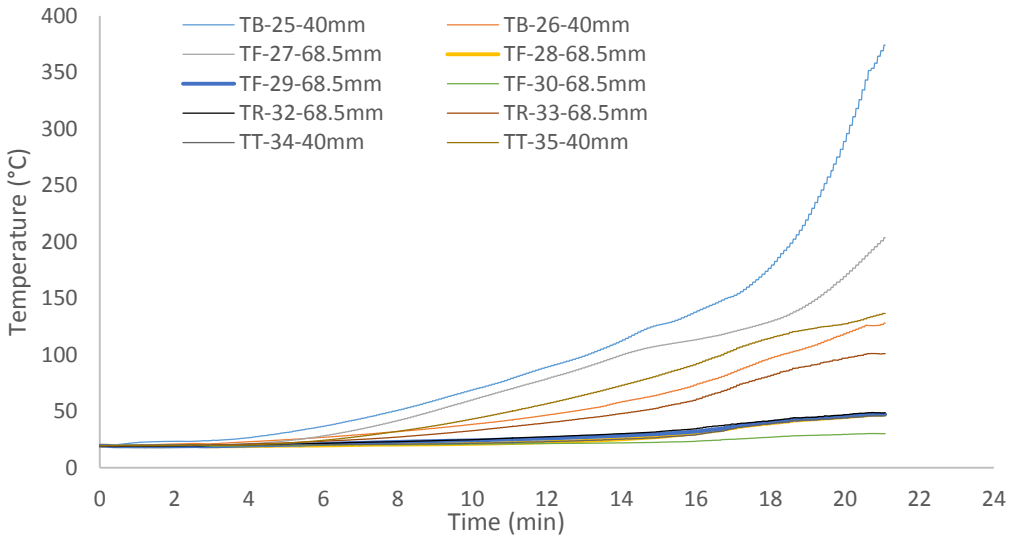

Figure 4.59 Temperature distribution at the mid-span of beam (SE - 60%)

In all three plots, temperature within the inner core remained a little over ambient, and below 100°C at which bound water in the specimen starts to evaporate.

The average temperature-depth distribution with time at the joints is presented in Figure 4.60. At 20 mm depth from the front and rear face of the beam, an average temperature of 845°C and 790°C was recorded at failure respectively. At 40 mm depth from the front face, through to the interior of the beam, the temperature remained slightly above ambient.

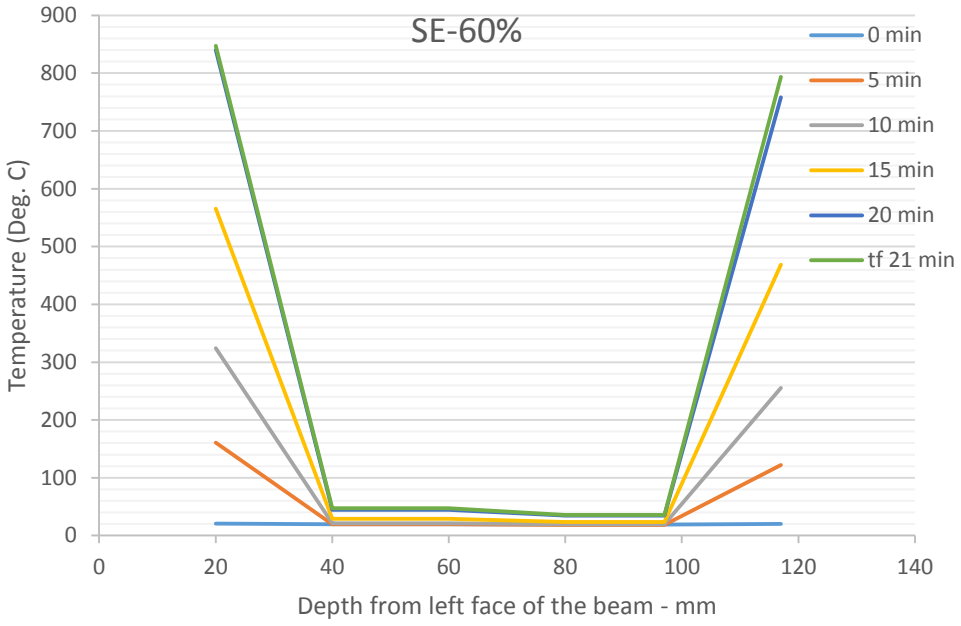

Figure 4.60 Temperature-depth distribution against time (SE-60%)

4.6.5 Charring Rate

The average and real charring rate was computed from the plots of temperature distribution and residual cross-section measurements. An average charring rate of 1.94 mm/min and 1.90 mm/min was found for the connection ends and mid-span of beam respectively (Table 4.8). The average char rate of the entire beam was 1.94 mm/min.

Computations from the reduced cross-section however produced a real charring rate of 1.16 mm/min at the connections and 1.10 mm/min at the mid-span (Table 4.9). An average char depth of 24 mm, accounting for 35% of the original cross-section width was estimated for the entire beam section at failure.

Table 4.8 Average charring rate of beam as computed from Temperature Profile plots (SE-60%)

Specimen	Section of beam	Depth (mm)	Thermocouple	Time to 300°C (min)	Charring Rate (mm/min)
7	Connection End (Close to door)	20	*TR-16-20mm*	12	1.67
			TR-17-20mm	10	2.00
			TR-19-20mm	12	1.67
			TF-22-20mm	7	2.86
			TF-23-20mm	10	2.00
			TF-24-20mm	11	1.82
		111	*TB-20-111mm*	n/a	n/a
			TB-21-111mm	n/a	n/a
	Mid-span	40	*TB-25-40mm*	21	1.90
			TB-26-40mm	n/a	n/a
			TT-34-40mm	n/a	n/a
			TT-35-40mm	n/a	n/a
		68.5	*TF-27-68.5mm*	n/a	n/a
			TF-28-68.5mm	n/a	n/a
			TF-29-68.5mm	n/a	n/a
			TF-30-68.5mm	n/a	n/a
			TR-32-68.5mm	n/a	n/a
			TR-33-68.5mm	n/a	n/a
	Connection End	20	*TR-16a-20mm*	12	1.67
			TR-17a-20mm	9	2.22
			TR-18a-20mm	11	1.82
			TR-19a-20mm	11	1.82
			TF-22a-20mm	13	1.54
			TF-23a-20mm	9	2.22
		95.5	*TB-20a-111mm*	n/a	n/a
			TB-21a-111mm	n/a	n/a
				Average char rate =	**1.94**

Table 4.9 Real charring rate (mm/min) as measured from the reduced cross-section of beams (SE-60%)

Length	1880	mm
thickness	137	mm
Height	222	mm
t_f	21	min
LR	60%	

Calculating char rate			
	Connection End	**Mid-Span**	**Connection End (Close to furnace door)**
Thickness of residual section	87.33	90.60	89.50
Char depth, c (mm)	24.83	23.20	23.75
Char rate (mm/min) at different sections	1.18	1.10	1.13
Average Thickness of residual section(mm)	89.14		
Average char depth, c (mm)	23.93		
Real Char Rate β (mm/min)	**1.14**		

4.7 Test 8 – Seated Shear Tab Connection

Specimen 8 involving the Seated Shear Tab Connection Assembly under a 100% load ratio was tested on the 18th of September, 2014. The glulam beam used had dimensions of 137 mm x 222 mm with a measured moisture content of 11%.

4.7.1 Loading

At 9:45 am, a load of 118 KN corresponding to 100% of the ultimate capacity was applied to the beam. Figure 4.61 shows the applied load curve with time after commencement of the fire test. The initial lower load at the start of the test is as a result of oil leakage in the hydraulic cylinder of the load application system.

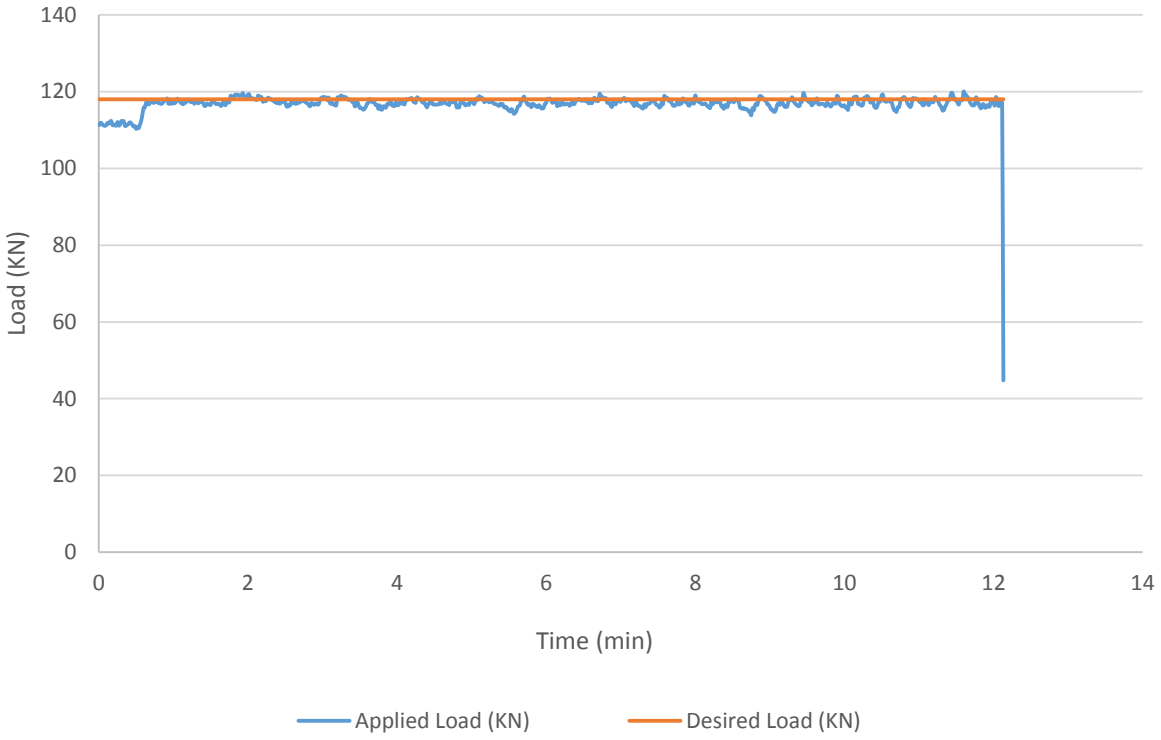

Figure 4.61 Graph of Desired and Applied Load vs Time (SE - 100%)

4.7.2 Furnace Temperature

With the constant load of 118 KN applied to the beam, the burners in the furnace were ignited at 10:16 am to commence exposure of the assembly to the non-standard time temperature curve. The furnace temperatures as recorded by the thermocouples and the plate thermometers are shown in Figures 4.62 and 4.63. The temperature in the furnace went as high as 980°C at failure of the specimen (Fig. 4.64). There was a delay in ignition of approximately 1 minute (Fig. 4.64).

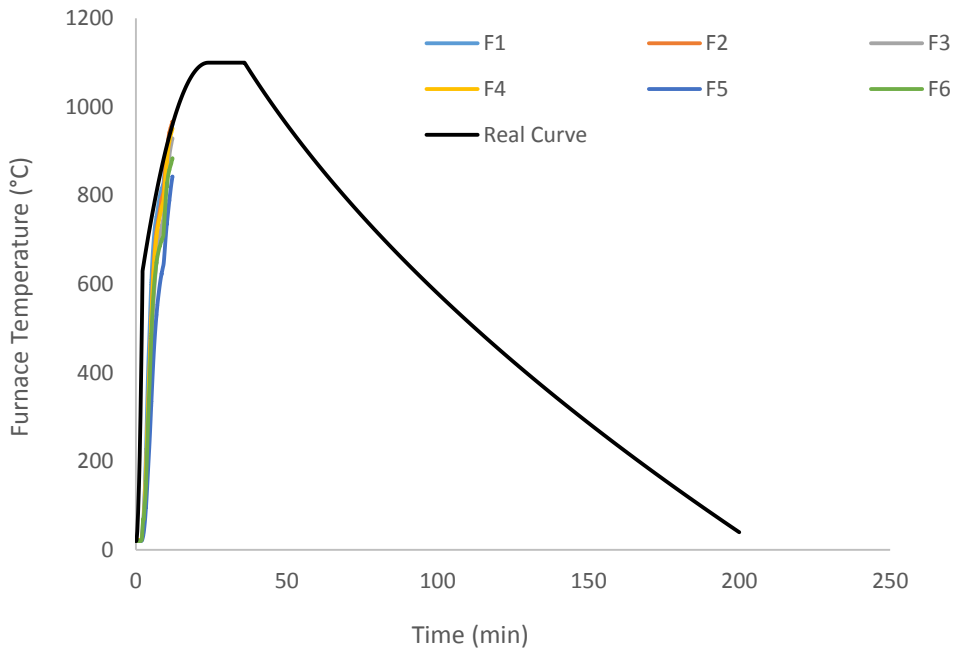

Figure 4.62 Furnace temperature as recorded by the thermocouples (SE-100%)

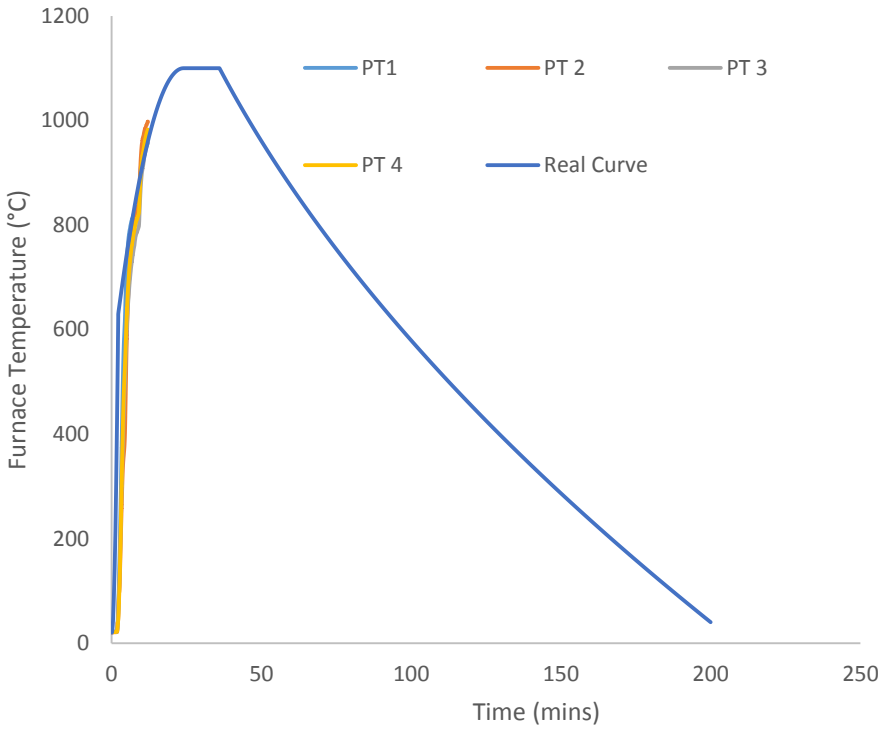

Figure 4.63 Furnace temperature as recorded by the plate thermometers (SE-100%)

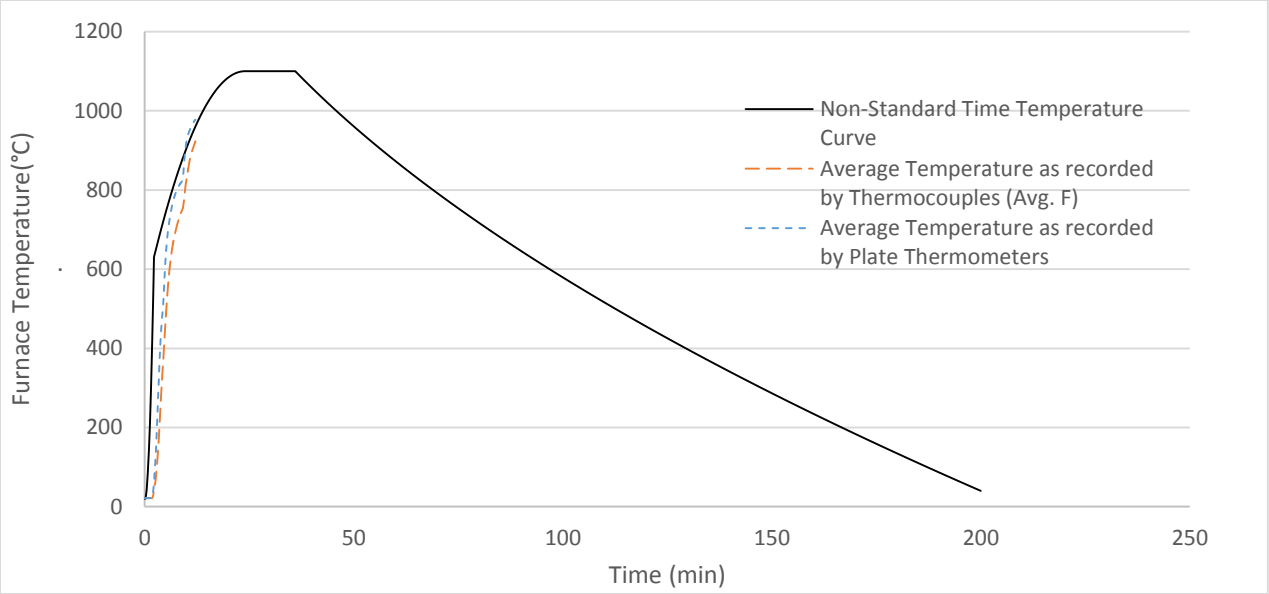

Figure 4.64 Average Furnace Temperature (SE - 100%)

4.7.3 Failure Mode and Failure Time

Specimen 8 resisted the applied constant load and fire exposure for approximately 12 minutes before failing due to bending at the mid-span (Fig. 4.65).

Figure 4.65 Specimen 8 after test (SE-100%)

Bending failure resulted in a fracture at one of the finger joints holding the laminates together in the tensile region of the beam (Fig. 4.66).

Figure 4.66 Fracture at finger joint of beam at almost mid-span (SE-100%)

4.7.4 Heat Transfer and Temperature Profiles

Figures 4.67, 4.68 and 4.69 show the measured temperature profiles at the left connection, at the right connection and at the mid-span of the beam respectively. At the sections close to the connection, temperature profile at immediate depths remain at ambient for the first 2 minutes of exposure to the real fire curve. Beyond this point, temperature rise is gradual and quite linear (Figs. 4.67 and 4.68). Thermocouples TF-22 and TF-24 measured the temperature profile with time at a depth of 20 mm from the front face. TF-22 which was at the mid-height of the beam had higher temperatures with a peak of 555°C at failure. TF-24 installed close to the insulated top face of beam recorded a temperature of approximately 300°C at failure. At the right connection end, TF-22a and TF-24a had peak temperatures of 250°C at failure. Temperatures at 20 mm depth from the

rear face ranged from 290 - 390°C at sections close to the connection. All three figures show that the temperature in the inner core remained at ambient with TB-21a recording a temperature of 75°C at failure at 111 mm depth from the bottom face of the beam.

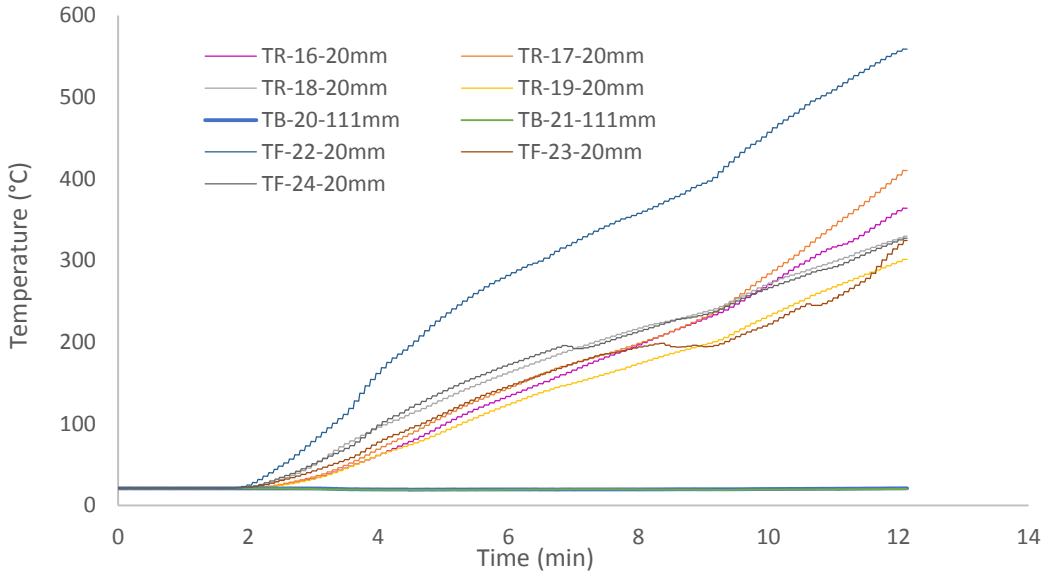

Figure 4.67 Temperature distribution at the left connection end of beam (SE-100%)

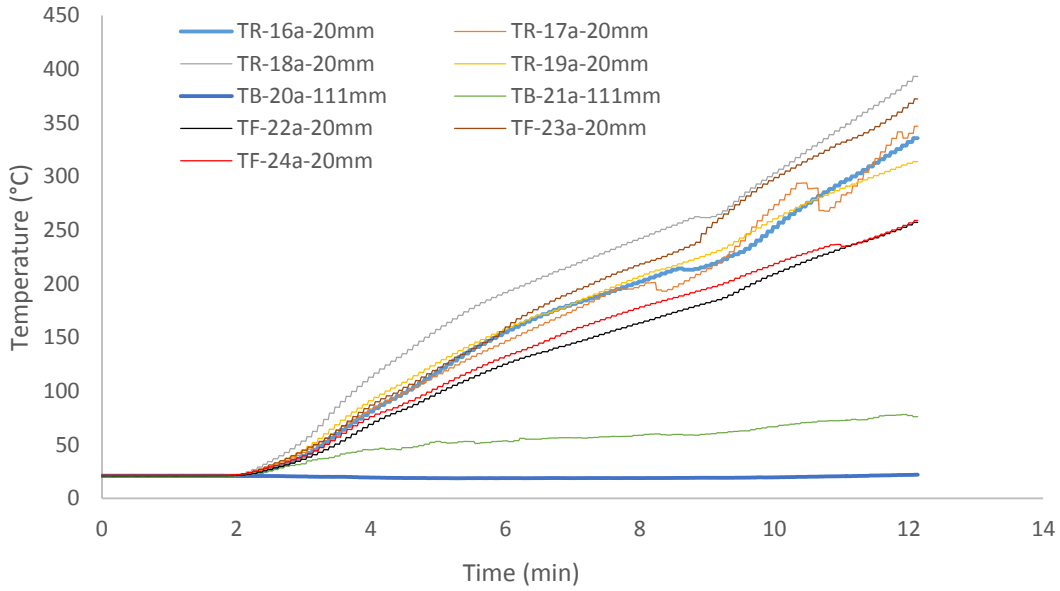

Figure 4.68 Temperature distribution at the right connection end of beam (SE - 100%)

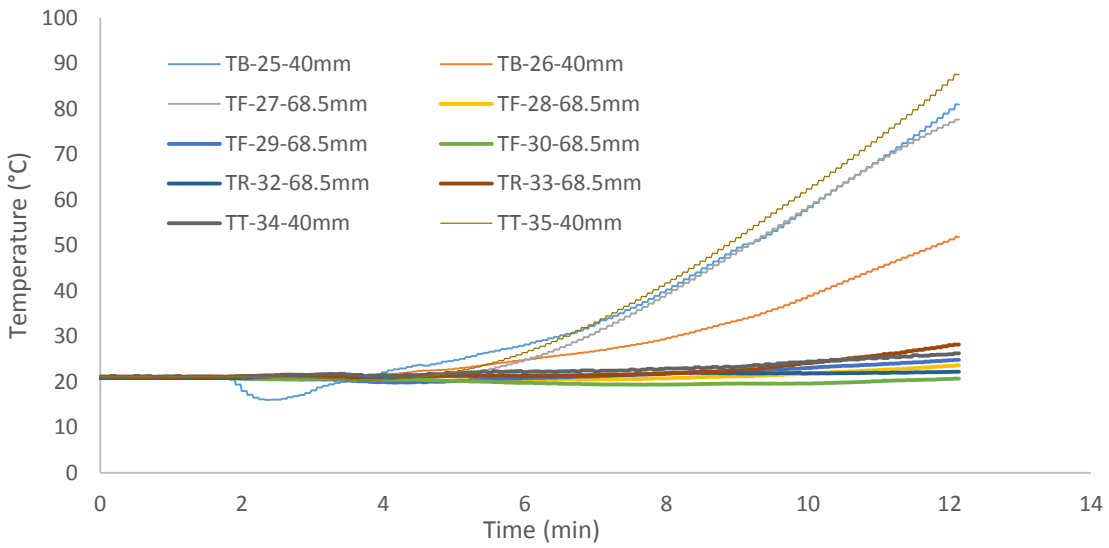

Figure 4.69 Temperature distribution at the mid-span of beam (SE - 100%)

Figure 4.69 shows the variation of the average connection temperature with time at each depth of installed thermocouples in the beam. At the failure time of 12 minutes, the average temperature varied from 400°C at 20 mm from the front face to ambient at 40 mm depth, through to 100 mm, before rising to 350°C at 120 mm depth from the front face.

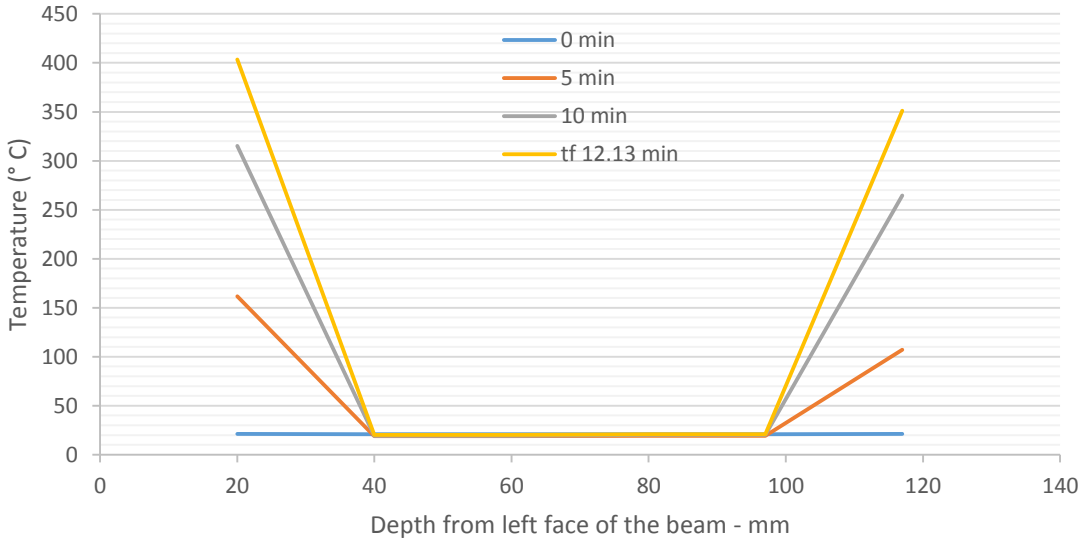

Figure 4.70 Temperature-depth distribution against time (SE-100%)

4.7.5 Charring Rate

An average charring rate of 1.92 mm/min (Table 4.10) and a real charring rate of 1.03 mm/min (Table 4.11) was found for the entire beam after failure.

Table 4.10 Average charring rate of beam as computed from Temperature Profile plots (SE-100%)

Specimen	Section of beam	Depth (mm)	Thermocouple	Time to 300°C (mins)	Charring Rate (mm/min)
8	Connection End (Close to furnace door)	20	*TR-16-20mm*	10.6	1.89
			TR-17-20mm	10.4	1.92
			TR-18-20mm	11.1	1.80
			TR-19-20mm	12	1.67
			TF-22-20mm	6.6	3.03
			TF-23-20mm	11.8	1.69
			TF-24-20mm	11.4	1.75
		111	*TB-20-111mm*	n/a	n/a
			TB-21-111mm	n/a	n/a
	Mid-span	40	*TB-25-40mm*	n/a	n/a
			TB-26-40mm	n/a	n/a
			TT-34-40mm	n/a	n/a
			TT-35-40mm	n/a	n/a
		68.5	*TF-27-68.5mm*	n/a	n/a
			TF-28-68.5mm	n/a	n/a
			TF-29-68.5mm	n/a	n/a
			TF-30-68.5mm	n/a	n/a
			TR-32-68.5mm	n/a	n/a
			TR-33-68.5mm	n/a	n/a
	Connection End	20	*TR-16a-20mm*	11.4	1.75
			TR-17a-20mm	11.4	1.75
			TR-18a-20mm	10	2.00
			TR-19a-20mm	11.2	1.79
			TF-22a-20mm	n/a	n/a
			TF-23a-20mm	10	2.00
			TF-24a-20mm	n/a	n/a
		95.5	*TB-20a-111mm*	n/a	n/a
			TB-21a-111mm	n/a	n/a
				Average char rate =	**1.92**

Table 4.11 Real charring rate (mm/min) as measured from the reduced cross-section of beams (SE-100%)

Length	1880	mm
thickness	137	mm
Height	222	mm
t_f	12.13	min
LR	100%	

Calculating char rate			
	Connection End	**Mid-Span**	**Connection End** (Close to furnace door)
Thickness of residual section	113.6	111.3	111.16
Char depth, c (mm)	11.7	12.83	12.917
Char rate (mm/min) at different sections	0.96	1.06	1.06
Average Thickness of residual section(mm)	112.03		
Average char depth, c (mm)	12.48		
Real Char Rate β (mm/min)	**1.03**		

Under 100% load ratio, there was no significant difference in the charring rates at the sections close to the connections and the mid-span of the beam. An approximate real charring rate of 1.0 mm/min was found for the three cut sections. An average char thickness of 12.5 mm accounting for 25% loss of cross-section width was measured for the glulam beam at failure.

4.8 Summary

In this section, results are discussed for the different shear tab connections tested, and compared to the results obtained from full scale tests on similar specimens exposed to the standard time-temperature cure of CAN/ULC S-101.

4.8.1 Concealed Shear Tab Connection (CN)

A typical isometric and side view of the concealed shear tab connection (CN) is shown in Figure 4.71.

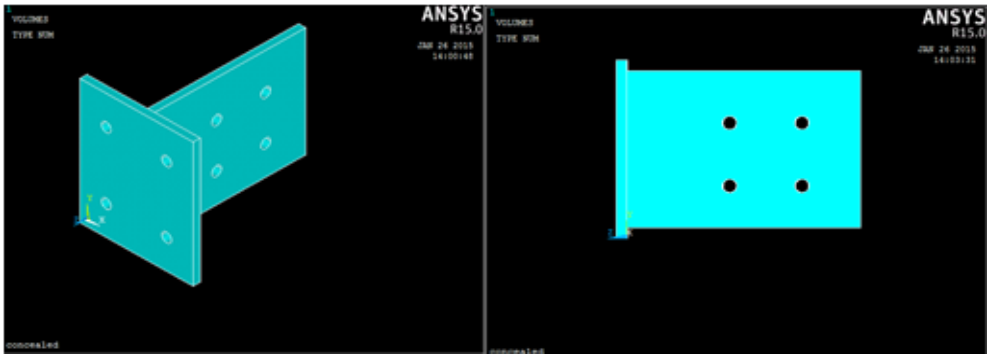

Figure 4.71 Isometric and side view of a CN connection type

It connects the glulam beam to the steel column by means of bolts, with the central plate slid in a central notch in the beam. This connection system offers the advantage of protecting the centrally positioned plate from direct exposure to extreme heat in fire. However, there is the disadvantage of reduced shear capacity at the support due to the presence of the notch, as well as direct transmission of heat from the bolts and plates to the inner core of the beam at the joints.

Table 4.12 Summary of results for CN connection type

Concealed Shear Tab Connection (CN)	**Test 5 - 60% LR**	**Test 6 - 100% LR**
Average Moisture Content (%)	10	9
Applied Load (KN)	43	71.8
Time of temperature rise from ambient at 20 mm depth at joint (min)	1.6	1
Time to failure (min)	12	3
Mode of Failure	Splitting at the joints along the grain of wood	Longitudinal split at the left joint
Peak Average Furnace Temperature at Failure (Deg. C)	930	590
Average Charring Rate at Connection End as measured from Temperature Profiles (mm/min)	2.64	–
Thickness of char layer at joint (mm)	16.5	7.13
Real Charring Rate at Connection End as measured from reduced cross-section of beam (mm/min)	1.39	2.6
Thickness of char layer at mid-span of beam (mm)	15.3	7
Average Charring Rate at beam mid-span as measured from Temperature Profiles (mm/min)	–	–
Real Charring Rate at beam mid-span as measured from reduced cross-section of beam (mm/min)	1.35	2.55

Table 4.12 presents a summary of the results obtained from exposing the concealed connection system under the two load ratios to the modeled non-standard fire curve. It is evident that the applied load had a significant influence on the time to failure of the assembly. Times to failure of 12 and 3 minutes were recorded under the 60% and 100% load ratios respectively. Failure of the specimens were characterised by longitudinal splits initiated at the joint bolt holes. Measured real charring rates at the beam mid-span and joints showed no significant difference under both load ratios of 60% and 100%. At failure, charring rate values of 1.39 mm/min and 1.35 mm/min were recorded under 60% load ratio for the joints and the mid-span of beam respectively. For the fairly low failure time of 3 minutes under 100% load ratio, a mean real charring rate of approximately 2.6 mm/min was produced across the entire length of the beam.

4.8.2 Exposed Shear Tab (EX) Connection

Unlike the concealed connection, the exposed shear tab connection (Fig. 4.72) consists of two side plates attached to the beam and directly exposed to heat. Depending on the thickness of these side plates, a considerable amount of delay to the transmission of heat to the inner core of the glulam beam at the joint can be provided. Some researchers also argue that the steam generated at the interface between the steel plate and the wood at temperatures near 100°C can also contribute to the delayed charring to the inner core (Samake et al., 2014). In Table 4.13, a summary of the results obtained from tests on the assemblies using the exposed connection is shown.

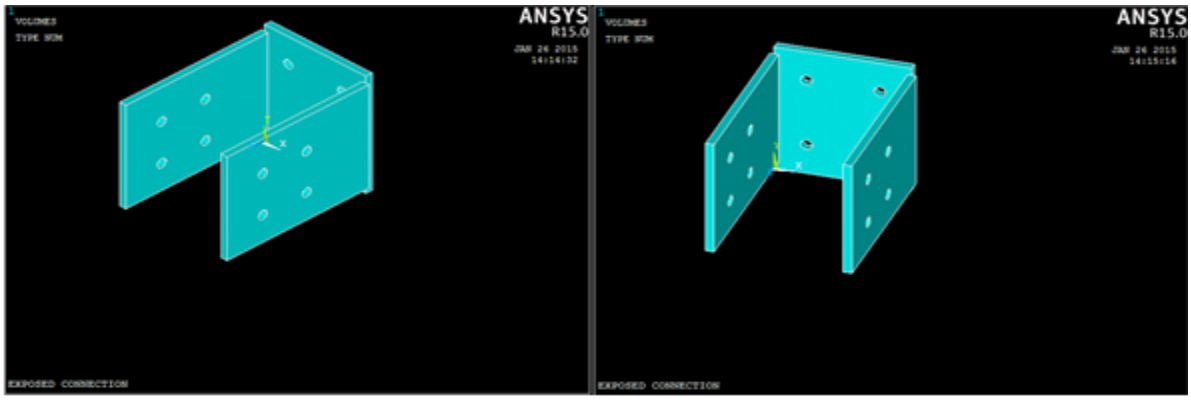

Figure 4.72 Isometric and oblique view of a typical EX connection type

Table 4.13 Summary of results for EX connection type

Exposed Shear Tab Connection (EX)	**Test 4 - 60% LR**	**Test 2 - 100% LR**
Average Moisture Content (%)	9	10
Applied Load (KN)	59	98
Time of temperature rise from ambient at 20 mm depth at joint (min)	1	1.6
Time to failure (min)	18	12
Mode of Failure	*Longitudinal split stretching almost the entire span of beam *Accompanying embedment of bolts	*Longitudinal Split at the joint *Accompanying bending failure involving rupture of finger joint holding laminates together
Peak Average Furnace Temperature at Failure (Deg. C)	1054	825
Average Charring Rate at Connection End as measured from Temperature Profiles (mm/min)	2.51	2.05
Thickness of char layer at joint (mm)	18.1	14.2
Real Charring Rate at Connection End as measured from reduced cross-section of beam (mm/min)	1.04	1.16
Thickness of char layer at mid-span of beam (mm)	18.9	13.8
Average Charring Rate at beam mid-span as measured from Temperature Profiles (mm/min)	–	–
Real Charring Rate at beam mid-span as measured from reduced cross-section of beam (mm/min)	1.08	1.12

The assemblies failed mainly by splitting along the grain of wood. Decrease in the load ratio from 100% to 60% increases the failure time of the connection. However, failure of the specimens still remain sudden and without any significant warnings. At the connection ends, charring rate values measured from the residual cross-section averaged 1.04 mm/min and 1.16 mm/min under 60% and 100% load ratios respectively. Compared to the concealed connection which had an average char rate above 1.30 mm/min, char rate values were relatively lower at the time of failure of the assembly. This can be attributed to the partial protection of wood due to stagnation of escaping vapour at interface between steel side plate and wood at temperatures close to 100°C (Samake et al., 2014). There was no significant variation in the charring rate at the sections of the wood close to the joint and at the mid-span.

4.8.3 Seated (SE) Shear Tab Connection

The seated connection (Fig. 4.73) though similar to the exposed connection, has a bearing plate to support and transfer the vertical loads to the columns. The mechanism of heat transfer from the surrounding environment through the plates, and to the wood is similar to that of the exposed connection. The exposed steel side plates directly transmit heat to wood surface in contact with it, and then to the inner core. The thicker bearing plate and the two side plates offer an improved partial protection to the enclosed wood as compared to the exposed connection (Akotuah et al., 2014).

Figure 4.73 Isometric and side view of a typical SE connection type

In one of the tests, a single bolt was utilized to hold the beam in the brackets. This however had no significant effect on the mechanical and thermal behavior of the wood. The probability of the high temperatures reaching the inner core of the beam via the bolts is reduced drastically compared to the exposed connection.

Table 4.14 presents a summary of the results obtained from the tests of the assemblies using the seated connection type.

Table 4.14 Summary of results for SE connection type

Seated Shear Tab Connection (SE)	**Test 7 - 60% LR**	**Test 8 - 100% LR**
Average Moisture Content (%)	9	10
Applied Load (KN)	70	118
Time of temperature rise from ambient at 20 mm depth at joint (min)	1	2
Time to failure (min)	21	12
Mode of Failure	*Initial bending failure *subsequent twisting as cross-section reduced	*Bending failure at mid-span *Accompanying rupture of finger joint holding laminates together at mid-span
Peak Average Furnace Temperature at Failure (Deg. C)	1100	980
Average Charring Rate at Connection End as measured from Temperature Profiles (mm/min)	1.94	1.92
Thickness of char layer at joint (mm)	24.3	12.31
Real Charring Rate at Connection End as measured from reduced cross-section of beam (mm/min)	1.16	1.01
Thickness of char layer at mid-span of beam (mm)	23.2	12.83
Average Charring Rate at beam mid-span as measured from Temperature Profiles (mm/min)	1.9	–
Real Charring Rate at beam mid-span as measured from reduced cross-section of beam (mm/min)	1.1	1.06

Specimens failed mainly in flexure at the mid-span. Under both load ratios, the seated connection recorded the highest failure time at 21 minutes and 12 minutes under the 60% and 100% load ratios

respectively. Despite the extreme temperatures reached in the furnace, the charring rate at the connection ends went as high as 1.1 mm/min. There was no significant variation in the charring rate at the joint and at the mid-span of beam.

4.8.4 Relative Failure Times of the Connections

In this section, a relationship is established between the fire resistance ratings of the three different connection types under the load ratios of 60% and 100%. As defined in section 3.3, the load ratio is a measure of the fraction of the total design load of the assembly in the event of a fire. Buchanan (2002) noted that most buildings usually have about 50% of the load capacity present in the event of a fire. This could even be less in structures purposefully designed to resist more catastrophic events such as earthquakes. Lower load ratios result in better fire performance of the assemblies as it was seen in the presented results.

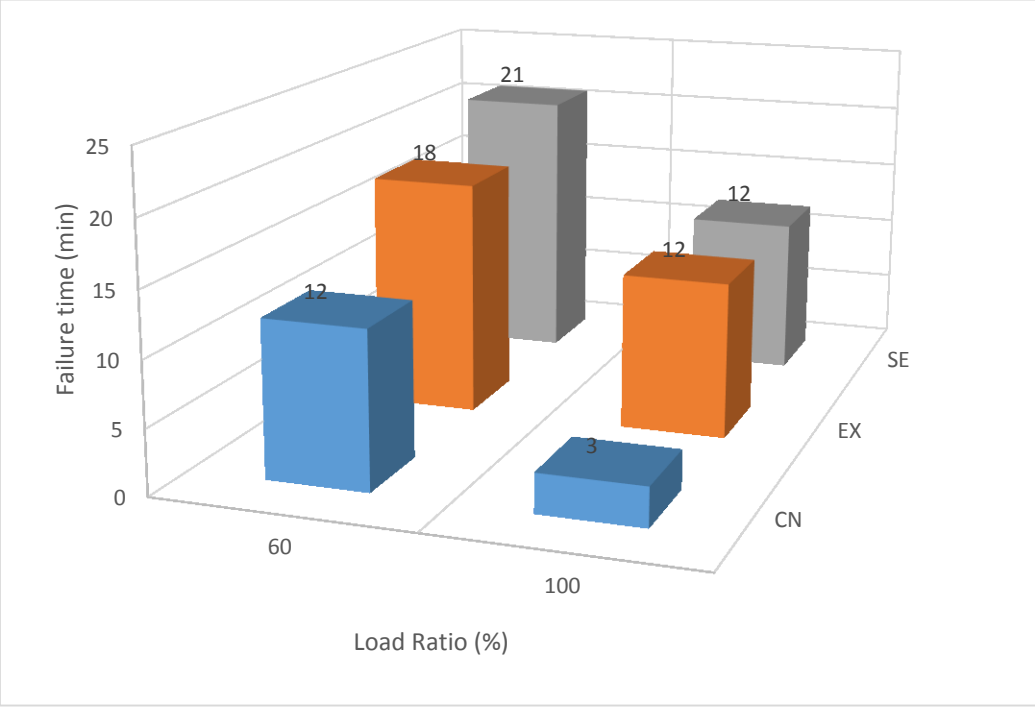

Figure 4.74 Relative time to failure of the connections

In Figure 4.74 above, the times to failure of the assemblies under different connection types and load ratios of 60% and 100% are presented. The influence of the load ratio on the time to failure can be clearly seen. An increase in the load ratio significantly leads to a decrease in the time to failure.

For the lower load ratio of 60%, the seated connection provides the best time to failure at 21 minutes. The time to failure of the assemblies is improved in the order of concealed to exposed to seated under the lower load ratio. There is an improvement of 75% in the time to failure provided by the seated connection as compared to the concealed. The exposed connection offers an extra 50% increase in the time to failure from that of the concealed. This increase in time to failure of the connections with exposed steel side plates can be attributed to the partial protection provided by these side plates (*Akotuah et al., 2014*). The thicker the side plate, the longer the time taken for the heat front to travel to the wood surface underneath. Moreover, the absence of a steel plate in the inner core of the beams restricts propagation of the char front to that from the outer surface only. With the concealed connection, the presence of the steel plate in the central notch initiates charring in the inner core as the temperature in the furnace increases prior to failure. This in addition to char propagating from the exposed sides increases the thickness of the char layer with time, leading to early failure as the strength bearing cross-section is reduced.

Table 4.15 Average char rate of glulam (mm/min) for each connection type

Fire Curve	Charring rate at mid-span of beam (mm/min)	Concealed connection (mm/min)	Exposed connection (mm/min)	Seated connection (mm/min)
Non-Standard	1.25	2.0	1.1	1.09
CAN/ULC S-101 (Ali et al.,2014)	0.78	0.94	0.56	0.57

In Table 4.15, the char rates of the assemblies are presented for exposure to the non-standard and CAN/ULC S-101 fire curves. Lower charring rate values of 1.09 mm/min and 1.1mm/min were recorded for the seated and exposed connections respectively under exposure to the non-standard time-temperature curve. For the concealed connection, a higher charring rate of 2.0 mm/min was recorded after testing. Average char rate values of 0.78 and 1.25 mm/min were observed for the beams when exposed to the CAN/ULC S-101 and the non-standard fire curves respectively. The average char rate of the beams tested (1.25 mm/min) under exposure to the non-standard fire curve was close to the char rate value of 1.1 mm/min reported by Lange et al. (2014) during his tests on glulam beams in natural fires. The average char rates in the real fire were twice as large as that in the standard fire defined by the CAN/ULC S-101 fire curve.

Failure of the connection assemblies were as a result of loss of strength in the wood member due to thermal degradation of the wood in elevated temperatures. Possible failure of the steel plates were always preceded by that of the wood member. Table 4.16 summarises the main mode of failure of the tested connection assemblies.

Table 4.16 Failure Modes of the Connection Assemblies

Connection Type	Failure Modes
Concealed (CN)	Longitudinal Split at the joint.
Exposed (EX)	Longitudinal split at the joint and rupture of a finger joint in the tensile region of the beam at mid-span.
Seated (SE)	Bending failure with subsequent twisting under loading when the full load capacity is applied.

4.8.5 Correlation between exposure to the Real and Standard fire curves using the Radiant Exposure Area Concept of Equivalent Severity (Nyman, 2002)

In this section, the severity of the real and standard exposure models on the assembly is analysed. Ali et al. (2014) conducted full scale tests to assess the behavior of similar connection assemblies under exposure to the CAN/ULC S101 standard fire curve. The results presented are used to present a correlation between the failure times of the assemblies in the standard fire and the non-standard fire.

Studies have shown that the severity of fires on an element can be determined by the amount of heat flux impinging and penetrating it (*Harmathy et al., 1983*). In this paper he concludes that the integral of the heat release rate in a fire with time alone is sufficient to describe the severity on compartment boundaries made of the same materials. This method was referred to as the Normalized Heat Load method, and was deemed applicable to design steel structures for fire safety. The Normalized Heat Load, H was defined as

$$H = \frac{1}{\sqrt{(k\rho c)}} \int_0^\tau q \, dt \qquad \textbf{Equation 4.1}$$

Where kpc is the thermal inertia of the compartment boundary, t is the exposure time and q is the heat release rate in the compartment. This offered a way of comparing the severity of two fires, and is a better approach when spread of fires to adjacent boundaries through openings is considered.

Nyman (2002) proposed a method for correlating real fire severity and standard fires severity using the cumulative radiative heat energy build up in a compartment. It is an improvement of the equal area concept proposed by Ingberg in the 1920s. This approach is built on the three main modes of heat transfer of conduction, convection and radiation from a fire to adjacent materials. In post flashover fires, the contributions of conduction and convection are negligible. As such radiation can be assumed to be the main mode of heat transfer. Moreover, the growth and spread of fires in buildings is highly influenced by radiative heat transfer. It affects how structural elements deplete in strength when involved in fires. As such it is theoretically appropriate to use the concept of radiative energy to establish an equivalent severity of a fire. It is a refinement of the Normalized Heat Load approach by Harmathy (1983). Nyman (2002) found the equivalent time of exposure in a real fire that would produce an equal radiative heat energy on elements under exposure to a standard fire curve at failure. In essence, he expressed the severity of a fire as a function of the integral of the emissive power curve with time.

$$E = \sigma\varepsilon \int_0^t T^4 \, dt$$ **Equation 4.2**

where

$E = Radiative\ heat\ energy\ \left(\frac{MJ}{m^2}\right)\ impinging\ an\ element$

$\sigma = Stefan\ Boltzmann\ Constant = 5.67 \times 10^{-8}\ Wm^{-2}K^{-4}$

$\varepsilon = emissivity\ assumed\ equal\ to\ 1\ (Law\ 1978)$

$$T = Gas\ temperature\ (K)$$

$$t = Exposure\ time\ (s)$$

According to Nyman (2002), the equivalent time to failure of an element in a real fire (t_{equiv}) can be predicted if the temperature profile in the real fire and time to failure (t_f) in the standard fire are known. This method can therefore be applied to predict the equivalent time to failure in the real fire, and compare the results with the actual failure times recorded during the full scale tests.

4.8.5.1 Radiant Exposure Area Correlation applied to the tested assemblies

The method of evaluating the equivalent severity is based on the failure times as found from exposure of the specimens to the real fire curve and the standard time-temperature curve defined by CAN/ULC S-101 (2007). Table 4.17 shows the failure times of each connection type under exposure to the two fire curves.

Table 4.17 Times to failure (CAN/ULC S-101 vs Non-standard Time-Temperature Curves)

Connection Type		**Failure Times (min)**		**Non-Standard/Standard**
		Standard, CAN/ULC S-101 (Ali et al., 2014)	Non-standard	
Concealed	CN 60	31	12	0.39
	CN 100	20	3	0.15
Exposed	EX 60	39	18	0.46
	EX 100	23	12	0.52
Seated	SE 60	34.5	21	0.61
	SE 100	15	12	0.8

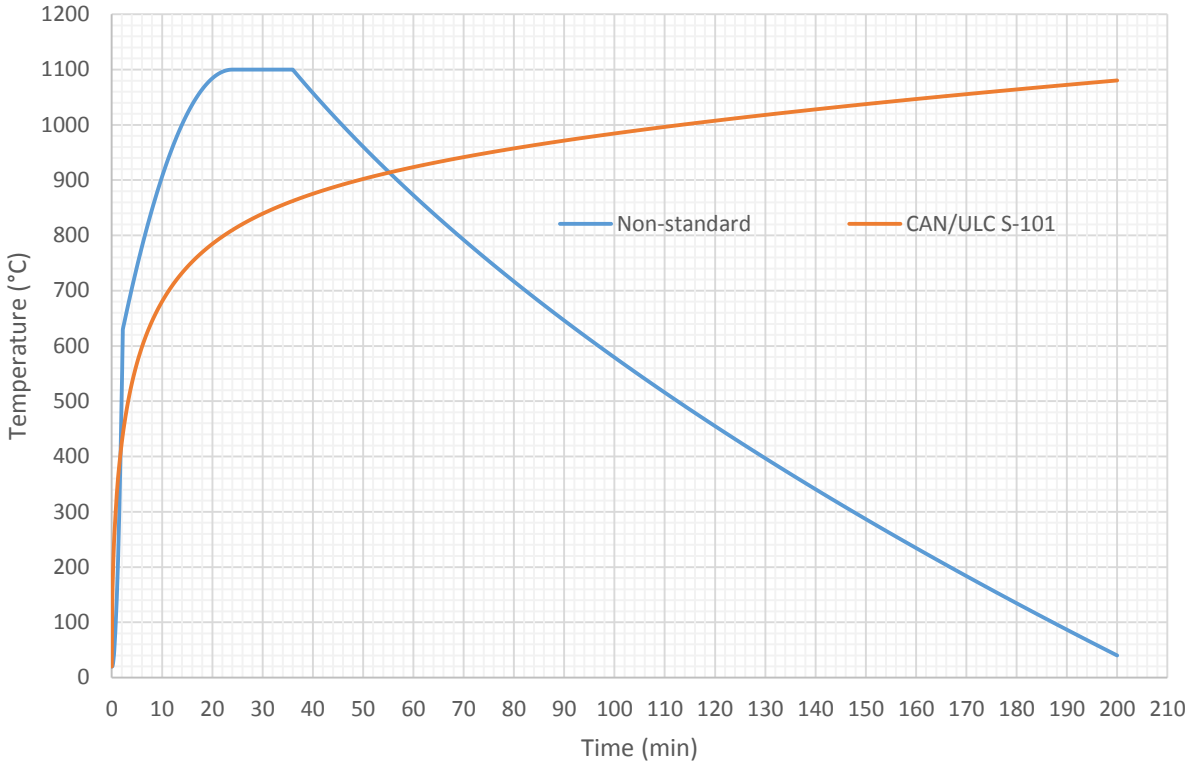

Figure 4.75 Standard (CAN/ULC S-101) vs Modeled Non-standard Fire Curve

The ratio of the failure times of the assemblies in the non-standard fire to the failure times in the standard fire defined by CAN/ULC S-101 ranged from 15% to 80%. This difference is due to the fast rise of the non-standard fire curve beyond the first 2 minutes of ignition (Fig. 4.75). This fast heating rate of the non-standard fire curve effects high radiant heat energies on the assemblies within a relatively shorter time frame, leading to early failure.

The severity of the standard and non-standard time temperature curves is evaluated in the succeeding sections.

4.8.5.1.1 Assembly involving Seated Shear Tab Connection (SE) – 60% Load Ratio

Testing of the assembly using the SE connection under 60% load ratio in the standard CAN/ULC S-101 fire curve lasted 34.5 minutes after exposure to a radiant heat energy of 123.9 MJ/m^2. Using the radiant exposure area concept, the predicted equivalent time of failure in the real fire at exposure to the same radiant energy is 21 minutes (Fig. 4.76) which is exactly the recorded failure time in the real fire test. The concept is therefore very accurate in predicting the equivalent time of failure of the seated connection under a load ratio of 60%.

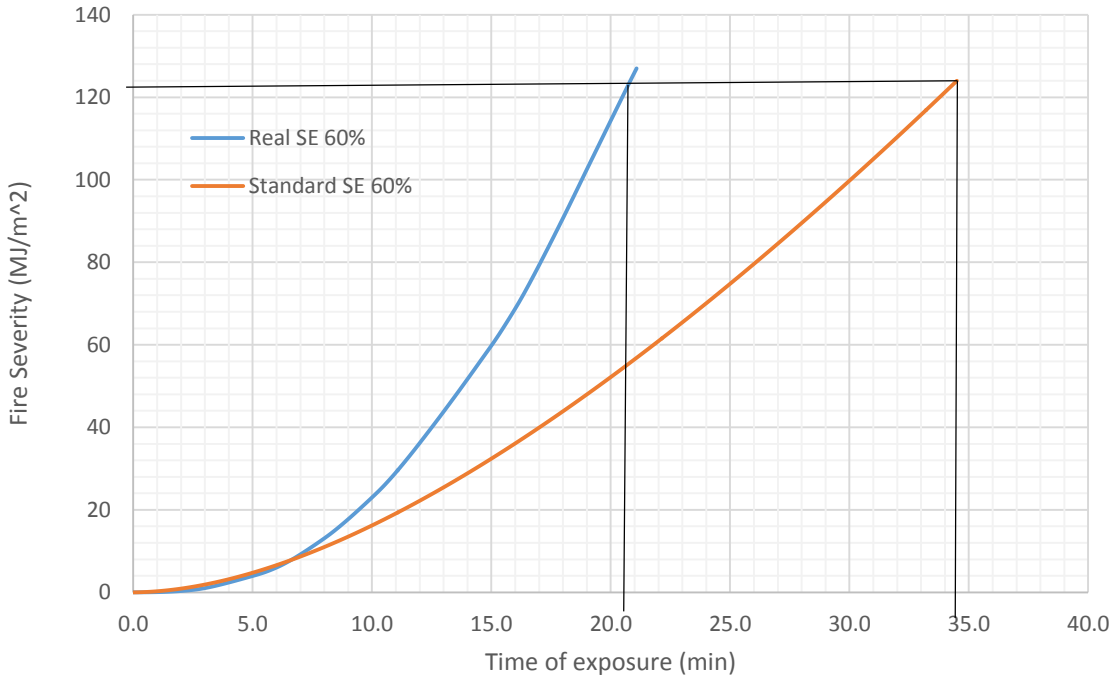

Figure 4.76 Radiant Exposure Correlation Graph (SE-60%)

4.8.5.1.2 Assembly involving Exposed Shear Tab Connection (EX) – 60% Load Ratio

After exposure to the CAN/ULC S-101 standard fire curve, the assembly involving the exposed connection under 60% load ratio failed after 39 minutes of exposure, with a radiant energy of 149.7

MJ/m^2. The predicted equivalent severity in the real fire is 23.5 minutes of exposure (Fig. 4.77) which is higher than the actual time of failure of 17.5 minutes in the real fire.

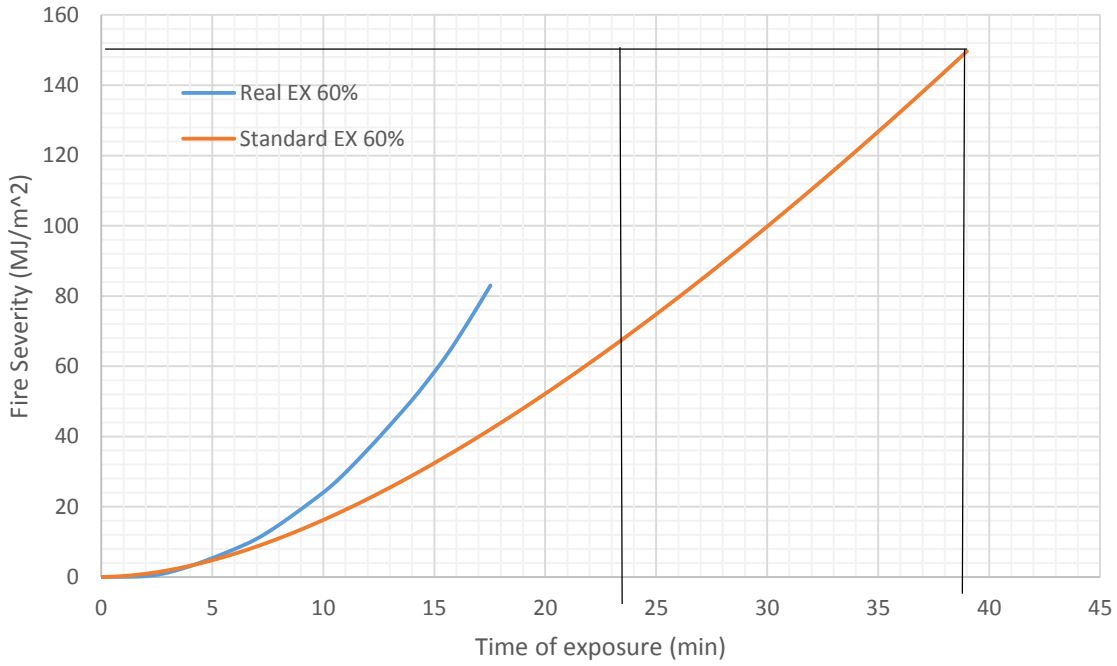

Figure 4.77 Radiant Exposure Correlation Graph (EX-60%)

4.8.5.1.3 Assembly involving Concealed Shear Tab Connection (CN) – 60% Load Ratio

The CN connection under 60% load ratio was exposed to a radiant heat energy of 105 MJ/m^2 after an exposure time of 31 minutes in the standard fire curve. The radiative energy area concept predicted a failure time of 18 minutes (Fig. 4.78) in the real fire, which is much lower than the time to failure of 12 minutes in the real fire.

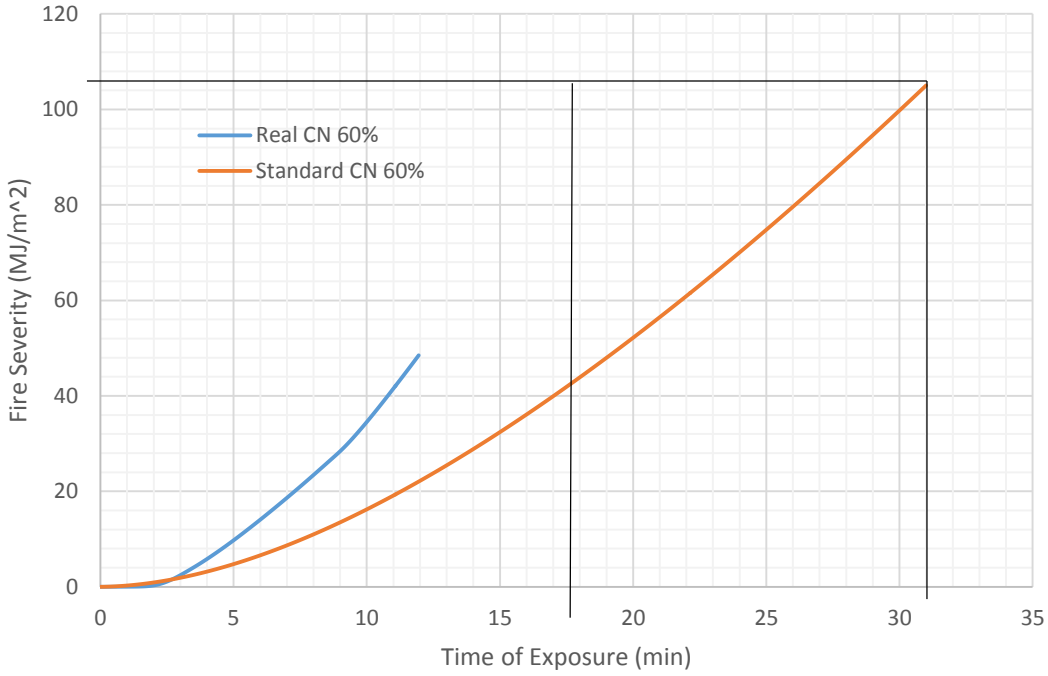

Figure 4.78 Radiant Exposure Correlation Graph (CN-60%)

4.8.5.1.4 Assembly involving Seated Shear Tab Connection (SE) – 100% Load Ratio

Under the full capacity of the assembly, the SE connection lost its structural integrity in the standard furnace after the 15th minute, at which time it had been exposed to a radiant heat energy of 32.4 MJ/m^2 (Fig. 4.79). The assembly is exposed to an equivalent severity in the real fire at 11 minutes, compared to an actual failure time of 12 minutes. Hence, the method is conservative in predicting the equivalent failure time in the real fire. The predicted failure time agrees well to the actual time of failure in the real fire test.

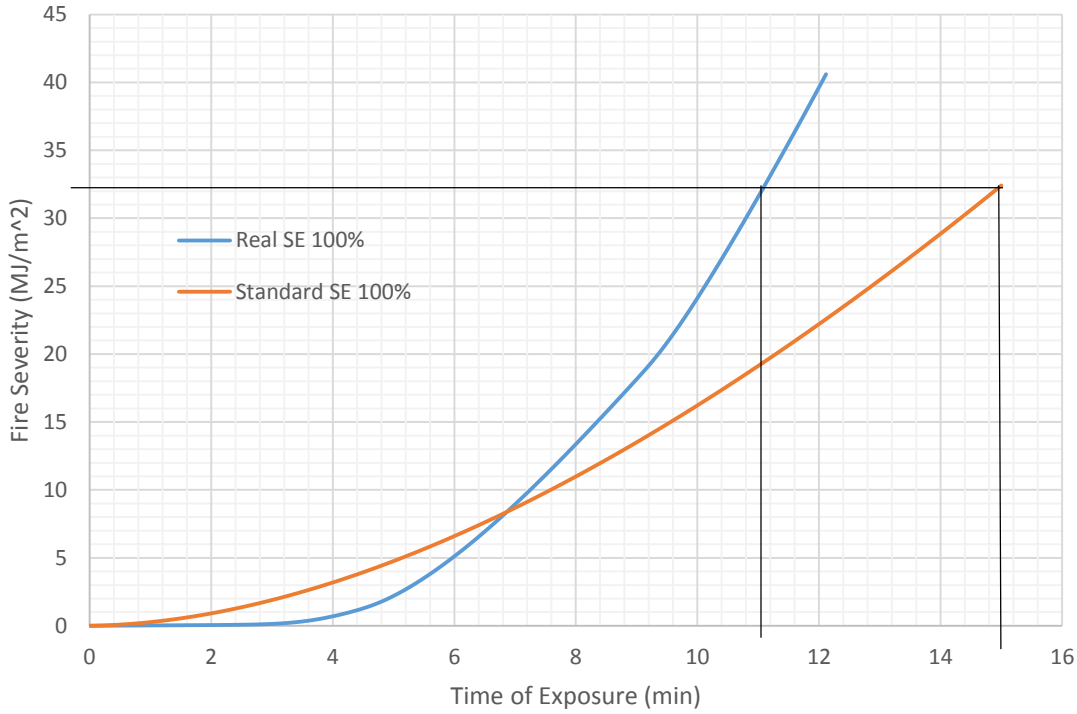

Figure 4.79 Radiant Exposure Correlation Graph (SE-100%)

4.8.5.1.5 Assembly involving Exposed Shear Tab Connection (EX) – 100% Load Ratio

In the standard furnace test, the EX connection under an applied load equal to the ambient capacity failed after 23 minutes. It was exposed to a radiant heat energy of 65.4 MJ/m^2 at this failure time. The radiant heat energy area method predicted a failure time of 18 minutes in the real fire as compared to the actual failure time of 12 minutes (Fig. 4.80). The method is therefore not conservative in estimating the equivalent time of failure in the real fire. The assembly fails 6 minutes earlier than the estimated failure time.

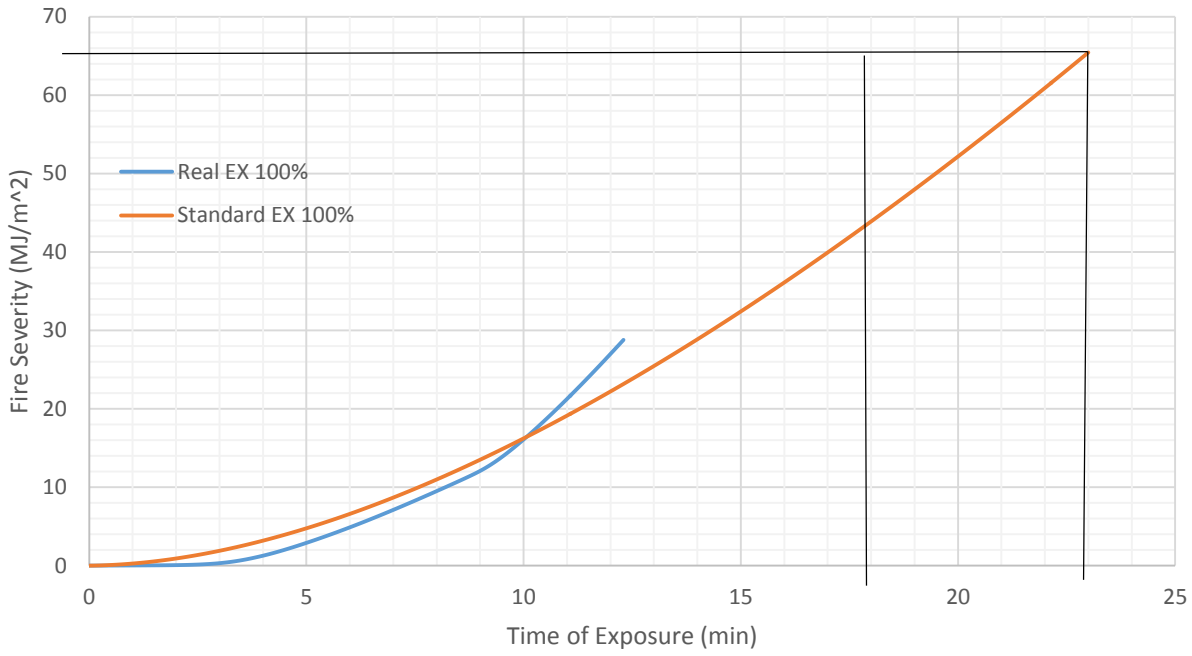

Figure 4.80 Radiant Exposure Correlation Graph (EX-100%)

4.8.6 Equivalent Fire Severity Summary

In the preceding section, the Radiant Heat Energy Area Concept was utilised to estimate the relationship between the severity of the real and standard fire curves on the connection assemblies. This method though recommended for insulation failure prediction of non-load bearing assemblies by Nyman (2002), provides fairly good and reliable results for the prediction of structural integrity failure of connection assemblies. A summary of the recorded failure times during testing and the predicted ones by the radiant energy concept is presented in Table 4.18. As it can be seen, the method gives fairly accurate and conservative estimates of the failure time for the seated connections. Under both lower and higher load ratios, there is no significant variation between the failure times during testing in the real fire and the equivalent time to failure by the discussed method.

The results is however non-conservative for fire tests involving the exposed and the concealed connections. Regardless of the load ratio, the method predicts a failure time 6 minutes longer than that recorded during testing of these assemblies in the real fire.

Table 4.18 Summary of recorded and predicted failure times of the assemblies

Assembly Reference	Time to failure (min)			
	Dimension (mm)	CAN/ULC S-101 (Ali et al., 2014)	Real Fire Curve	Radiant Heat Energy Area Prediction ($t_{equivalent}$)
SE-60%	137 x 222	34.5	21	21
SE-100%	137 x 222	15	12	11
EX-60%	137 x 222	39	17.5	23.5
EX-100%	137 x 222	23	12	18
CN-60%	140 x 191	31	12	18
CN-100%	140 x 191	20	3	- [1]

[1] *The Concealed Connection Assembly (CN-100%) failed relatively early in the real fire test and so radiant heat energy build up in the furnace room was not high enough to make feasible predictions of the equivalent failure time*

5 CONCLUSIONS AND RECOMMENDATIONS

In this research, nine (9) unprotected hybrid connection assemblies involving glulam beams and insulated steel columns were tested in a furnace under exposure to a modelled real fire curve. The glulam beams spanning 1.88 m were subjected to two-point constant transverse loads corresponding to load ratios of 60% and 100%. As defined in Section 3.3, the load ratio is the ratio of the applied loading during testing to the load capacity of the beam assuming simply supported end restraints at ambient temperature. Three main beam-to-column connections of seated, exposed and concealed were studied.

5.1 Conclusions

Based on the results and observations made, the following conclusions can be drawn:

1. The connection types with side plates (Seated and Exposed Connection Assembly) recorded an average charring rate of 1.09 mm/min as compared to 2.0 mm/min for the concealed connection type. This confirms the contribution of the slotted in steel plate in advancing the char front to the inner core of the beam at the connections. As such the beam with the concealed connection has charring commencing and proceeding from the exposed surfaces and inner core in contact with slotted in steel plate leading to quicker loss of section in fire. The exposed connection on the other hand has its inner core protected from extreme heat by the insulating char layer, and the thermo-hydric reaction between the steel side plate and the wood surface during the incipient stage of the fire. This hydric flux at temperatures in the region of 100°C slows down the combustion process of wood as a layer of steam is formed at the interface between wood and steel. This reaction process however depends on the moisture content of wood and the thickness of the steel side plate.

2. Charring rate of wood in the real fire used for the tests exceeded the value of 0.65 mm/min obtained in standard fire tests and employed in the design of wood for fire safety. In this research, charring rate values exceeding 1.0 mm/min were recorded for the glulam beam.
3. In this research, average char rate values of 1.09 mm/min, 1.1 mm/min and 2.0 mm/min were recorded for the seated, exposed and concealed connections respectively. Ali et al. (2014) reported charring rates of 0.57 mm/min, 0.56 mm/min and 0.94 mm/min for the seated, exposed and concealed connections under exposure to the standard fire defined by the CAN/ULC S-101 fire curve. The average charring rates recorded under exposure to the real fire curve were twice as large as that recorded in the standard fire curve.
4. Though the assemblies were designed to fail in one dominant mode, it was observed during testing that failure involved a combination of two or more modes. Splitting of wood was the dominant failure mode for the exposed and concealed connection, with an accompanying embedment of bolt holes, and fracture of glulam beam at mid-span in the tensile regions. Failure of the SE connection assembly involved cracking in the tensile region at mid-span, and lateral torsional buckling. It is important to mention that the presence of a floor system in a typical structure will prevent the latter, as enough restraint is provided. This also confirms Law's claim in 1981 (*Law, 1981*) of the unclear definition of restraint in standard furnace testing, and how it can give results far from failures in compartment fires.
5. The effect of the ratio of applied load in fire to the capacity of a member in ambient conditions cannot be underestimated. Decreasing the load ratio from 100% to 60% significantly increased the time to failure of the tested connection assemblies. The seated connection had a 75% increase in failure time, with the exposed having an increase of 50%.

6. Based on the analysis of results obtained, it can be concluded that the seated connection assembly offers the best fire resistance rating, with failure times that are 17% and 75% higher than that of the exposed and concealed connections respectively, under a load ratio of 60%.
7. To compare the severity of the real fire curve and the CAN/ULC S101 fire, the radiant exposure area method proposed by Nyman (2002) was used. The radiant exposure method by itself was found to be not appropriate for connections due to the numerous parameters such as the effect of charring rates (average value of 0.78 mm/min in the standard fire curve defined by CAN/ULC S-101, and 1.25 mm/min in the real fire curve), load ratio and different connections, that affect its structural behavior in a fire. The closest predictions were made for the seated connection. Results of the equivalent fire severity in the real fire were conservative for the seated connection only as the method predicted an equivalent time of failure almost equal to that recorded in the actual real fire test. The method predicted an equivalent failure time in the real fire curve with a variation of -8.33%, 34% - 50%, and 50% for the connection types of seated, exposed and concealed respectively.
8. The test furnace is capable of replicating real fires using the two propane burners for full scale tests.

5.2 Recommendations

1. In order to derive correlations and equations to relate the severity of the standard fire and the real fire for each connection type, future studies involving more specimens for each connection type is recommended.

2. In this research, one bolt diameter of 12.7 mm was employed for all connection types. The use of different bolt diameters is highly recommended in future studies to investigate their influence on fire resistance of connection assemblies in real fires.
3. Test on the Concealed (CN) Assembly under 100% load ratio unexpectedly failed after 3 minutes of exposure to the non-standard fire curve. Repetition of this test in future studies is therefore recommended.
4. Evaluation of achieved results with numerical modeling is recommended for future studies.

References

AFPA (1999). Details for Conventional Wood Frame Construction. Washington, DC: U.S.A. American Forest & Paper Association.

Aguanno, M. (2013). *Fire Resistance Tests on Cross-Laminated Timber Floor Panels: An Experimental and Numerical Analysis*. Department of Civil and Environmental Engineering: Carleton University.

Ali, S. G., Akotuah, A. O., Erochko J., & Hadjisophocleous, G. V. (2014). Performance of Hybrid Timber Connections with Full-scale Tests and Finite Element Modelling. *8th International Conference on Structures in Fire, 511-519*.

ASTM E119. (2000). Standard Test Methods for Fire Tests of Building Construction & Materials. American Society for Testing and Materials.

Babrauskas, V. (2004). Wood char depth: Interpretation in fire investigations. International Symposium on Fire Investigation. Fire Service College, Moreton-in-Marsh: United Kingdom.

Babrauskas, V. (2010). Performance-based building codes: What will happen to the levels of safety?. Fire Science and Technology Inc. 9000-300th Place SE. Issaquah WA 98027: U.S.A.

Benichou, N., & Sultan. M. A. (2000). Fire Resistance Performance of Lightweight Wood-framed Assemblies. *Fire Technology, 36, 3, 184-219.*

Buchanan, A. H. (2002). Structural Design for Fire Safety. Chichester, UK: John Wiley & Sons Ltd.

CAN/CSA-O86-09. (2010). Engineering Design in Wood. Canadian Standards Association. ON, Canada.

CAN/CSA S16-09. (2009). Design of Steel Structures. Canadian Standards Association. ON, Canada.

CAN/ULC S-101. (2007). Standard Methods of Fire Endurance Tests of Building Construction & Materials. Underwriter's Laboratories of Canada. Scarborough, Canada.

Canadian Mortgage & Housing Corporation (CHMC). (2014). Canadian Wood Frame House Construction. Canada. Library & Archives Canada Cataloguing.

Drake, G., Berry, M., & Schroeder, D. (2015). Effect of Cold Temperatures on The Shear Behavior of Glued Laminated Beams. *Cold Regions Science & Technology, 112, 45-50.*

EC3. (1995). Eurocode 3: Design of Steel Structures, EN 1993-1-2: General Rules-Structural Fire Design. European Committee for Standardization. Brussels, Belgium.

EC5. (2004). Eurocode 5: Design of timber Structures, EN 1995-1-2: General-Structural Fire Design. European Committee for Standardization. Brussels, Belgium.

Erchinger. C., Frangi. A., & Fontana, M. (2010). Fire Design of Steel-to-timber Dowelled Connections. *Engineering Structures, 32, 580-589.*

Frangi, A., & Fontana, M. (2003). Charring Rates & Temperature Profiles of Wood Sections. *Fire and Materials, 27, 91-102.*

Gerhards, C. C. (1982). Effect of the Moisture Content and Temperature on the Mechanical Properties of Wood: An Analysis of Immediate Effects. *Wood and Fibre, 14, 1, 4-36.*

NFPA 921. (2001). Guide for Fire and Explosion Investigations. Quincy, MA. National Fire Protection Association.

Harmathy, T. Z., & Mehaffey J. R. (1983). Post-flashover Compartment Fires. Division of Building Research. National Research Council. Canada.

He, M., Li, Z. (2012). Evaluation of Lateral Performance of Timber-Steel Hybrid Lateral Resistant System through Experimental Approach. Wood Conference on Timber Engineering, Auckland.

Hertz, K. (2012). Parametric Fires for Structural Design. *Fire Technology, 48, 807- 823*.

ISO 834. (1999). Fire Resistance Tests-Elements of Building Construction, Part 1: General Requirements. International Organization for Standardization, Switzerland.

Johnsson, H. (2004). Plug Shear Failure in Nailed Timber Connections, Avoiding Brittle and Promoting Ductile Failures. Lulea University of Technology.

Kathleen, H., & Almand, P. E. (2012). Structural Fire Resistance Experimental Research-Priority Needs of U.S. Industry. Quincy, MA. Fire Protection Research Foundation, NIST.

Kodur, V. K. R., & Harmathy, T. Z. (2002). Properties of Building Materials. SFPE Handbook of Fire Protection Engineering. Quincy, MA. National Fire Protection Association.

Konig, J. (2005). Structural Fire Design of Timber Structures According to Eurocode 5. Fire Safety Science-Proceedings. 8th International Symposium. 303-313.

Konig, J. (2006). Effective Thermal Actions and Thermal Properties of Timber Members in Natural Fires. *Fire and Materials, 30, 51-63*.

Konig, J., Noren, J., Olesen, F. B., & Hansen, F. T. (1997). Timber Frame Assemblies Exposed to Standard and Parametric Fires Part 1-Fire Tests. Stockholm. EN 1363-1.

Lange, D., Bostrom, L., Schmid, J., & Albretsson, J. (2014). Charring Rate of Timber in Natural Fires. 8th International Conference on Structures in Fire. Shanghai, China. 521-528.

Law, M. (1971). A relationship between fire grading and building design and contents. Fire Research Note No. 877. Fire Research Station, UK.

Law, M. (1973). Prediction of fire resistance. Paper in Symposium No. 5, Fire-Resistance Requirements of Buildings, a New Approach. Department of the Environment and Fire Offices Committee Joint Research Organization. London, UK.

Law, M. (1978). Fire Safety of External Building Elements - The Design Approach. Engineering Journal, 2nd Quarter, 59 – 74. American Institute of Steel Construction (AISC), USA.

Law, M. (1981). Designing Fire Safety for Steel-Recent Work. Proceedings of the ASCE Spring Convention. Pp 16. American Society of Civil Engineers. New York, NY.

Lie, T.T. (1972). Fire and Buildings. London, UK. Applied Science Publishers Ltd.

Maciulaitis, R., Lipinskas, D., & Lukosius, K. (2005). Singularity and Importance of Determination of Wood Charring Rate in Fire Investigation. *Materials Science, 12, 42-46*.

McGregor, C. (2012). Contribution of Cross-Laminated Timber Panels to Room Fires. Department of Civil & Environmental Engineering: Carleton University.

Mehaffey, J. R. (2003). Fire Performance of Heavy Timber Connections. Report No. 3223, Forintek Canada Corp. Ottawa, ON, Canada.

Morris, L. J., & Plum, D. R. (1996). Structural Steelwork Design to BS 5950. Prentice-Hall.

NBCC. (2010). National Building Code of Canada. Canadian Commission on Building and Fire Code. National Research Council of Canada. Ottawa, ON, Canada.

Nyman, J. F. (2002). Equivalent Fire Resistance Ratings of Construction Elements Exposed to Realistic Fires. University of Canterbury, New Zealand.

Building Code Act 1992. (2012). Ministry of Municipal Affairs & Housing. Ontario, Canada.

Peng, L., Hadjisophocleous, G., Mehaffey, J., & Mohammad, M. (2010). Fire Resistance Performance of Unprotected Wood-Wood-Wood and Wood-Steel-Wood Connections: A Literature Review and New Data Correlations. *Fire Safety Journal, 45, 392-399*.

Pettersson, O. (1973). *The connection between a real fire exposure and the heating conditions according to standard fire-resistance tests – with special application to steel structures*. Document CECM 3-73/73. European Commission for Constructional Steelwork.

Pettersson, O., Magnusson, S. E., & Thor, J. (1976). Fire Engineering Design of Steel Structures. Publication No. 50. Swedish Institute of Steel Construction.

Purkiss, J. A. (2007). Fire Safety Engineering Design of Structures. Aston University.

reThink Wood (2012). Evolving Building Codes and Wood Revolution: Pushing the boundaries of innovative wood design and construction. www.rethinkwood.com

SAA. (1990). Timber Structures, Part 4: Fire Resistance of Structural Timber Members. AS 1720-4-1990. Standards Associates of Australia.

Samake, A., Taazount, M., Audebert, P. & Palmili, P. (2014). Thermo-Hydric Transfer within Timber Connections under Fire Exposure: Experimental and Numerical Investigations. *Applied Thermal Engineering, 63, 254-265*.

SFPE Handbook of Fire Protection Engineering. (2002). Society of Fire Protection Engineers.

Solomon, T., & Siegfred, F. S. (2014). Special Issue on Performance of Timber and Hybrid Structures. *Journal of Performance of Constructed Facilities 28, Special Issue*.

SNZ. (1993). Code of Practice for Timber Design, NZS 3603. Standards New Zealand, Wellington, New Zealand.

Tannert, T., Vallee, T., & Muller, A. (2012). Critical Review on the Assessment of Glulam Structures using Shear Core Samples. *Journal of Civil Structural Health Monitoring 2:6572.*

Walton, W. D., & Thomas, P. H. (2002). Estimating Temperatures in Compartment Fires. SFPE Handbook of Fire Protection Engineering, Chapter 6, 3, 134 – 147.

Wood Design Manual. (2010). The Complete Reference for Wood Design in Canada. Canadian Wood Council.

Wood Handbook (1999). Wood as an Engineering Material. United States Department of Agriculture, Forest Service, Forest Products Laboratory. General Technical Report FPL-GTR-190.

Zi-Tao, Y., Xu, X., Li-Wu, F., Ya-Cai, H., & Ke-Fa, C. (2011). Experimental Measurements of Thermal Conductivity of Wood Species in China: Effects of Density, Temperature, and Moisture Content. *Forests Products Journal, 61, Issue 2, 130 – 135.*

Appendices

Appendix A – Detailed Drawings of Connections

All shear tab plates are CSA G40.21, Grade 300W.

Bolt Grade – A 327, 12.7 mm diameter.

Seated Shear Tab Connection

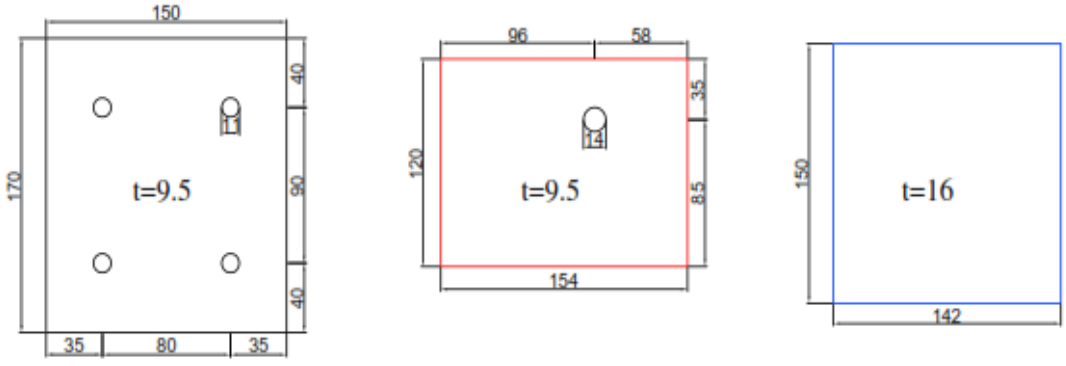

Column Plate Side Plate Bearing Plate

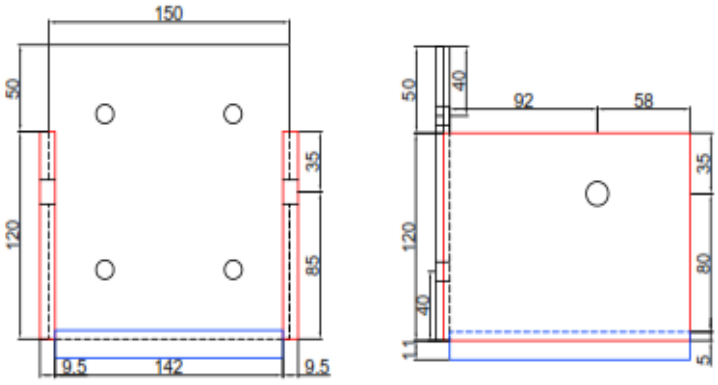

Back View Side View

Concealed Shear Tab Connection

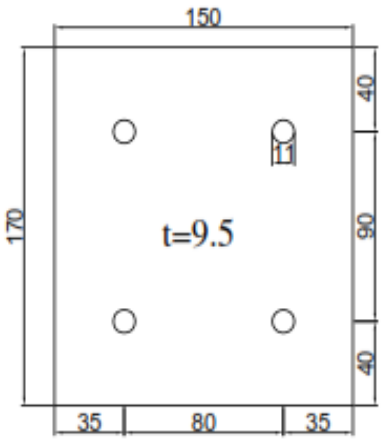

Column Plate

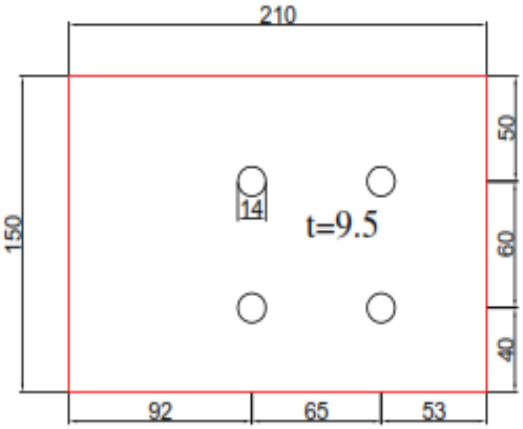

Side Plate

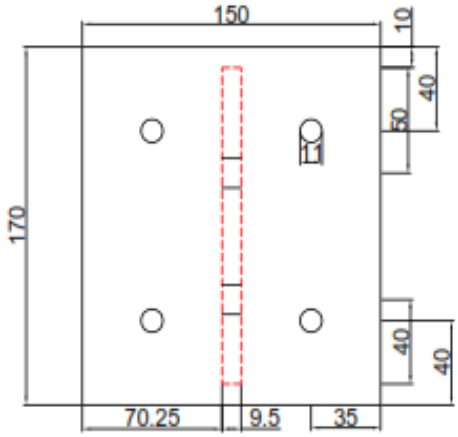

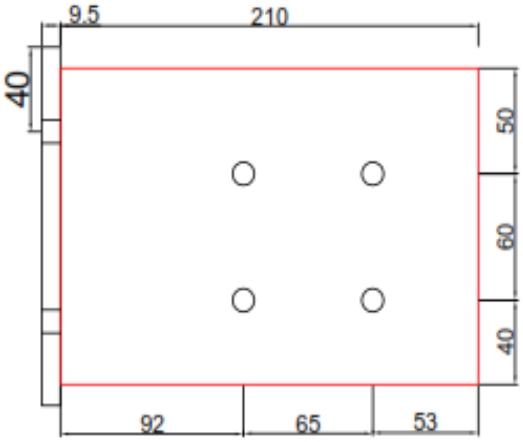

Exposed Shear Tab Connection

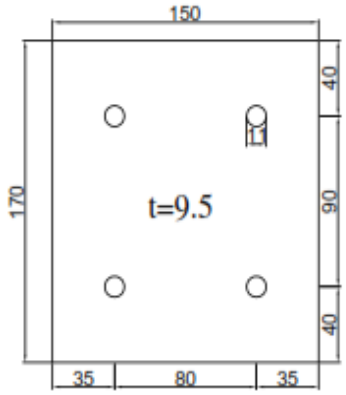

Column Plate

Side Plate

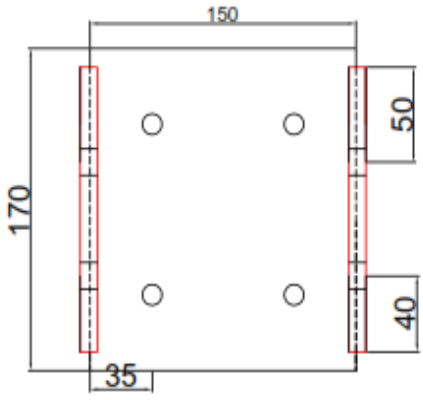

Back View

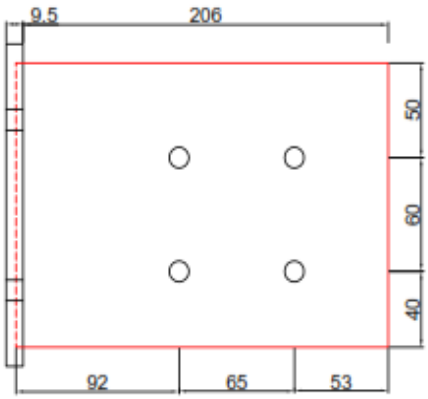

Side View

Appendix B – Design Calculations for Beams per provisions in CSA O86-09 (2010)

Design for Shear CL 6.5.7

Provisions for shear resistance of glulam beams in the CSA O86-09 is by either the simplified method or the detailed one. The simplified method, also applied in evaluating the shear resistance of sawn lumber works well for beams less than 2 m^3 in volume. The detailed method is a factor of both the load pattern and the volume of the member. It can be applied to all beams. It however produces a higher factored shear resistance when employed in beams of volume less than 2 m^3.

Simplified Method

Under this method, the factored shear resistance, V_r must be greater than the maximum factored shear force, V_f acting on the beam.

$$V_r = \emptyset F_v \frac{2A_g}{3} K_N$$

$where$

$\emptyset = 0.9$

$A_g = gross\ cross - sectional\ area\ of\ member, mm^2$

$K_N = notch\ factor\ (Cl\ 6.5.7.2.2)$

$F_v = f_v(K_D K_H K_{SV} K_T)$

$where$

$f_v = specified\ shear\ strength, MPa$

$K_D = load\ duration\ factor\ (Cl\ 4.3.2)$

$K_H = system\ factor\ (Cl\ 6.4.3)$

$K_{SV} = service\ condition\ factor\ for\ longitudinal\ shear\ (Cl\ 6.4.2)$

$K_T = treatment\ factor\ (Cl\ 6.4.4)$

Detailed Method

For all beams, the factored shear resistance, V_r must be greater than the sum of all factored loads, W_f, acting on the beam.

$$V_r = \emptyset F_v 0.48 A_g K_N C_V Z^{-0.18}$$

$$where$$

$$Z = beam\ volume, m^3$$

Design for Bending CL 6.5.6

The bending strength of glulam beams of regular cross-section is found per provisions in Cl 6.5.6.5 of the CSA O86-09. It is taken as the lesser of M_{r1} or M_{r2} calculated as shown below:

$$M_{r1} = \varphi F_b S K_X K_{Zbg}$$

$$M_{r2} = \varphi F_b S K_X K_L$$

$$where$$

$$\varphi = 0.9$$

$$S = Section\ modulus, mm^3$$

$$K_X = curvature\ factor\ (Cl\ 6.5.6.5.2)$$

$$K_{Zbg} = 1.03(BL)^{-0.18} \leq 1.0$$

$$where$$

$$B = beam\ width\ (for\ single - piece\ laminations) or\ the\ width\ of\ the\ widest\ piece\ (for\ multiple - piece\ laminations$$

$$L = length\ of\ beam\ segment\ from\ point\ of\ zero\ moment\ to\ point\ of\ zero\ moment, m$$

$$K_L = lateral\ stability\ factor\ (Cl\ 6.5.6.4)$$

$$F_b = f_b(K_D K_H K_{Sb} K_T)$$

$$where$$

$K_{Sb} = service\ condition\ factor\ for\ bending\ at\ the\ extreme\ fibre$

Design for Connection Yielding and Splitting Resistance CL 10.4.4.2

Clause 10 of CSA O86-09 makes provisions for the design of fastenings such as bolts, dowels, rivets, screws and shear plate connectors. It is assumed there is equal distribution of stresses on each fastener in a group of fastenings. For loading of beams perpendicular to grain, probable failure modes are due to yielding of bolts and embedding of the bolts, or splitting along the grain of the wood. Simple beam end bolted connections were used in this research study.

Yielding Resistance Cl 10.4.4.3

Foe double shear connections, the unit yielding resistance of bolts is calculated. The factored lateral yielding resistance $N_{r,}$ must be greater than or equal to the factored load N_f on the joint.

The factored yielding resistance is calculated as:

$$N_r = \emptyset_y n_u n_s n_f$$

$where$

$\emptyset_y = resistance\ factor\ for\ yielding\ failures = 0.8$

$n_u = unit\ lateral\ yielding\ resistance, N\ (Cl\ 10.4.4.3.2)$

$n_s = number\ of\ shear\ planes\ in\ the\ joint$

$n_f = number\ of\ fasteners\ in\ the\ joint$

For loading perpendicular to the grain of wood and three member connections, the unit lateral resistance n_u of a bolt is found as the smallest of the equations below as copied from CSA O86-09:

(a) $f_1 d_F t_1$

(c) $\frac{1}{2} f_2 d_F t_2$

(d) $f_1 {d_F}^2 \left(\sqrt{\frac{1}{6} \frac{f_2}{(f_1+f_2)} \frac{f_y}{f_1}} + \frac{1}{5} \frac{t_1}{d_F} \right)$

(g) $f_1 {d_F}^2 \sqrt{\frac{2}{3} \frac{f_2}{(f_1+f_2)} \frac{f_y}{f_1}}$

where

$f_1, f_2 = embedment\ strength\ of\ members\ 1\ and\ 2\ (Cl\ 10.4.4.3.3)\ where\ member\ 1\ is\ the\ side\ member, MPa$

$d_F = diameter\ of\ fastener, mm$

$t_1, t_2 = member\ thickness\ or\ dowel\ bearing\ length\ in\ accordance\ with\ Cl\ 10.4.2.2, mm$

$f_y = yield\ strength\ of\ fastener\ in\ bending, in\ accordance\ with\ Cl\ 10.4.4.3.3.3, MPa$

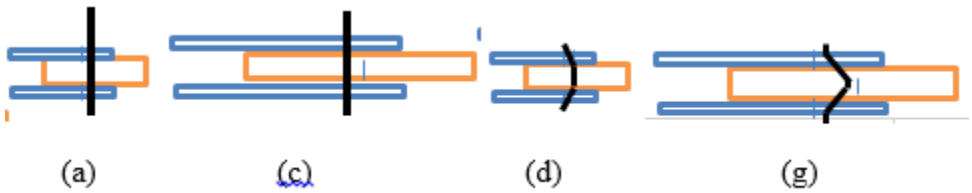

Perpendicular-to-grain Splitting Resistance for Wood Cl 10.4.4.7

Splitting failure is the brittle fracture of wood across a joint with bolts under tension loading perpendicular-to-grain (Wood Design Manual 2010). Provisions for splitting resistance in the CSA O86-09 are based on fracture mechanics formula taken from Eurocode 5. The splitting resistance at a joint is given as the lesser of the sum of the splitting resistance of all side members or that of the main member. The code also highlights the sensitiveness of the loaded edge distance on the splitting failure of members. In three-member connections, splitting resistance can be improved by ensuring equal thickness of the wood side members to avoid eccentricity loading.

$$QS_{rT} = \sum QS_{ri}$$

$where$

$QS_{rT} = Total\ factored\ splitting\ resistance\ of\ a\ joint, N$

$QS_{ri} = Factored\ perpendicular - to - grain\ splitting\ resistance\ of\ wood\ member\ i, N$

$QS_{ri} = \emptyset_W QS_i(K_D K_{SF} K_T)$

$where$

$\emptyset_W = resistance\ factor\ for\ brittle\ failures = 0.7$

$$QS_i = 14t\sqrt{\frac{d_e}{1 - \frac{d_e}{d}}}$$

$where$

$t = member\ thickness, mm$

$d_e = effective\ member\ depth, mm$

$= d - e_p$

$where$

$d = member\ depth, mm$

$e_p = unloaded\ edge\ distance, mm$